SEMMELWEIS EGYETEM

DOKTORI ISKOLA

Ph.D. értekezések

2843.

LASZLOVSZKY TAMÁS KRISTÓF

Funkcionális Idegtudományok
című program

Programvezető: Dr. Sperlágh Beáta, c. egyetemi tanár

Témavezető: Dr. Hangya Balázs, tudományos főmunkatárs

Characterization of functionally distinct basal fore-brain cholinergic cell types

PhD thesis

Tamás Kristóf Laszlovszky

János Szentágothai Doctoral School of Neurosciences

Semmelweis University

Supervisor:	Balázs Hangya, MD, PhD
Official reviewers:	László Magor Lőrincz, PhD
	Róbert Bódizs, PhD habil
Head of the Complex Examination Committee:	Bereczki Dániel, MD, PhD, DSc
Members of the Complex Examination Committee:	Emília Madarász, PhD, DSc
	Alán Alpár, MD, PhD, DSc

Budapest

2023

TABLE OF CONTENTS

1. LIST OF ABBREVIATIONS

AAV – adeno-associated virus

ac – anterior commissure

ACG – autocorrelogram, autocorrelation

ACh – acetylcholine

AD – Alzheimer's Desease

AHP – afterhyperpolarization

AIC – Akaike information criteria

Am - amygdala

AP – action potential

AP (axis) - anteroposterior

aq – cerebral aqueduct

Async – asynchronous firing

ATP – adenosine triphosphate

aW – active wake

BF – basal forebrain

BFCN - basal forebrain cholinergic neuron

BI – burst index

BIC – Bayesian information criteria

BLA – Basolateral amygdalar nucleus

BO – Bulbus olfactorius

Burst-BFCN – bursting basal forebrain cholinergic neuron

Burst-BFCN-SB – strongly bursting subgroup of Burst-BFCNs

Burst-BFCN-PL – Poisson-like firing subgroup of Burst-BFCNs

CB – calbindin

CCG – cross-correlogram, cross-correlation

Cer - Cerebellum

Ch1-Ch8 – 8 Major cholinergic projection neuron groups

ChAT – choline acetyltransferase

ChR - channelrhodopsin

CS – superior colliculus

Cm - centimeter

CPu – caudate-putamen

CR – calretinin

CR (behavioral trial outcome) – correct-rejection

dB - decibel

DBB – diagonal band of Broca

DMH – dorsomedial nucleus of the hypothalamus

DR – dorsal nucleus raphe

EEG - electroencephalogram

EF – early firing

EMG – Electromyography

ERS – event-related spectrogram

f – fornix

FA – false alarm

GABA – gamma-aminobutyric acid

GAD – Glutamic acid decarboxylase

Gad2 – GABA synthesizing enzyme

GAL - galanin

Gnrh – Gonadotropin-releasing hormone

GP – globus pallidus

HDB – horizontal limb of the diagonal band of Broca

HI – Hippocampus

HIP – Hippocampal region

Hz - hertz

ic – internal capsule

IPN – inter-peduncular nucleus

IR – infrared

ISI – interspike interval

kg/m^2 - kilogram/square meter

kHz - kilohertz

Kv (and subtypes) – Voltage dependent potassium channel

Kv2.2 – delayed rectifier potassium channel

LED – light-emitting diode

LF – late firing

LFP – local field potential

LH – Lateral habenula

LHA – Lateral hypothalamic area

lo – lateral olfactory tract

LV – lateral ventricule

LVA – low voltage activated calcium currents

μm - micrometer

μM – micromole

μV - microvolt

M1/M2 – motor cortex

mAChR – muscarinic acetylcholine receptor

MCPO – Magnocellular regions of the preoptic nucleus

MDF – medium-density fiberboard

mGP – medial part of the Globus Pallidus

MH – Medial habenula

mm – millimeter

mPFC – medial prefrontal cortex

ms – millisecond

MS/DBB – medial septum/diagonal band of Broca

MS – Medial septal nucleus

msec - millisecundum

MS/VDB – medial septum/vertical diagonal band of Broca

mt – mamillothalamic tract

mV - millivolt

nAChR – nicotinic acetylcholine receptor

Nb – neurobiotin

NB – nucleus basalis

NkR – Neurokinin receptor

nM - nanomol

NMDA - N-methyl-D-aspartic acid

NOS – Nitric oxide synthase enzyme

NPY – neuropeptide Y

NREM – non-rapid-eye-movement

Opt – optic tract

P75 – neurotrophin receptor

pA - picoampere

PAG – phosphate-activated glutaminase

pChAT – putative choline neuron

PETH – peri-event time histogram

PFC – prefrontal cortex

PL – poisson like

PPN – pedunculopontine nucleus

PS – paradoxical sleep

PSTH – peri-stimulus time histogram

PV – parvalbumin

PWM – pulse-width modulation

Reg-BFCN – regular firing basal forebrain cholinergic neuron

Reg NB – unidentified regular firing neuron

REM – Rapid eye movement

RV – rabies virus

s – secundum

SB – strongly bursting

scgn – secretagogin

Scp – superior cerebellar peduncles

SD – standard deviation

SE – standard error

SI – substantia innominata

SI/EA – substantia innominata/extended amygdala

Slc32a1 – vesicular GABA transporter

Sm – stria medullaris

SNr – substantia nigra reticularis

SOM – somatostatin

SPL – sound pressure level

STA – spike-triggered average

STS – spike-triggered spectrograms

Sync – synchronous firing

SWS – slow-wave sleep

TAN – tonically active interneuron

Th – thalamus

TI – theta index

tPS – transition to paradoxical sleep

TTL – transistor-transistor logic (pulse)

TTX – tetrodotoxin

UT - untagged

V - volt

VDB – vertical limb of the diagonal band of Broca

vGAT – vesicular GABA transporter

vGluT(1-3) – vesicular glutamate transporter (subtypes 1 to 3)

VIS – Visual cortex

VMH – ventromedial hypothalamic nucleus

VO/LO – ventral/lateral orbitofrontal cortices

vPFC – ventral Prefrontal Cortex

VTA – Ventral tegmental area

W - watt

W (sleep) - wake

2. INTRODUCTION

2.1 General introduction

Basal forebrain cholinergic neurons (BFCNs) have been associated with a wide variety of cortical processes from synaptic plasticity, learning, and memory, to the modulation of sleep-wake cycle, brain states and oscillations (Chubykin et al., 2013; Everitt & Robbins, 1997; Hasselmo & Sarter, 2011). The timescale of these processes can vary from fast, millisecond-based to slow, second, minute or even hour-based neuronal firing changes. The cholinergic system is capable of fast, phasic reactions – for instance to a sudden sensory input – or slow, tonic activity changes, modulating brain states by altering acetylcholine concentration in the cortex. To control these markedly different processes, cholinergic cells are expected to exhibit a large set of firing patterns, in course of which the synchronous or asynchronous co-firing of individual units enables the system to produce adequate cholinergic output for every different modulatory scenario. Hypothetically speaking, this broad temporal modulatory output (from fast phasic to slow tonic actions) by the BFCNs can be achieved in two ways. By their firing abilities they can be either "generalists", meaning that individual cholinergic cells express all types of activity patterns, or they are "specialists", so that there are subgroups among them, each supporting a specific function. Earlier *in vitro* studies (Khateb et al., 1992; Simon et al., 2006; Zaborszky, van den Pol, et al., 2012) characterized two distinct types of firing patterns among BFCNs, the so-called early and the late firing neurons. The early firing neurons are more excitable, and show strong spike frequency adaptation; moreover, they are capable of reaching depolarization blockade. In contrast, the late firing neurons are less excitable with the ability to maintain this low frequency discharge rate for prolonged periods. Functionally, the early firing cells are better suited for fast, phasic changes causing a sudden acetylcholine release in the cortical target areas triggered by a sudden sensory input. This fast cholinergic mechanism is a key feature in the generation of cortical processes such as learning (especially reinforcement learning), attention, synaptic plasticity, and memory (Gu & Yakel, 2011; Yang, Thankachan, et al., 2017). Conversely, cortical acetylcholine release can be controlled by slow, tonic activity changes of the late firing neurons, regulating cortical processes such as arousal (Sarter et al., 2009; Teles-Grilo Ruivo et al., 2017) on a longer timescale. The distinct electrophysiological properties of the cholinergic neurons are in accordance with the diverse cholinergic modulatory

functions, exhibiting phasic and tonic activity changes in the cortex. The *in vitro* data suggest the existence of distinct BFCN subgroups, but these have not yet been linked to *in vivo* functions. Whether "generalist" BFCNs are producing all the distinct functional modes or various "specialist" BFCN types can be attributed to segregated functions is still a debate.

We addressed this by conducting *in vitro* and *in vivo* measurements of BFCNs. BFCNs' intracellular properties were probed by precisely controlled *in vitro* experiments. These measurements were designed to characterize the electrical properties of the BFCNs by controlling their input parameters while testing if they are capable of exhibiting phasic and tonic firing patterns for a given input. Uncovering the correlation between BFCNs' firing and distinct behavioral processes, and if they synchronize their activity with each other, required *in vivo* behavioral measurements where multiple cholinergic single-unit activity can be registered simultaneously with cortical local field potential (LFP) recordings during controlled behavioral events.

BFCNs can respond to salient sensory inputs with short, 18 milliseconds (ms) latency, and high temporal precision (Hangya et al., 2015). Therefore, we had to measure the stimulus presentations to the animal with the same accuracy, to precisely align the evoked action potentials (APs) to these events. To achieve this, we designed an *in vivo* data acquisition setup (Solari et al., 2018) precise enough to operate at millisecond order temporal resolution during the delivery of cue and feedback stimuli, which allowed us to train the animals on specific learning tasks while measuring concurrent neuronal activity. Additionally, we registered the specific responses of the animals (such as licking for water) in parallel with the registration of their neuronal activity. This experimental setup enabled us to test both the electrophysiological and the functional heterogeneities among the cholinergic cells.

The data presented in the current thesis was recorded in mice either in *in vitro* experiments to study BFCNs intrinsic properties or in *in vivo measurements* to examine their behavioral functions. *In vitro* measurements were designed to precisely control and monitor the membrane potential of the neuron and the strength of the activation. To determine the functional differences among the BFCNs, we also recorded them *in vivo* using extracellular tetrode recordings with optogenetic identification while the animals performed an

auditory detection task requiring sustained attention. Data analysis was performed on a large *in vivo* (n=78) and *in vitro* (n=60) dataset by built-in and custom written Matlab scripts (further detailed in the Methods).

My personal contribution was designing and building the *in vivo* data acquisition setup and performing delay measurements of stimulus presentations on it. Furthermore, I performed the data analysis, model fitting, and data visualization for the entire *in vivo* dataset supervised by Balázs Hangya.

In the following introduction sections, we give an overall review on basic anatomical and functional properties of the basal forebrain (BF), followed by the identification of distinct cholinergic cell types with specific synchronization and behavioral properties.

2.2 Cholinergic cells in the Central Nervous System

2.2.1 Projection neurons

Nowadays most of the studies in neuroscience are based on rodent experiments, mostly using genetically modified mouse lines; however, the pioneers of this area were often using primates to study the cholinergic system. Therefore, earlier studies are using partly different nomenclature for the anatomical parts of this system. One of these early studies was a complete anatomical characterization of the BF and all the other central cholinergic nuclei in primates by Mesulam and colleagues (M. M. Mesulam & van Hoesen, 1976). They differentiated eight major groups of projection neurons (Ch1-Ch8) in rhesus monkeys. Group Ch1 corresponds to the medial septal area located between the lateral ventricles and the corpus callosum, dorsally from the hypothalamus. Ch2 corresponds to the cholinergic neurons in the vertical limb of the diagonal band of Broca (VDB). These first two groups send their projections to the hippocampus. Group Ch3 is located more ventrally, and it corresponds to the horizontal limb of the diagonal band of Broca (HDB), which is the source of the cholinergic fibers targeting the olfactory bulb. Group Ch4 includes the substantia innominata (SI) and the magnocellular regions of the preoptic nucleus (MCPO) and the nucleus basalis of Meynert, and they send their projections to the cortex and to the amygdala. Ch3 and Ch4 contain the largest number of cholinergic neurons, which are also the main cholinergic input to the prefrontal cortex (M. -Marsel Mesulam et al., 1983). Ch5 and Ch6 are located in the pedunculopontine nucleus (PPN) sending

ascending projections to the hypothalamus and to the thalamus as well as descending projections towards the pons targeting the nucleus vestibularis, locus coeruleus and some of the raphe nuclei. Ch7 is located in the habenula and innervates the interpeduncular nucleus. The last group is Ch8, which can be found in the parabigeminal nucleus and it projects to the superior colliculus (von Bohlen und Halbach, O., Dermietzel, R., 2006). This classification has been adapted to rodent experiments as it is shown in Figure 1.

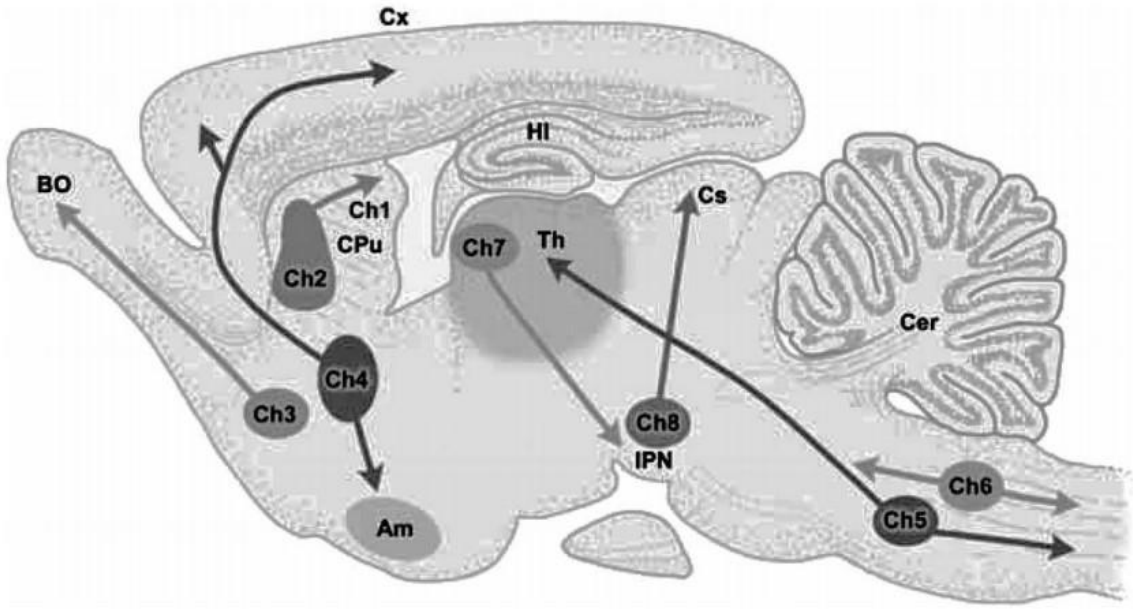

FIGURE 1 | Central cholinergic cell groups and their projections in the rat brain. Abbreviations: Am=amygdala, BO=Bulbus olfactorius, Cer=cerebellum, CS=superior colliculus, CPu=caudate-putamen, HI=hippocampus, IPN=inter-peduncular nucleus, Th=thalamus (von Bohlen und Halbach, O., Dermietzel, R., 2006)

2.2.2 Cholinergic interneurons

Cholinergic cells are typically associated with long projections and distant target areas; however, there is a subgroup of cholinergic interneurons and local projecting cells. A well-known example is the striatal cholinergic interneurons (Tanimura et al., 2019), which can modulate the dopaminergic terminals from the substantia nigra locally. These cells are exhibiting a tonic firing pattern; however, their synchrony with each other, and how they reset their firing after an input signal is markedly different from the tonically firing cholinergic projection neurons of the BF (discussed later). Moreover, cholinergic interneurons are present in the cortex, the hippocampus and in the olfactory bulb as well,

modulating a wide variety of neuronal processes. In our studies we focused on the projecting cholinergic subgroup; therefore, these locally projecting cells are not part of our measurements.

2.3 The basal forebrain

2.3.1 Cell types of BF, local connections

The projection neurons of the BF are implicated in the modulation of learning, memory, plasticity, attention, reward processing, sleep-wake control, and even consciousness (Chubykin et al., 2013; Everitt & Robbins, 1997; Froemke et al., 2007; Gu & Yakel, 2011; Hasselmo & Sarter, 2011; Yang, Thankachan, et al., 2017). Classically these functions were associated with the cholinergic BF neurons only; however, functional studies shed light on an intricate system built by neurochemically distinct cell populations (Lin et al., 2015). To understand the specific cholinergic effects, which is the main focus of this dissertation, it is inevitable to consider the BF's gamma-aminobutyric acid containing (GABAergic) and glutamatergic components and their interactions as well.

2.3.2 Main groups of the BF

Based on the cells' neurotransmitter profile the BF can be subdivided into three major groups (Anaclet et al., 2015; Mckenna et al., 2013; Xu et al., 2015; Zaborszky, van den Pol, et al., 2012), such as the cholinergic, the GABAergic and the glutamatergic cell populations. During neurotransmitter synthesis each group utilizes different synthesizing enzymes, which are then taken up by distinct vesicular transporters. These specific enzymes and transporters are often used as markers for a specific subgroup. Cholinergic cells are usually labeled by their acetylcholine synthesizing enzyme choline acetyltransferase (ChAT) (Armstrong et al., 1983). GABAergic cells are identified by their intrinsic vesicular GABA transporter (vGAT), while glutamatergic neurons are identified by one of the glutamatergic transporters (vGluT) or by the glutaminase enzyme (PAG). These populations can be further divided in case of the GABA and glutamate expressing cells. These subcategories are based on the cells' projections, calcium-binding protein expression, the presence of neuropeptide receptors, ion channels, and their intrinsic electrical properties (Figure 2.).

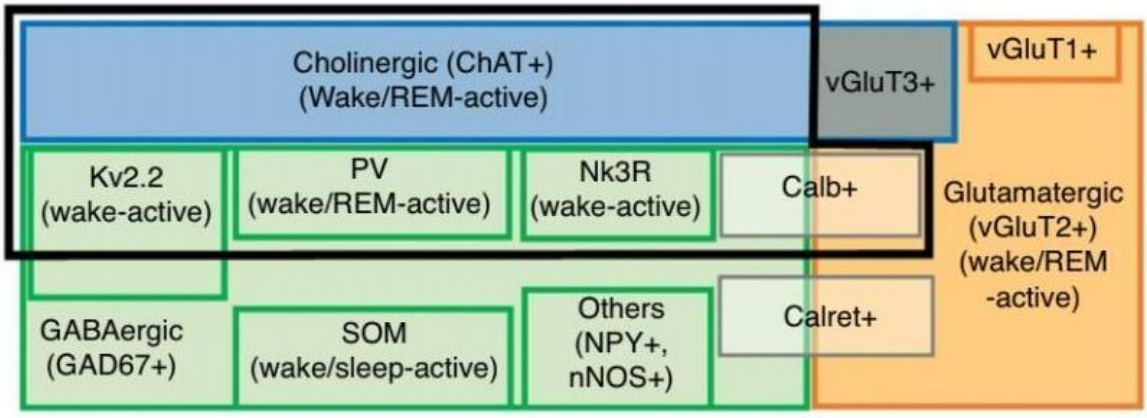

FIGURE 2 | Basal forebrain cell groups by their neurotransmitter profile and activity pattern during sleep-wake states. Blue, ChAT+ population of the BF (~10-20% of the BF neuronal population)((Zaborszky, van den Pol, et al., 2012); green, GAD67+/Gabaergic population (largest group of BF neurons)(Gritti et al., 2006); orange, Glutamatergic population (mainly vGluT2+, with small numbers of vGluT1+ and vGluT3+ neurons)(Hur & Zaborszky, 2005); A few vGluT3 neurons are cholinergic (grey/blue box) and project to the amygdala. The black frame represents cortically-projecting neuronal subtypes, including most cholinergic neurons, three different types of GABAergic neurons and glutamatergic (vGluT2) neurons. (Yang et al., 2017).

2.3.3 Cholinergic cells

Although BFCNs are the most studied of the above-mentioned three groups, they are only representing 10-20% of the overall neuronal population in the BF (Zaborszky, van den Pol, et al., 2012). The diagonal band of Broca (DBB) is the densest structure in the BF with respect to cholinergic cells and the substantia innominata (SI) is the least dense (Gritti et al., 2006). Typically, they are large neurons (>20 μm) (Mckenna et al., 2013; Yang et al., 2014) and most of them express the low affinity neurotrophin receptor p75 (Zaborszky, van den Pol, et al., 2012) which makes them capable of regulating fear extinction consolidation (Boskovic et al., 2018). They heavily innervate the entire cortex, showing target specific topographic organization. A newly discovered calcium binding protein secretagogin (scgn) showed co-expression with cholinergic cells in the medial and lateral septal areas, as well as in the DBB and amygdala (Gyengesi et al., 2013). The functional relevance of this co-expression is still unclear. A specific subset of BFCNs

targets the amygdala (Nickerson Poulin et al., 2006; Unal et al., 2015; Zaborszky, van den Pol, et al., 2012) and these neurons have unique properties, such as the lack of p75 receptors, and some of them even express the third subtype of the vesicular glutamate transporter (vGluT3) (Nickerson Poulin et al., 2006). This property makes them capable of synthesizing both acetylcholine (ACh) and glutamate (Gritti et al., 1997). Of note, this is not a unique feature of the BF, as cholinergic neurons in the medial habenula and in the striatum are also known as co-synthesizing ACh and glutamate (Figure 2.).

Furthermore, a second neurotransmitter group shows colocalization with acetylcholine. Saunder and colleagues (Saunders et al., 2015) optogenetically activated BFCNs and measured the postsynaptic currents in layer 1 interneurons in the cortex. These BFCNs are expressing the GABA synthesizing enzyme Gad2 and the vesicular GABA transporter (Slc32a1). They proved that their axon terminals are capable of monosynaptic release of both ACh and GABA. This process can be further characterized based on how they release ACh and GABA to the synaptic cleft. Theoretically they can release them from the same vesicle pool (co-release), or each type of the vesicles are released in a spatially and/or temporally distributed way (co-transmission). In hippocampal terminals of BFCNs cholinergic and GABAergic co-transmission has been described which can evoke complex postsynaptic potentials (Takács et al., 2018).The ability of co-expressing neurotransmitters by BFCNs further complicates the understanding of their cortical modulatory role.

2.3.4 GABAergic cells

The most abundant cells in the BF are the GABAergic ones, which are identified by their glutamic acid decarboxylase 67 (GAD67), or by their vesicular-GABA-transporter (vGAT) expression (Anaclet et al., 2015; Mckenna et al., 2013; Xu et al., 2015). They are mostly small or medium-sized neurons (<20 μm) but a small subset of them are large sized (>20 μm) projection cells (Gritti et al., 2003; Mckenna et al., 2013). The densest GABAergic location within the BF can be found laterally to the magnocellular preoptic nucleus. A subgroup of the GABAergic cells is positive for the calcium binding protein parvalbumin (PV). PV+ neurons are characterized by fast-spiking activity pattern, capability of high frequency bursting, narrow action potentials (APs), large H-currents, and depolarized membrane potential (Brown & McKenna, 2015; Lin et al., 2015; Mckenna et

al., 2013). They are involved in the modulation of cortical gamma band oscillations (Kim, Thankachan, et al., 2015). They are also expressing the Kv3.1 channel (Figure 2.), which is known for fast opening kinetics, which plays a crucial role in the generation of bursts. Another large population among BF GABAergic cells are expressing the delayed rectifier potassium channels Kv2.2 (Hermanstyne et al., 2010). These neurons are typically present in the HDB and in the MCPO. The third most numerous BF GABAergic subgroup is the Neurokinin B receptor (Nk3R) expressing one (Furuta et al., 2004). They have a specific role in the secretion of the gonadotropin-releasing hormone, and they are forming a spatially separate population among the cortically-projecting BF GABAergic cells. Smaller subgroups of GABAergic neurons exist, marked by the expression of the neuropeptides somatostatin (SOM), neuropeptide Y (NPY), or calcium binding proteins such as calbindin (CB) and calretinin (CR), or the nitric oxide synthase (NOS) enzyme (Gritti et al., 2003; Yang, Thankachan, et al., 2017; Zaborszky, van den Pol, et al., 2012).

CR is also expressed in glutamatergic cells, while CB can be found in all three major groups of BF cells. Alzheimer's Disease (AD) patients are demonstrating BFCN cellular atrophy, which is manifested in a specific way within the CB containing subpopulation. During the advanced stages of the disease the residual cholinergic cells are showing reduced CB levels, which leads to increased intracellular calcium concentration, which is a key malfunction during the apoptosis of the cells (Riascos et al., 2014). While most of the aforementioned neurons project to distant regions of the cortex, there are GABAergic neurons which projects locally within the BF. Another subset of them is distinguished by their small cell bodies and by their unique intrinsic electrical properties, which shows similarity to striatal medium-spiny neurons.

GABAergic cells exhibit a diverse set of firing patterns modulating a wide range of cortical processes. A subset of them are the PV positive cells that show sleep-wake cycle-related activity (Figure 3), firing with maximal intensity during wakefulness and rapid eye movement sleep (REM) epochs (Hassani et al., 2009; Mckenna et al., 2013; Xu et al., 2015). Their APs are in correlated with cortical gamma oscillations, which suggests their role in the modulation of attention (Hangya et al., 2015). Contrary to the PV+ cells, SOM or NPY positive neurons are characterized by showing maximal firing activity during non-REM sleep, linked to cortical delta activity (Duque et al., 2000; Xu et al., 2015). The remaining GABAergic cells do not express known markers that would serve as unique

identifiers for this subgroup; however, these cells are exhibiting REM-sleep coupled maximal activation and firing activity inversely proportional to EMG activity (Hassani et al., 2009). Recent functional studies showed a wake-promoting effect of the BF PV+ GABAergic cells by chemogenetic activation, and an increase in high frequency cortical oscillations (Anaclet et al., 2015; Kim, Thankachan, et al., 2015; Xu et al., 2015). Selective activation of the PV+ subgroup resulted in cortical gamma enhancement by synchronizing their cortical target PV+ interneurons (Kim, Thankachan, et al., 2015; Xu et al., 2015). SOM+ cells are heterogeneous based on their correlations with sleep-wake stages. There are a few of them which are active during wake and REM; however, the overall effect induced by stimulating SOM-expressing BF neurons is reduced wake periods and increased non-REM sleep (Xu et al., 2015). Relatively small amounts of data have been gathered about the Kv2.2 and the Nk3R positive neurons' functional properties; however, c-fos expression of these neurons was enhanced after wakefulness and they supposedly reduce cortical delta oscillation during sleep (Hermanstyne et al., 2013).

2.3.5 Glutamatergic cells

The glutamatergic population is divided into three groups according to their vesicular glutamate transporter subtype (vGluT) expression (Figure 2.). The most significant subset is the vGluT2 positive population, which sends cortical projections mostly from the ventromedial parts of the BF; however, these fibers are a relatively small subset (~5%) compared to the GABAergic and cholinergic projections (Hur & Zaborszky, 2005; Zaborszky, van den Pol, et al., 2012). In contrast to their weak cortical projections, they are heavily innervating subcortical regions such as the lateral habenula, which plays an important role in reward processing (Xu et al., 2015). Similarly to GABAergic cells, they are exhibiting local projections within the BF and they express calcium binding proteins (Gritti et al., 2003). CB-expressing glutamatergic cells are targeting the cortex, while CR-expressing neurons are sending their projections locally or caudally from the BF (Anaclet et al., 2015; Gritti et al., 2003). vGluT2-containing cells located in the rostral part of the BF are containing the gonadotropin-releasing hormone (Wu et al., 2009). An additional subset of the glutamatergic BF cells are the vGluT3-containing cells that coexpress acetylcholine (Nickerson Poulin et al., 2006). vGlut2 neurons are the most well-studied

regarding their firing patterns and AP properties. They are capable of firing bursts, although not as fast as the GABAergic ones, with a maximal firing rate around 50Hz *in vitro* (Xu et al., 2015; Yang, McKenna, et al., 2017). Some of them are exhibiting low-threshold calcium currents and moderate H-currents, which show spatial variability. Their APs are showing positive correlation with wake and REM phases (Figure 3.) and their activation can cause sustained wakefulness or it can decrease the power of delta oscillations during non-REM sleep (Xu et al., 2015). They increase their firing after negative reinforcers and their rostrally located subgroup is modulating hippocampal theta and locomotor activity (Fuhrmann et al., 2015; Robinson et al., 2016).

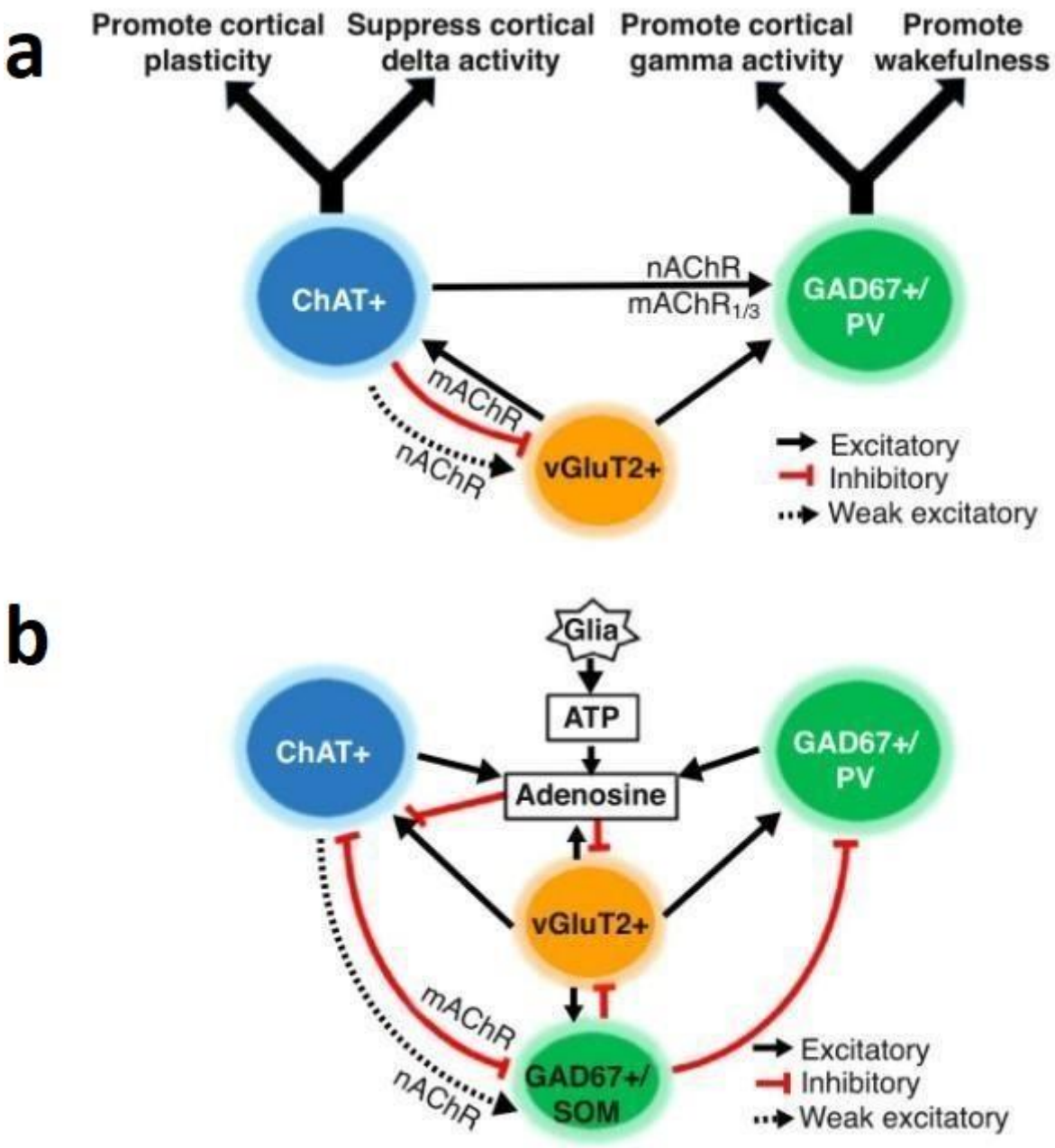

FIGURE 3 | Schematic model of the basal forebrain (BF) circuits controlling sleep–wake behavior. Solid lines with arrowheads indicate excitatory effects on the target neurons. The black dashed lines indicate a weak excitatory effect. Lines with flat ends indicate inhibitory effects. (a) BF circuits promoting wakefulness, cortical activation and adaptive responses to behaviorally relevant stimuli. An important subset of GABAergic neurons containing parvalbumin (PV) regulates cortical gamma band activity. Cholinergic (ChAT+) and glutamatergic (vGluT2+) neurons promote wakefulness and cortical activation indirectly via excitatory effects on GABAergic/parvalbumin (GAD67+/PV)

neurons, as well as via their direct cortical projections. Cholinergic neurons promote cortical plasticity in response to reinforcers. (b) BF circuitry involved in sleep promotion. During prolonged wakefulness (i.e., sleep deprivation) there is accumulation of extracellular adenosine due to direct release from neurons as well as breakdown from the neurotransmitter/gliotransmitter ATP. Adenosine inhibits BF cholinergic and GABAergic projection neurons by inhibiting their glutamatergic inputs via A1 receptors (Hawryluk et al., 2012; Kalinchuk et al., 2008), thereby promoting a homeostatic sleep response. Activation of a subset of GABAergic neurons containing somatostatin may facilitate spontaneous transitions into non-REM sleep by direct postsynaptic inhibition of wake-promoting cholinergic and GABAergic neurons. Abbreviations: ATP: adenosine triphosphate; choline acetyltransferase; GAD: glutamic acid decarboxylase; mAChR: muscarinic acetylcholine receptors; nAChR: nicotinic acetylcholine receptor; NREM: non-rapid-eye-movement; PV: parvalbumin; SOM: somatostatin; vGluT2: vesicular glutamate transporter type 2. (Yang et al., 2017)

2.3.6 Peptidergic cells

Most studies within the BF are focusing on the classical neurotransmitters and their modulatory roles. However, various neuropeptides are expressed in specific subsets of the BF cell population. These neuropeptides can trigger a prolonged change in the activity of the postsynaptic target neurons. BF neurons can be separated into three groups based on their neuropeptide expression (described in sections 2.3.3-2.3.5). Neuropeptide-Y (NPY), somatostatin (SOM), and galanin (GAL) are expressed in the BF with specific modulatory roles and interactions with the main neurotransmitter groups. NPY positive neurons are forming a local feedback-loop by suppressing the activity of the cholinergic projection cells. They are capable of tuning the cortical cholinergic output following a cholinergic activation epoch. SOM positive cells are implicated in the control of subcortical gamma oscillations and in the modulation of slow-wave sleep. They are sending local projections to PV-positive, glutamatergic, and to cholinergic neurons. They exert an inhibitory effect on BF cortically projecting neurons, resulting in the promotion of non-REM sleep. Furthermore, selective inactivation of SOM cells disrupted the amplitude of gamma oscillations in the ventral pallidum, which regulates locomotor speed, as well as interfered with

medial septal oscillatory activity, which modulates spatial working memory. These cells are synchronizing their local postsynaptic targets in the gamma band, exerting a modulatory drive to cortical brain states and cognitive processes.

GAL-positive cells attracted research interest when anatomical studies showed hypertrophy of galanin fibers during late stages of Alzheimer's disease (AD), which is characteristic of the cholinergic atrophy in the BF. Galanin fibers are "hyperinnervating" the remaining BF cholinergic cells in late stages of AD. Galanin is considered as a neuroprotective factor which is assumed to take part of the protective tissue response in AD. Galanin fibers showed an extensive arborization in the MS/DBB around cholinergic and GABAergic neurons. Whole-cell patch clamp recordings in the medial septum/diagonal band of Broca (MS/DBB) from acute slices described that galanin decreases the tetrodotoxin-sensitive spontaneous GABA release decreases the muscarinic receptor-mediated GABA release. Functional studies showed that galanin alters the cholinergic-GABAergic communication. Optogenetic activation of cholinergic neurons in the MS/DBB increased the GABA release back onto the cholinergic neurons. Galanin disrupts the feedback inhibition by the GABAergic MS/DBB cells reducing the inhibitory input received by the cholinergic cells (Damborsky et al., 2017). The local disinhibition within the BF in parallel with galanin hypertrophy during later stages of AD can serve as a compensatory mechanism to preserve the remaining BF cholinergic activity (Counts et al., 2010).

2.3.7 Glial cells

The BF also contains glial cells, which tend to receive more and more focus in recent years due to their crucial role in neuronal energy balance, inflammatory processes, and even in the modulation of cognitive processes. Regarding the BF, microglia is a key player in the maturation and the sustainment of the BFCNs (Jonakait et al., 2012). Moreover, recent data suggests that adenosine is a key regulator of sleep and wakefulness. Sleep-deprivation increased the level of extracellular adenosine in the BF (Kim, Ramesh, et al., 2015). This can be the consequence of direct neuronal adenosine release or glial cells releasing ATP which then breaks down into adenosine. The increased level of extracellular adenosine is inhibiting vGluT2 neurons through their A1 receptors. Tuning down these neurons are shutting down the excitatory inputs from the glutamatergic cells

to the BF cholinergic and GABAergic projection neurons. By blocking the glutamatergic excitation to the wake promoting cells, adenosine triggers a homeostatic sleep response. Although cholinergic and glutamatergic neurons' firing activities also showed correlation with adenosine levels, only the selective glutamatergic ablation resulted in impaired sleep homeostasis, suggesting that the glutamatergic cells are key components in the adenosine-based modulation of the sleep-cycle (Halassa et al., 2009).

2.4. Input-Output profile of the BF

Projection neurons of the basal forebrain are sending their axons throughout the entire cortical mantle. Each of the BFCNs are releasing ACh in specific cortical target areas where the ACh emission is regulated on different timescales across the different cortical areas. Such specific modulatory roles can be achieved by distinct inputs targeting these BF cholinergic cells, generating specific output patterns. Therefore, the input-output relations of the BF can give answers to the following questions: Which BF cells are responsible for the modulation of a specific cortical area? Which are the inputs that are driving these BF cells?

Despite the recent state-of-art anatomical data by tracing and genetic experiments there is still much debate about how the BF modulates numerous cortical processes.

2.4.1. Basal forebrain efferents

Classical anterograde and retrograde tracing studies determined the targets of the projection neurons of the BF (Saper, 1985). According to the location of the cell body within the BF and their target within the cortex, these fibers can be grouped into two fiber tracts. Neurons of the medial septum, HDB, SI and the medial part of the Globus Pallidus (mGP) are targeting the frontal cortex, the hippocampus the anterior cingulate cortex and the retrosplenium. These projections are forming the so-called medial-tract by mostly cholinergic and PV positive GABAergic BF neurons. The remaining fibers are forming the lateral tract with the cell bodies located in the MS, DBB, and the medial preoptic area, targeting the enthorinal, the piriform, and the perirhinal cortices. Additionally, cells of the SI and GP are projecting also to the neocortex through the internal capsule (Figures 4-6).

As distinct function is often the consequence of distinct anatomical connections, the question of whether BF cells target multiple areas ("generalists") or have specific cortical targets ("specialists") arose. Despite the thorough investigation of the BF connectome, data from the Zaborszky, the Dan, and from the Qiu labs (Do et al., 2016; Gielow & Zaborszky, 2017; Li et al., 2017) are still leaving questions about the target specificity. Contradictory data can be a result of the different techniques that were utilized by the aforementioned labs and the anatomical heterogeneity of the BF.

The Zaborszky concept supports the "specialist" paradigm claiming that each cell is responsible for the innervation of one target area, and projections to multiple targets from the same BF cell do not exist. In case of the cholinergic fibers, they showed that cells in the medial-rostral part of the BF tend to project to the medial parts of the cortex, whereas lateral and caudal BF cells are targeting lateral cortical areas. The more the two types of projection cells are intermingled the more their cortical targets are interconnected.

In contrast, the Qiu lab presented a massive dataset visualizing almost the entire arborization of the BFCNs, the analysis of which led to a significantly different concept. They presented individual BFCNs with multiple cortical targets. Interestingly, an individual BFCN can target distinct cortical regions that are responsible for markedly different cognitive functions.

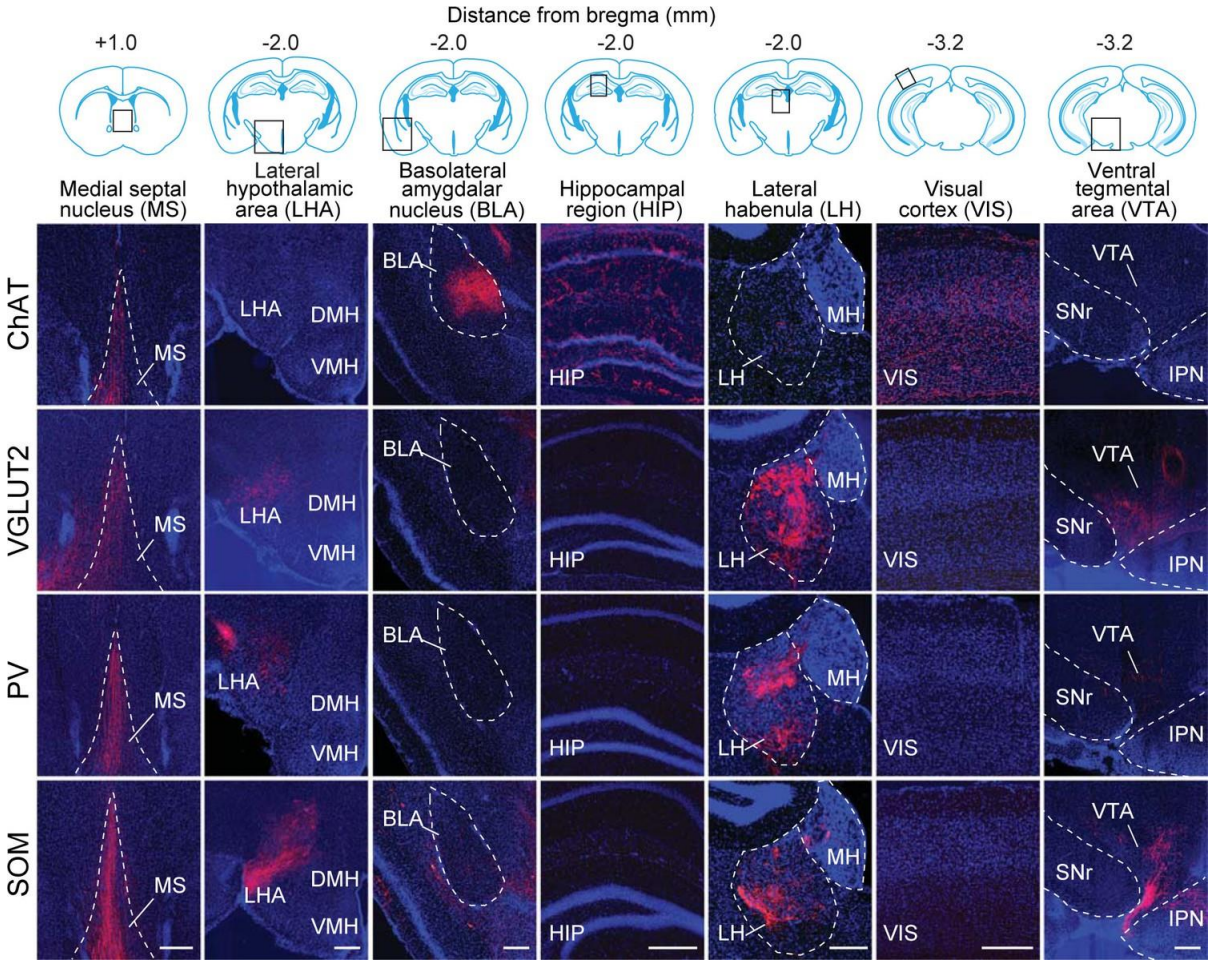

FIGURE 4 | Axon projections of each BF cell type to selected brain regions. Examples of axon projections from each of the four BF cell types to seven selected brain structures (black box in each coronal diagram). Scale bar, 250 mm. DMH, dorsomedial nucleus of the hypothalamus; IPN, interpeduncular nucleus; MH, medial habenula; SNr, substantia nigra reticularis; VMH, ventromedial hypothalamic nucleus. Upper panel, brain outlines adapted from Figures 23, 48, 57, from The Mouse Brain in Stereotaxic Coordinates, 3rd edition, Franklin, K.B.J. and Paxinos, G (copyright Elsevier, 2008. All Rights Reserved). (Do et al., 2016)

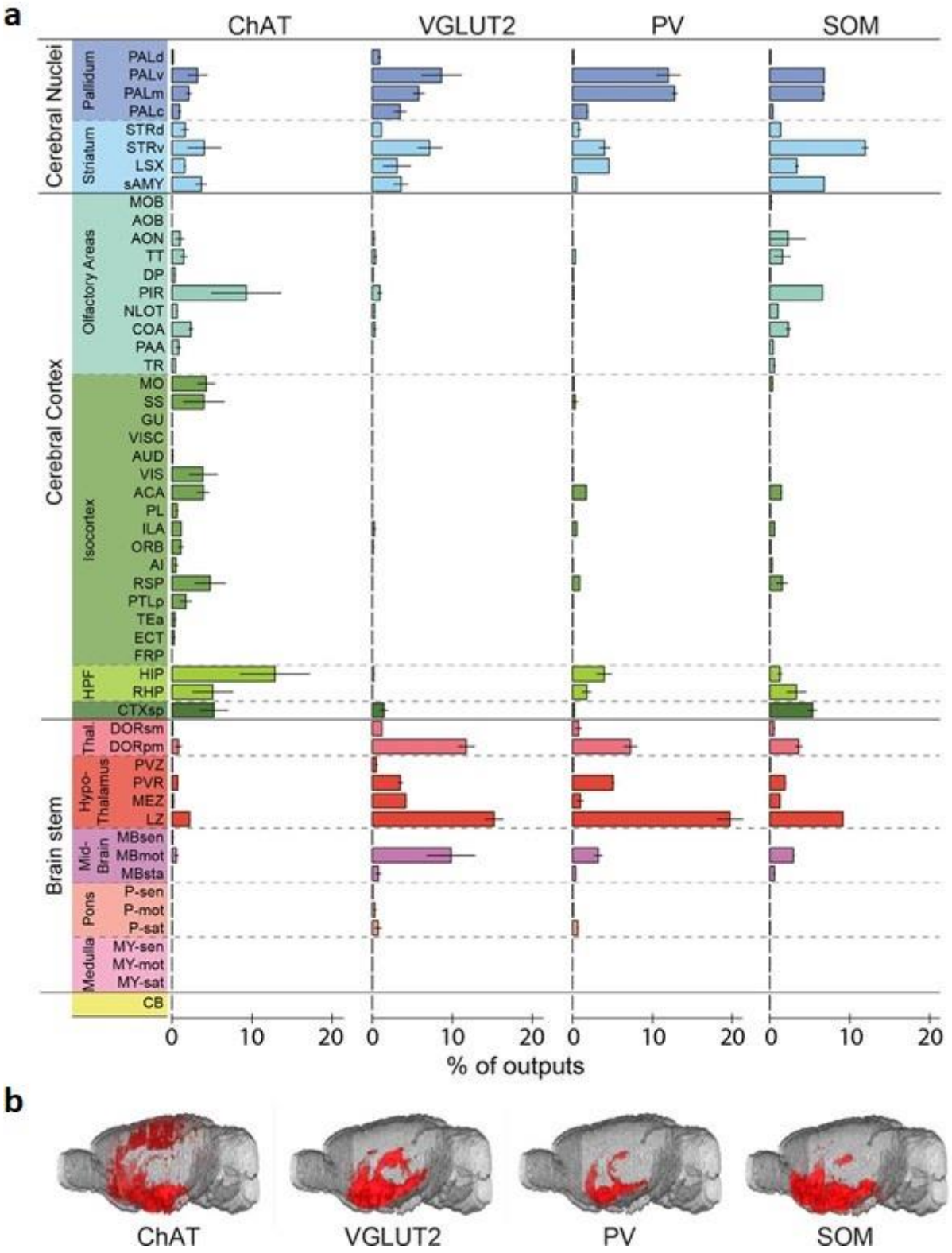

FIGURE 5 | Whole-brain distributions of axonal projections from the four BF cell types. (a) Percentages of labeled axons in 53 brain areas (ChAT, n = 3 mice; VGLUT2, n = 3; PV, n = 3; SOM, n = 3). Error bar, ± s.e.m. (Abbreviations of the 53 brain areas and their

percentages of inputs are listed in Do et al.'s Figure 6—source data 1). (b) Whole-brain 3D reconstruction of axon projections from each of the four BF cell types. Note that although VGLUT2+ and PV+ neuron projections showed the similar spatial distribution, there were fewer labeled axons from PV+ than VGLUT2+ neurons. (Do et al., 2016)

ACh is not only affecting the postsynaptic cells but also modulates presynaptic axon terminals expressing various muscarinic and nicotinic receptors. The numerous types of target receptors and their capability to modulate the cortical target cells both indirectly via their presynaptic partners or directly through their postsynaptic receptors makes the BF cholinergic system capable of controlling cortical processes across different cortical areas and timescales. BF projection neurons are innervating subcortical targets as well. One of the most well-studied subcortical targets of the cholinergic cells is the basolateral amygdala, but they are also innervating the striatum and the pallidum to a lesser extent.

As mentioned earlier, most of the fibers from the BF to the cortex are GABAergic and their postsynaptic partners are mostly GABAergic cells expressing PV, CB, or SOM. Interestingly, these cortical GABAergic target cells also receive modulatory input from cholinergic cells through their nicotinic ACh receptors. BF GABAergic cells are also innervating the striatum and the pallidum, specifically by the SOM and PV neurons. These cells are also projecting to the lateral hypothalamus and habenula, and to the VTA.

As we mentioned earlier, the BF sends efferents to subcortical targets as well, which is the preferred target of the vGluT2 positive cells. Glutamatergic cells are targeting the VTA, the habenula, the ventral pallidum, the striatum, the lateral hypothalamus, and the dorsal thalamus.

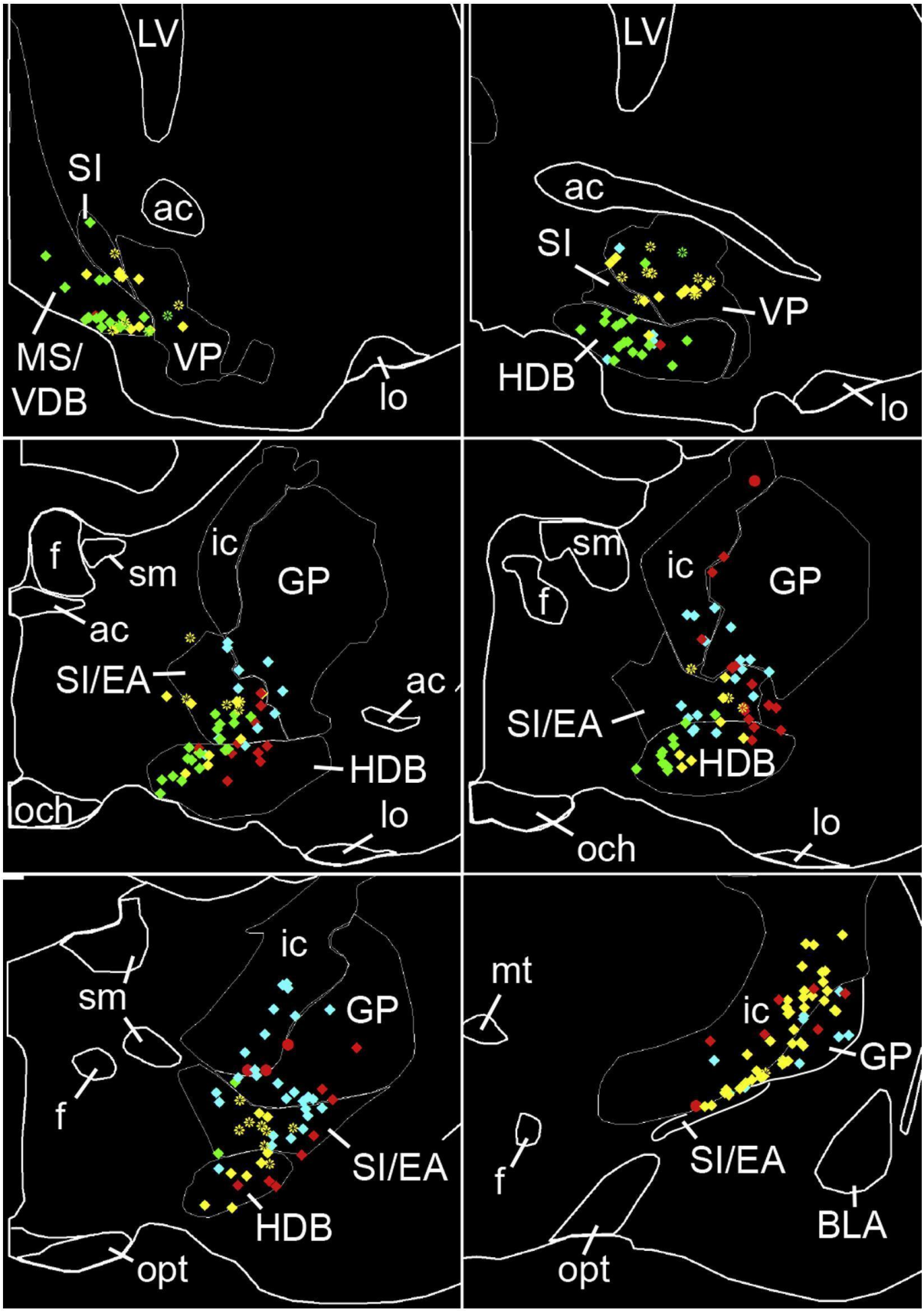
LV
SI
ac
MS/
VDB
VP
lo
LV
ac
SI
VP
HDB
lo
f
sm
ic
GP
ac
SI/EA
ac
HDB
och
lo
sm
ic
GP
f
SI/EA
HDB
och
lo
ic
sm
GP
f
SI/EA
HDB
opt
mt
ic
GP
f
SI/EA
BLA
opt

FIGURE 6 | Topography of BFCNs monosinaptically targeting distinct brain areas. Cre-dependent helper viruses were used in a ChAT::Cre rat line to selectively label cholinergic cells (expressing ChAT) in the BF (ChAT+ cells were labelled with mCherry, AAV-EF1a-FLEX-TVAmCherry). Retrograde rabies virus were injected in BF projection targets labelling a subset of BF cholinergic neurons (GFP +, AAV-CA-FLEX-RG). Cholinergic cells capable of spreading virus monosynaptically (mCherry + / GFP +) in 12 subjects following retrograde viral injection in M1/M2 (red), mPFC (green), VO/LO (blue), or amygdala (yellow). Double immunopositive BFCNs from individual cases (labeled with differently shaped symbols) were warped into a common template brain. ac, anterior commissure; BLA, anterior basolateral amygdala; f, fornix; GP, globus pallidus; HDB, horizontal diagonal band; ic, internal capsule; lo, lateral olfactory tract; LV, lateral ventricle; mt, mammillothalamic tract; MS/VDB, medial septum/ vertical diagonal band; opt, optic tract; sm, stria medullaris; SI/EA, substantia innominata/ extended amygdala. (Gielow & Zaborszky, 2017)

2.4.2 Basal forebrain afferents

Probably the most well-studied inputs of the BF are originating from the medial and ventral prefrontal cortex (vPFC) and terminating in the HDB, while the piriform cortex and the cortex insulae target the SI. The largest contributor to the BF afferents is the dorsal striatum; however, ventral striatal fibers are also present, targeting the BF cholinergic cells. Additional direct inputs are originating from various cortical areas mostly from the deeper layers (Figures 7-9).

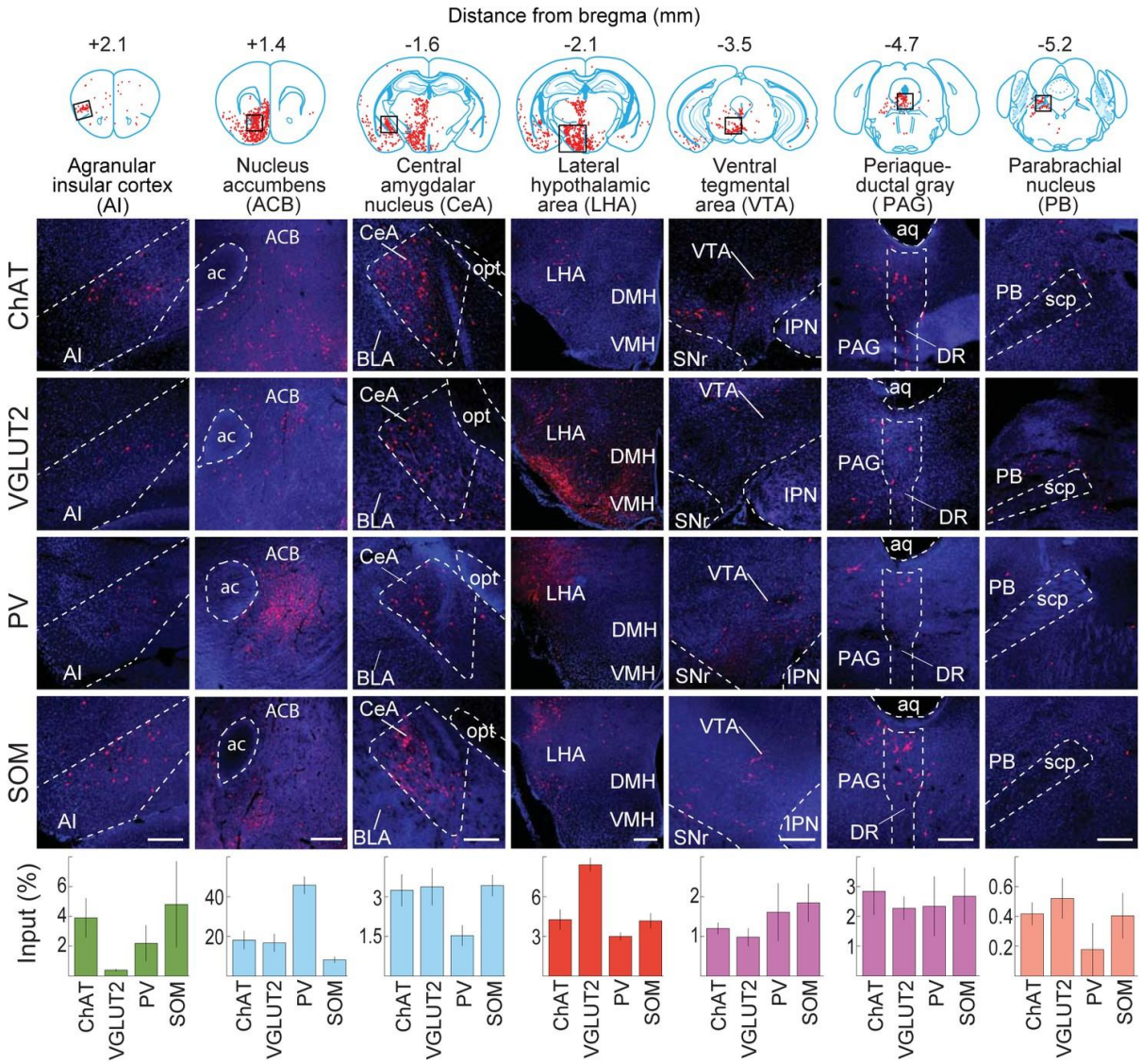

FIGURE 7 | Inputs to each BF cell type from selected brain regions. Examples of Rabies virus (RV) labeled input neurons to each of the four BF cell types in seven selected brain structures (black box in each coronal diagram). Scale bar, 200 mm. In each coronal diagram, RV-labeled neurons detected in all four brain samples are indicated by red dots. Bottom panel, mean percentage of input neurons in each brain structure for the four BF cell types. Error bar, ± s.e.m. Bar color indicates which of the 12 regions the given brain structure belongs to as depicted in Figure 9. ac, anterior commissure; aq, cerebral aqueduct; BLA, basolateral amygdalar nucleus; DMH, dorsomedial nucleus of the hypothalamus; DR, dorsal nucleus raphe; IPN, interpeduncular nucleus; opt, optic tract; scp, superior cerebellar peduncles; SNr, substantia nigra reticularis; VMH, ventromedial hypothalamic nucleus.

Upper panel, brain outlines adapted from Figures 13, 19, 44, 48, 60, 70, 74, from The Mouse Brain in Stereotaxic Coordinates, 3rd edition, Franklin, K.B. J. and Paxinos, G (copyright Elsevier, 2008. All Rights Reserved).(Do et al., 2016)

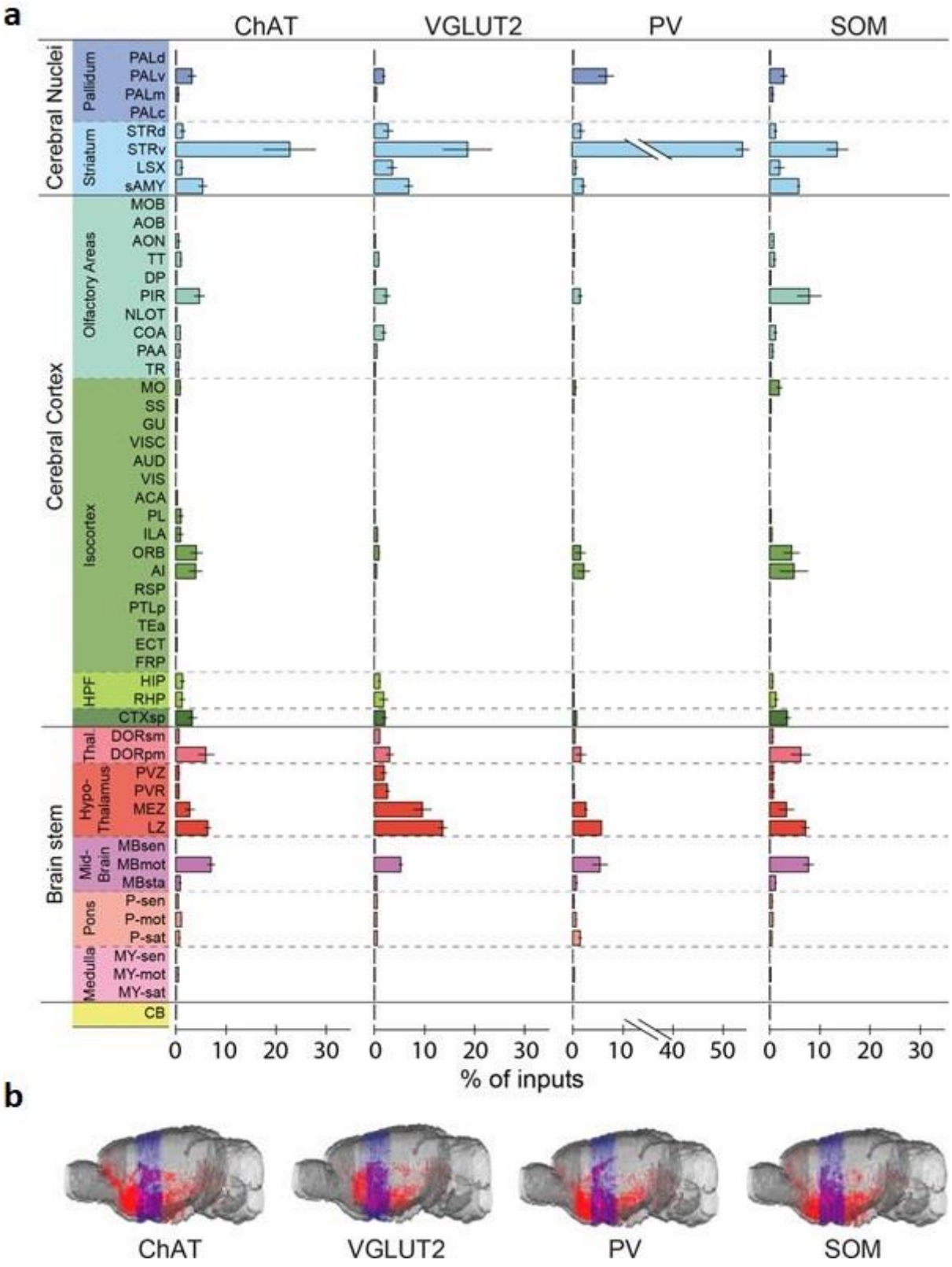

FIGURE 8 | Whole-brain distributions of inputs to the four BF cell types. (a) Percentages of retrogradely labeled input neurons in 53 brain areas (ChAT, n = 5 mice; VGLUT2, n

= 5; PV, n = 3; SOM, n = 4). Brain areas are grouped into 12 generalized, color-coded brain structures. HPF, hippocampal formation. Abbreviations of the 53 brain areas and their percentages of inputs are listed in Do et al.'s Figure 3—source data 1 (https://doi.org/10.7554/eLife.13214.009). Error bar, ± s.e.m. Since labeled neurons in coronal sections near the injection site were excluded from analysis (see Do et al.'s Figure 1—figure supplement 2, https://doi.org/10.7554/eLife.13214.004), inputs from the pallidum are likely to be underestimated. (b) Whole-brain 3D reconstruction of the inputs to the four BF cell types. The blue-shaded area denotes the region excluded for analysis due to potential local contamination (see Do et al.'s Figure 1—figure supplement 2, https://doi.org/10.7554/eLife.13214.004). (Do et al., 2016)

BF cells also receive significant subcortical inputs. Inputs from the BLA, LHA and nucleus accumbens are targeting specific BF subgroups, which send efferents to these areas, creating functionally relevant loops. The neurotransmitter profile of these input cells (noradrenergic, dopaminergic) can link distinct neuromodulatory systems to the BF population. Additionally, cells expressing orexin and hypocretin are targeting septohippocampal cholinergic partners which promote wakefulness through the activation of the cholinergic target cells. BF cholinergic cells receive inputs from various subcortical neuromodulatory systems. They have a key role in processing these mixed signals and transmit them towards the cortex.

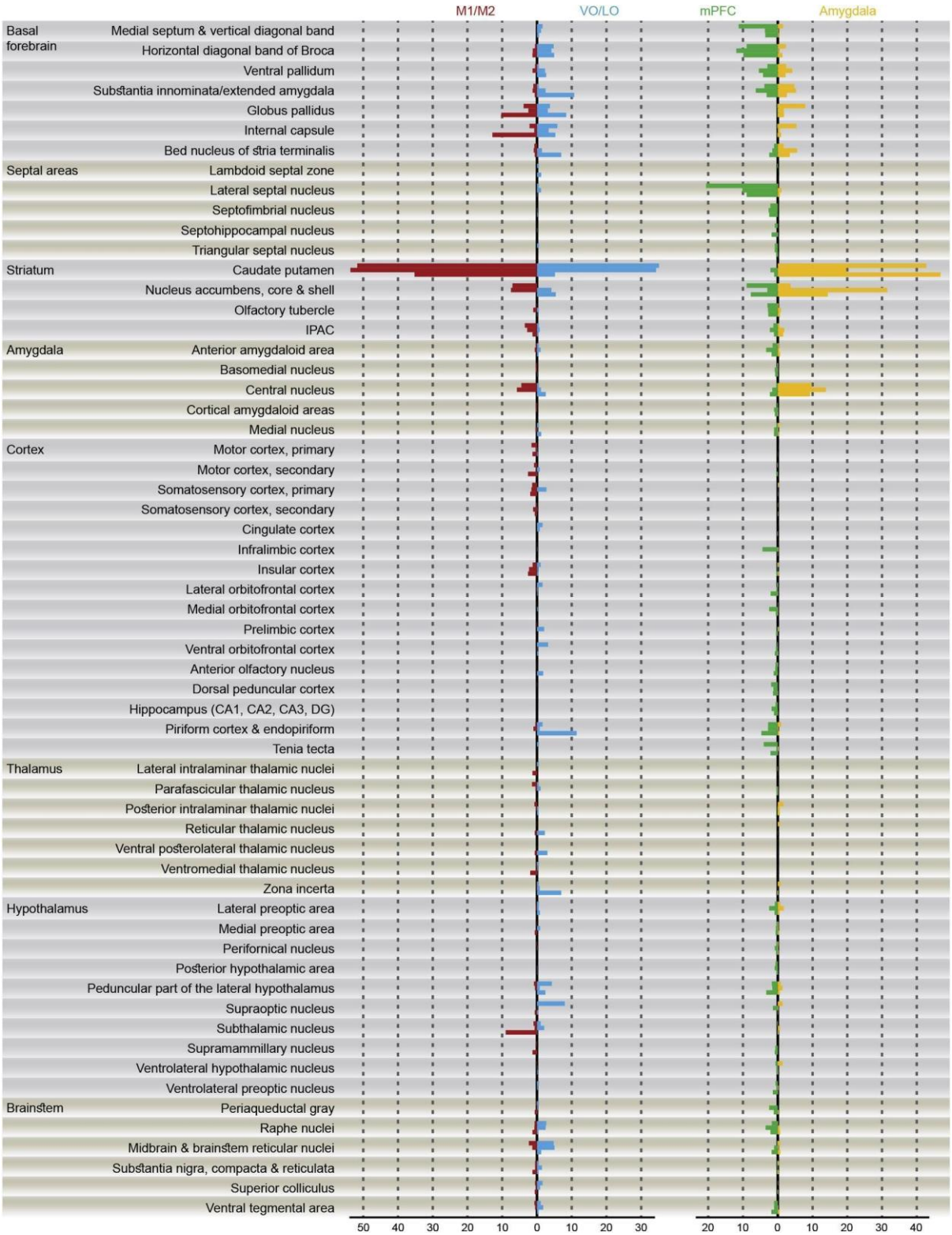

FIGURE 9 | Distribution of Inputs across All Brain Regions**.** Percentage of labeled inputs to BF cholinergic projection cells across all brain regions is shown per subject (individual bars clustered in groups of three). Regions of sparse input (where no injection group averaged >0.5%) are not shown. See also Gielow et al.'s Figures S3 and S4 and Table S2.

M1/M2, motor cortex; mPFC, medial prefrontal cortex; VO/LO, ventral/lateral orbito-frontal cortices. (Gielow & Zaborszky, 2017)

2.5. Electrophysiology of the BFCNs

2.5.1 In vitro

Cholinergic neurons showed distinct firing properties among all the BF cells measured in brain slices. One of the features that separated them from the other non-cholinergic BF cells was the presence of prominent calcium currents with a low threshold spike that makes them capable of rhythmical burst firing (Jones, 2004). Although non-cholinergic BF cells were also capable of rhythmic firing, they exhibited it in a completely different way, by firing non-adapting clusters of spikes (Alonso et al., 1996). Cholinergic cells produced rhythmic bursts with 2 or 3 spikes by receiving depolarizing current injections while their membrane potential was kept in a hyperpolarized state (Figure 10). Similar bursts could be induced when a hyperpolarizing membrane potential was released.

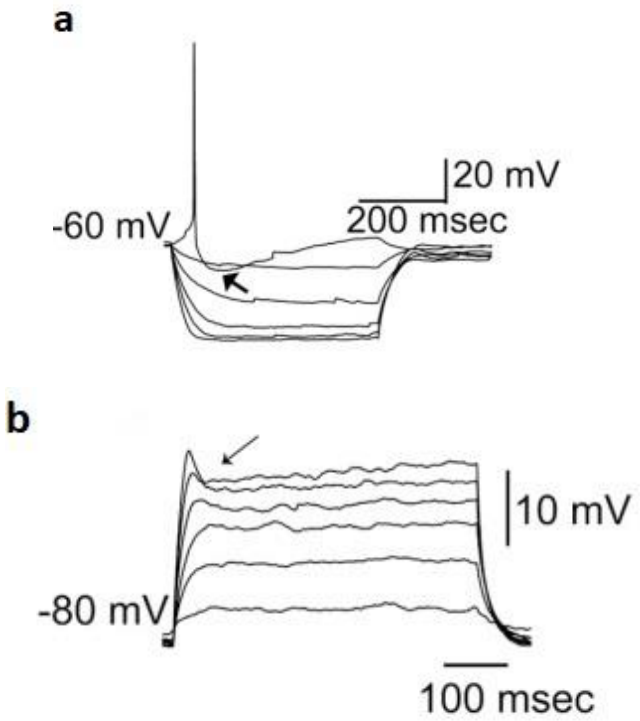

FIGURE 10 | (a) A cholinergic neuron at rest responding to negative and positive square pulses ranging between −100 and 20 pA in 20 pA increments. Zero pA step not shown. Note the prominent AHP following the single spike (indicated with arrow), and anomalous inward rectification at negative voltages. (b) The same neuron recorded in the presence of 1 μM TTX from a membrane potential of −80 mV in response to positive square current pulses from 20 to 120 pA in 20 pA increments. Note the voltage hump (indicated by arrow) and the outward rectification in the positive direction. (Zaborszky, Unal, et al., 2012)

The underlying mechanism behind the bursts was discovered by pharmacological blockage of specific ion channels. Sodium channel blockage by tetrodotoxin (TTX) revealed the broad, low-amplitude calcium spikes behind the fast bursts (Khateb et al., 1992). The evoked bursts appeared with a pre-hyperpolarization dependent delay. The degree of the preceding hyperpolarization affects the delay through a transient outward potassium current (the so-called A-current). After the decay of the bursts a slow, long-lasting (~300 ms on average) hyperpolarization follows caused by a calcium dependent potassium current. When the pre-pulse conditions were reversed from hyperpolarized to depolarized state, the following depolarizing current injections evoked only single spike firing (Figures 11-12).

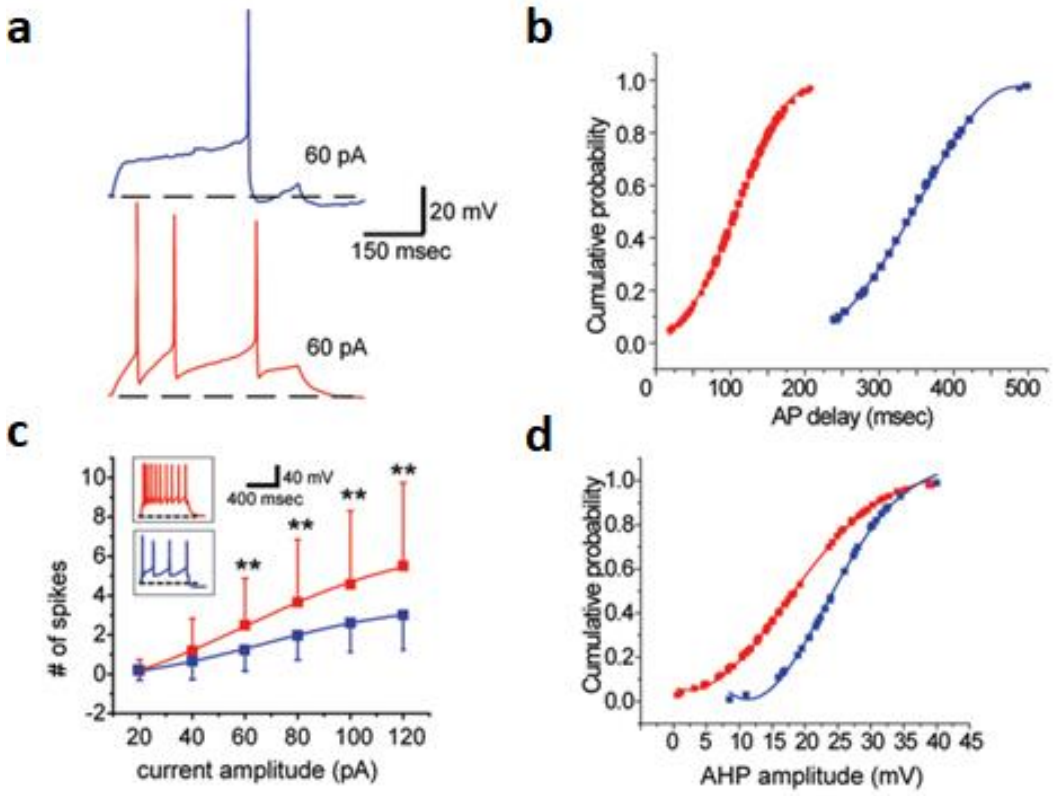

FIGURE 11 | Cholinergic BF neurons can be distinguished based on their firing properties. (a) A late firing (LF) neuron (blue trace, Top) and an early firing (EF) neuron (red trace, Bottom). The traces were obtained in response to a rheobase current injection (+60 pA in both cases). The scale bar applies to both traces. Dashed line corresponds to −70 mV. (b) Cumulative probability plot depicting the distribution of action potential latencies at rheobase. LF (blue) and EF neurons (red) fall into clearly distinguishable groups. (c) Scatter plot illustrating the current-frequency (I-F) curve of LF (blue) and EF neurons (red). Insets are representative examples of firing behavior in response to 120 pA current injections from −70 mV. Dashed lines correspond to −70 mV and the scale bar applies to both insets. (d) AHP amplitude distributions for LF (blue) and EF neurons (red). Despite some overlap, LF neurons had higher amplitude AHPs. (Zaborszky, Unal, et al., 2012)

The two types of the induced firing modes (single spike or burst) can differently modulate the postsynaptic partner of these BF cholinergic neurons. On a network level it is hypothesized that firing patterns like cholinergic burst firing can induce rhythmic

electroencephalogram (EEG) oscillations. Moreover, pharmacological studies of BF cholinergic cells revealed that muscarinic agonists and serotonin can hyperpolarize these cells while N-methyl-D-aspartic acid (NMDA) and noradrenaline can depolarize them. During *in vitro* conditions simultaneous administration of ACh and NMDA evoked rhythmic bursting in the cholinergic cells with a mean frequency of 6 Hz, which is in the middle of the theta range (Khateb et al., 1997). Not only neurotransmitters could evoke rhythmic firing of the cholinergic cells, but also neuropeptides such as neurotensin induced depolarization in the BF cholinergic cells evoking a slow rhythmic bursting. With prolonged neurotensin administration BFCNs started to synchronize their firing and evoke complex spindle-like activity patterns (Alonso et al., 1994). Few seconds long repetitive depolarizations and quiet periods alternates during these patterns accompanied by high frequency bursts during the depolarized periods. The effects on cortical oscillatory activity of these BF cholinergic firing patterns are further discussed in the *in vivo* section of the introduction.

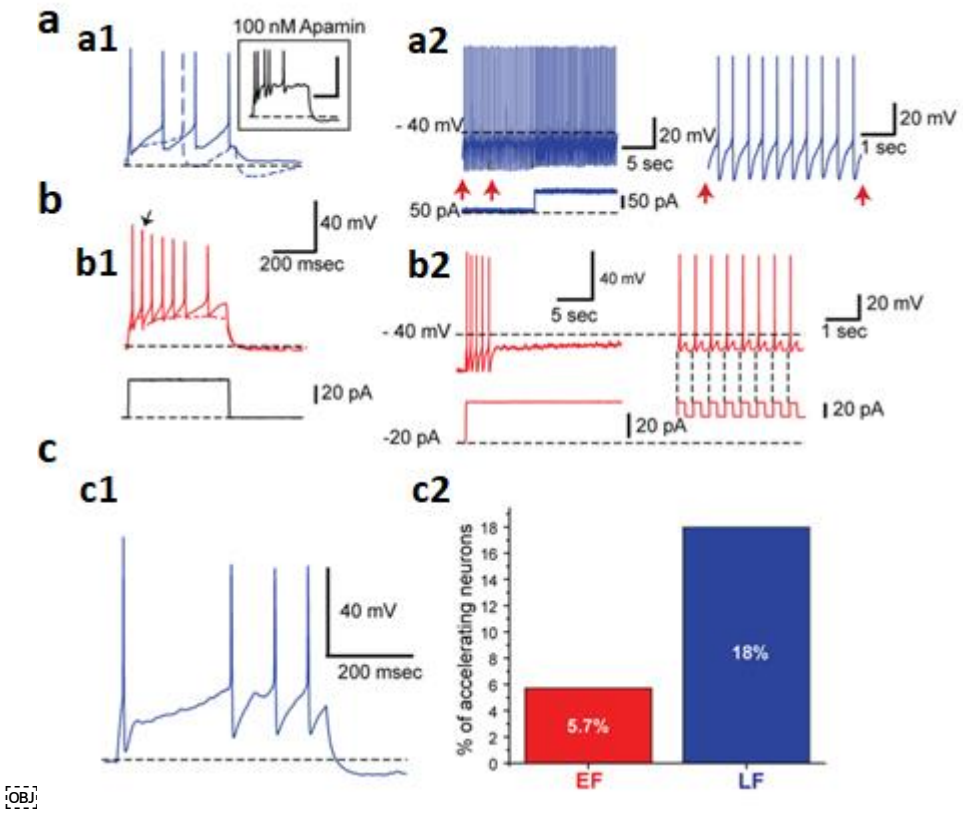

FIGURE 12 | EF neurons show higher spike frequency adaptation than LF neurons. (a) LF neurons. (a1) An LF neuron showing almost no spike frequency adaptation. Apamin

application increased the spike frequency adaptation (Inset). The dashed trace indicates response to a rheobase current injection. (a2) The same neuron fires regularly when prolonged background pulse is given. On the right is an expansion of the time indicated with vertical arrows. (b) EF neurons. (b1 and b2) The same arrangement as in a1 and a2. In b1 the arrow points out to the first action potential elicited with a rheobase current injection. The EF neuron fires transiently in response to a sudden positive shift in the injected current. This is followed by irregular low frequency firing and complete silencing. When hyperpolarizing current pulses are superimposed (b2, right side) on the positive background current, the neuron can sustain firing due to post inhibitory rebounds (see the vertical dashed lines at the ends of negative current pulses shown below). (c) Spike frequency acceleration. (c1) Example of an LF neuron exhibiting spike frequency acceleration. (c2) Percentage of neurons with spike frequency acceleration. (Zaborszky, Unal, et al., 2012)

Further *in vitro* studies measured BFCNs' evoked responses to current injections showing that two functionally different firing patterns exist among them. There were neurons which reacted to current injections with a fast phasic burst package; however, they showed prominent spike frequency adaptation, even reaching the depolarization blockade (Zaborszky, Unal, et al., 2012). They are the so-called early firing cholinergic cells. A second group of cholinergic cells were characterized by their slower activation kinetics and their ability to keep up this slower tonic firing pattern for a long time, hence they were called late firing cholinergic cells. They could be easily distinguished by the difference of their firing delay after current injections. LF neurons responded with an average 343 ms latency compared to the EF cells which could fire their first spike after a mean latency of 107 ms. Furthermore, current injections were followed by significantly higher firing rates and lower afterhyperpolarization (AHP) in EF cells compared to LF cholinergic cells. However, LF cells could output a precise firing pattern during a constantly applied current, while EF cells showed irregular firing patterns or fell silent after a few initial spikes. EF cells could be rescued from this depolarization blockade when steady depolarizing current was superimposed with rhythmic hyperpolarizing pulses, which probably de-inactivated the voltage-gated sodium-currents. LF neurons, unlike EF neurons showing spike frequency adaptation, displayed spike frequency acceleration after an

initial gap. This increase in the firing frequency continued until eventually reaching a regular steady state firing pattern. The more excitable EF cells were further separated from the LF group by their higher expression of low voltage activated calcium currents (LVA). The two groups separated by these markedly different electrokinetic parameters can be differently involved in cortical modulation resulting in distinct functional outcomes. In a speculative attempt to link these *in vitro* results to hypothesized cholinergic functions, the EF group was thought to be involved in phasic changes of cortical ACh release necessary for changes in attention, while the LF group was associated with general arousal by slow, tonic modulation of cortical ACh levels.

2.5.2 In vivo

Ealy studies in rhesus monkeys by DeLong and colleagues (Mitchell et al., 1987; Richardson & DeLong, 1986) focused on cells in the globus pallidus (GP) playing a role in movement control. Accidentally they discovered that a few cells recorded on the ventral border of the GP showed distinct firing characteristics compared to movement-related pallidal cells. Similar to more ventrally recorded substantia innominata cells, these neurons had regular firing patterns with gradual fluctuations. During these operant conditioning experiments some of these cells increased their firing during the delivery of positive reinforcement, whereas some of them decreased their firing. There were no simultaneous EEG recordings in these studies, but it was hypothesized that during the task, the monkey's cortex was in a continuously activated, aroused state. These phasic activity changes of the BF cells were the first results showing that BF cells can play a role in cognitive and other higher processes. Subsequent studies with cortical EEG recordings tested this hypothesis in cats, monkeys, and rats in awake or anesthetized conditions.

After these functional experiments BF cholinergic cells were characterized not only by their projection targets but how they coupled their firing activity to cortical EEG changes. Initially, two categories were described based on the BFCNs' firing rate and the frequency of the ongoing cortical EEG oscillation. The first group consists of BFCNs which exhibit high firing rate during fast cortical EEG activity, whereas the second group consists of BFCNs which has higher firing rate during EEG epochs characterized by slow waves (Détári et al., 1999). Cholinergic neurons are ideal candidates for conveying information

from the brainstem activating system to the cerebral cortex, yet they are intermingled with GABAergic and glutamatergic cortically projecting neurons. *In vivo* rodent experiments applying post hoc immunohistochemical identification of the recorded cells could link more specific functions to BF projection cells with distinct neurotransmitter profiles. Each of these BF projection cell groups differentially modulates the ongoing cortical EEG oscillations and high-level cortical processes, which will be presented in detail in the following section.

Functional studies with advanced measuring techniques discovered that BFCNs are showing increased firing rates during wakefulness and REM sleep, and a decreased activity during non-REM periods (Figures 13-14)(Lee et al., 2005; Xu et al., 2015).

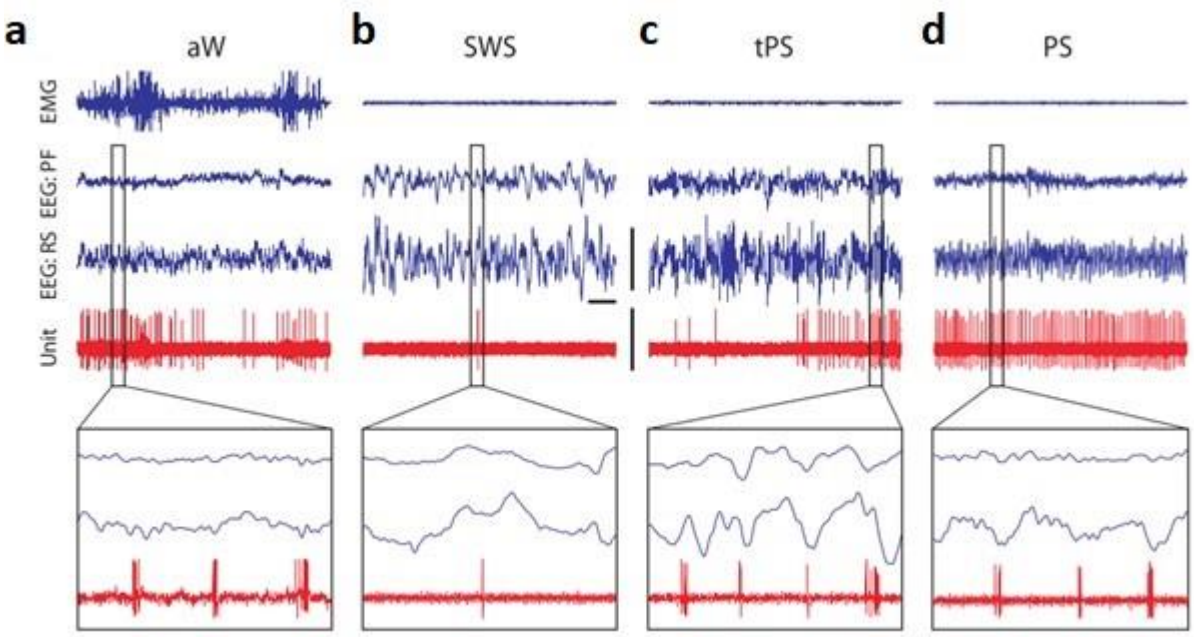

FIGURE 13 | Discharge of a Neurobiotin (Nb) labeled cholinergic neuron. (a–d), Record of Nb+/ChAT+ unit discharge together with EEG and EMG activity during 10 s periods of active wake (aW) (a), slow-wave sleep (SWS) (b), transition to paradoxical sleep (tPS) (c), and paradoxical sleep (PS) (d). The unit fired during aW, virtually ceased firing during SWS, resumed firing during tPS, and discharged maximally during PS. As evident in the expanded 0.5 s traces (bottom), the unit discharged in bursts of spikes with theta EEG activity that was present intermittently during aW, briefly at the end of tPS, and continuously during PS. Calibration: 1 s, 1 mV (EEG, EMG), 1.5 mV (Unit). (Lee et al., 2005)

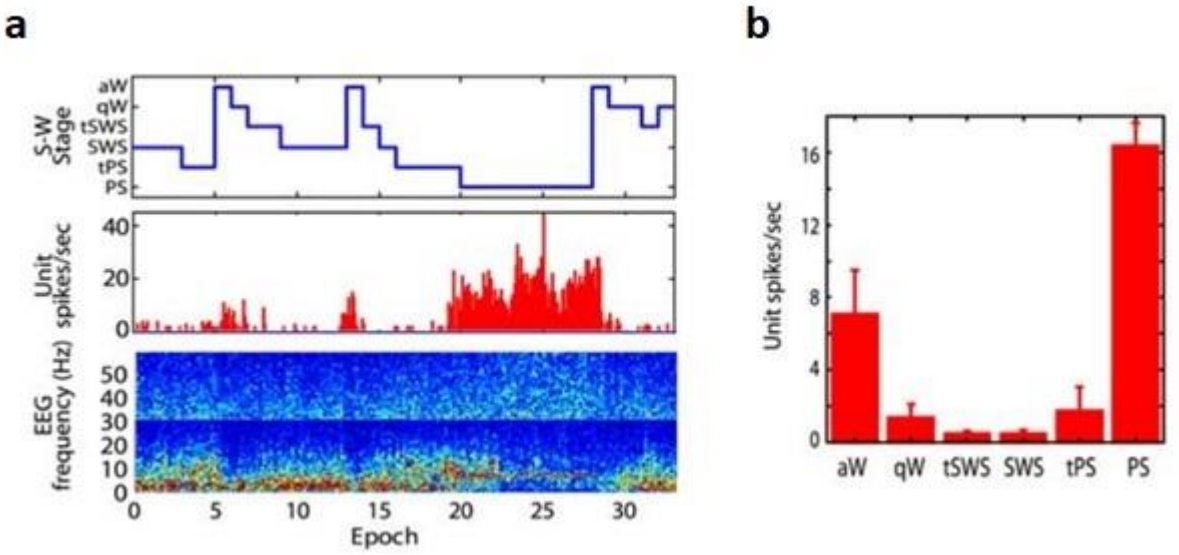

FIGURE 14 | Discharge profile and pattern of an Nb-labeled cholinergic neuron. (a) Across sleep–wake (S-W) states (shown in the sleep–wake hypnogram), the Nb+/ChAT+ cell discharged at variable rates (shown in unit rate histogram) in association with variable EEGs (shown in power spectral array). (b) Its average discharge rate was moderately high in aW, minimal in SWS, and maximal in PS. (Lee et al., 2005)

They can temporally couple to ongoing cortical oscillations; moreover, they are capable of firing burst packages during theta periods. Corticopetal cholinergic cell firing can be elicited by a positive or negative reinforcement signal (Hangya et al., 2015; Harrison et al., 2016). They have the ability to adjust their firing frequency in a wide spectrum and grouping their APs into bursts or keeping them separately as individual APs. This wide variety of firing patters makes them capable of evoking cortical activation (Metherate et al., 1992), promote sensory perception (Pinto et al., 2013), and even code the salience of the stimuli (Gritton et al., 2016). They are fine-tuning the activation of the postsynaptic partners by setting synaptic plasticity during behaviorally relevant events (Verhoog et al., 2016). This is a crucial role of the BFCNs, which create appropriate conditions to learn new things based on reinforcement. Neurodegenerative processes occurring during Alzheimer's Disease are disrupting this cholinergic teaching signal, preventing the ability to

learn and store new memories (McGaughy et al., 2000). In case of memory formation, it is known that sleep is indispensable for memory consolidation. Cholinergic cells are also implicated in the modulation of the sleep-wake states. Cholinergic activation can result in a prolonged alert state, or it can facilitate the transition to wakefulness (Han et al., 2014; Ozen Irmak & de Lecea, 2014). As mentioned earlier, these sleep regulatory effects are not exclusively modulated by the cholinergic cells but by the other two main BF projection cell groups too. Cholinergic firing is increasing cortical theta (Figure 15) (Han et al., 2014; Ozen Irmak & de Lecea, 2014; Xu et al., 2015; Zant et al., 2016), whereas suppressing delta oscillations (Chen et al., 2016; Shi et al., 2015).

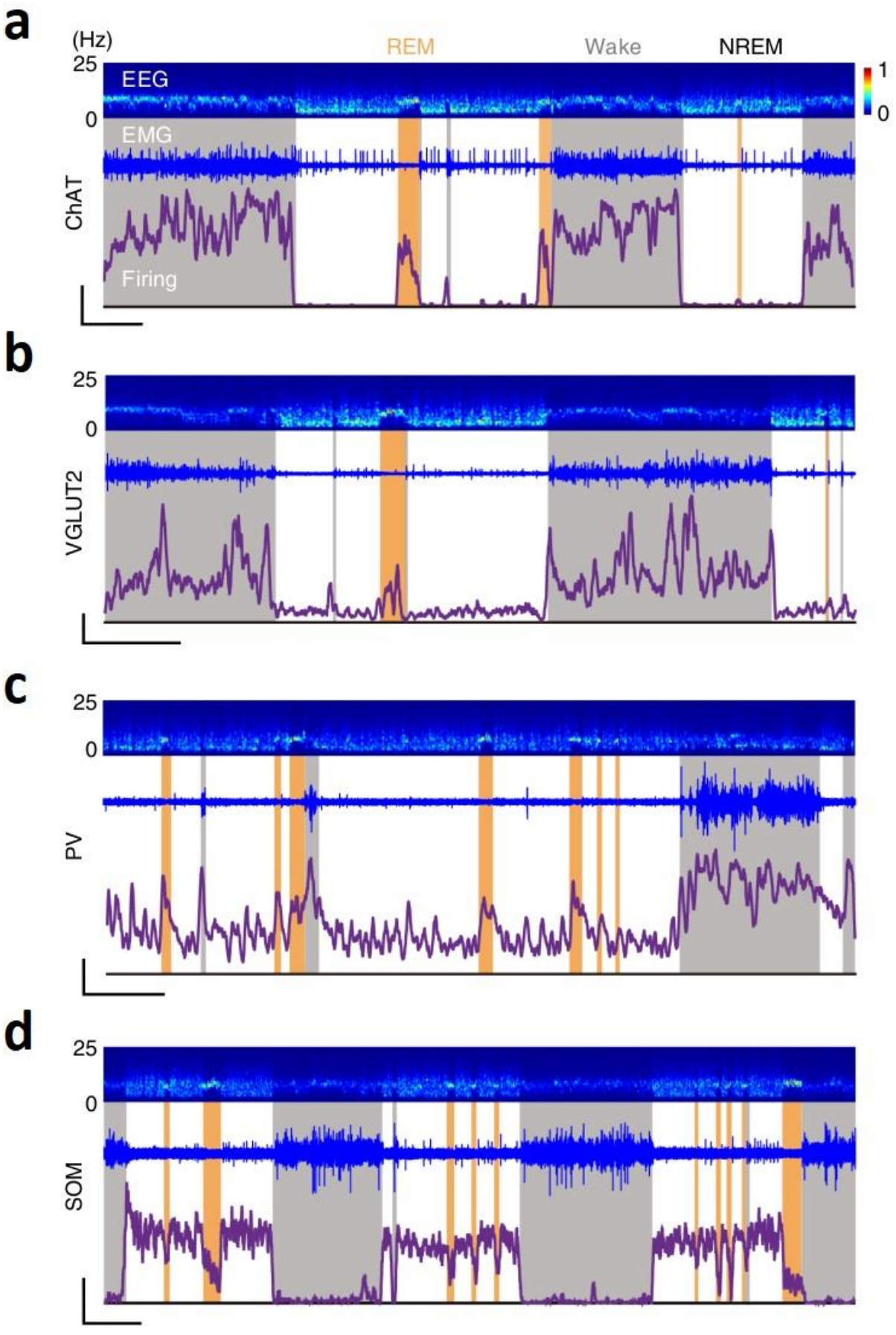
a
(Hz)
REM
Wake
NREM
25
EEG
0
1
0
EMG
ChAT
Firing
b
25
0
VGLUT2
c
25
0
PV
d
25
0
SOM

FIGURE 15 | Firing rates of identified BF cell types across natural sleep-wake cycles. (a) Firing rates of an example ChAT+ neuron over 108 min. Top, EEG power spectrogram (0-25 Hz). Middle, EMG trace. Bottom, firing rate of the ChAT+ neuron. Scale bars represent 3 spikes per s, 500 s. Brain states are color coded: wake (W), gray; REM, orange (R); NREM, white (NR). (b) Data presented as in A for VGLUT2+ neurons (six mice). (c) Data presented as in A and B for PV+ neurons (five mice). (d) Data presented as in A and B for SOM+ neurons (five mice). Scale bars represent 10 spikes per s, 500 s. (Xu et al., 2015)

2.5.3 Attention

Sustained attention is indispensable to detect potentially relevant stimuli from the external world. The capability to react to unexpected events or to select a specific stimulus from the environment that is relevant for the self-preservation of the subject are likely key features of the BF cholinergic population. There are many studies featuring experiments testing sustained attention of the animals, one of them is the reinforcement learning paradigm. By learning the association between the cue (usually a visual or an auditory stimulus) and the feedback (water, food, sucrose, etc.) animals become experts in maintaining their attention until they receive reward. Cholinergic cells are necessary for the formation of this association; moreover, these cells are coding salience regarding the size or the unexpectedness of a reinforcing signal (Hangya et al., 2015). With reduced cholinergic activity, the animals tend to make more errors in the detection and in the collection of the rewards suggesting the role of cholinergic cells in attention (Everitt & Robbins, 1997). Fast activation of the cortex after these events requires cholinergic cells to respond with short latency and high precision. This highlights the importance of phasic activation patterns exhibited by BF cholinergic cells (Hasselmo & Sarter, 2011; Parikh et al., 2007). Functional studies using optogenetic activation of the BF showed evoked cortical LFP desynchronization, which increased the detection performance of the animal. Inhibition of the same population resulted in cortical synchronization and decreased performance levels (Lin et al., 2015; Pinto et al., 2013).

2.5.4 Wakefulness

Wakefulness is a global brain state which determines alertness, detection performance, and reaction times. On top of the homeostatic regulation of brain states, significant sensory, emotional or biologically relevant events can increase the level of wakefulness and they are capable of prolonging these epochs. The association between increased wakefulness and gamma activity is well-known; however, the fact that synchronous BF activation can boost this oscillatory activity was only proved after *in vivo* functional studies appeared. However, this sleep related modulation is not exclusive to cholinergic cells since non-cholinergic BF populations are also directly as well as indirectly modulating arousal states (Buzsaki et al., 1988). The distinct populations employ different activation strategies, which lead to better signal-to-noise ratio in case of the detection of a relevant sensory stimulus. Some of these cells increased their firing rate before relevant stimulus presentation occurred. This pre-stimulus activation makes the cortex more susceptible to detect relevant stimuli. By the increasing general arousal, the system is more tuned towards a state where small inputs around the detection threshold are still registered (Lin et al., 2006; Lin & Nicolelis, 2008). The BF populations showed wake, REM and non-REM sleep specificity, which suggests that BF plays a modulatory role of the circadian rhythm. This slower modulatory process likely involves tonic changes of the cells' firing patterns, setting cortical ACh levels at longer timescales.

2.5.5 Learning, Memory

The BF not only adjusts cortical wakefulness based on the current sensory stimuli, but it is crucial for conveying event-specific information leading to learning new associations and memory formation. The key component during these processes is the hippocampus, which receives input from basal forebrain (mostly the MS) cholinergic neurons. The atrophy of these fibers results in the loss of the ability to learn new associations; however, the ones already learnt are not affected (McGaughy et al., 2000). Selective IgG-saporine-mediated lesions of BFCNs mimicked the neuronal cell death detected during AD. The animals showed reduced performance in learning new information and recalling them. Moreover, they showed a decreased performance in discrimination tasks and in exercises where sustained attention was crucial for performance (Baxter et al., 2013; Baxter & Chiba, 1999; McGaughy et al., 2000). A major component in memory formation is the

emotional information associated with a sensory event. Positive and negative reinforcement is followed by rapid BF cholinergic activation. The fast and precise cholinergic response forwarded to the cortex after a relevant event is crucial in reinforcement learning. Furthermore, these cholinergic responses are scaled by the unexpectedness of the stimulus (Hangya et al., 2015). Additional studies showed that BF stimulation in parallel with sensory inputs created rearrangement in the stimulus specific cortical receptive fields (Baxter et al., 2013; Baxter & Chiba, 1999; Chubykin et al., 2013; Disney et al., 2007; Kilgard & Merzenich, 1998).

2.5.6 Rodent cognition and psychophysics

The aforementioned functions require millisecond precise neuronal firing. To perceive the modulatory processes utilized by the brain to create distinct behaviors it is necessary to perform experiments with awake animals behaving in well-defined tasks. To interpret firing patterns, one needs to record and manipulate the animal's behavior with the same temporal resolution. Although there are a few companies that deliver experiment-ready solutions, the specific behavioral tasks required a higher degree of freedom to plan these experiments. We had to come up with a flexible system which enables us to perform custom behavioral training while maintaining precise temporal control. We performed delay measurements of stimulus and reinforcement delivery to address every temporal element in a behavioral task. We combined microcontroller-based behavior control with a sound delivery system for playing complex acoustic stimuli, fast solenoid valves for precisely timed reinforcement delivery and a custom-built sound attenuated chamber using high-end industrial insulation materials. Together this setup provides a physical environment to train head-fixed animals, enables calibrated sound stimuli and precisely timed fluid and air puff presentation as reinforcers. Combined with electrophysiology and optogenetic manipulations, the millisecond timing accuracy will help interpret temporally precise neural signals and behavioral changes. The development of these methods was crucial towards the discovery of the two distinct cholinergic cell types in the BF.

3. OBJECTIVES

3.0 The following objectives are summarizing the pre-defined goals of my PhD studies regarding the BF cholinergic neuronal experiments. Prior to these measurements a methodological development was initiated to create a suitable infrastructure for the *in vivo* experiments. This work is detailed in the following Methods section (4.1).

3.1 The first goal of my PhD thesis was to determine if separate groups exist among the identified basal forebrain cholinergic cells based on their *in vivo* firing properties. For this goal, we calculated burst index, theta index, and relative refractory period from their autocorrelograms (see methods) to map the cells' capabilities of burst firing, theta phase preference, and the distribution of their spikes based on their inter-spike refractory periods. To test bimodal distribution of their relative refractory periods we applied a model selection approach based on Akaike and Bayesian information criterion.

3.2 The second goal of my thesis was to address the synchronization among the BFCNs and with cortical oscillations. To test their co-activation we calculated cross-correlations between the firing of individual cells to detect synchronous or asynchronous relations among the cells. The impact of BFCNs on cortical oscillations (LFP recordings) was tested with spike-triggered average calculations (STA), with spike-triggered spectrograms (STS), with Morlet wavelets, and with peri-event time histograms (PETH).

3.3 My third objective was to address the effect of BFCN activation on the outcomes of an auditory detection task. Therefore, we tested the influence of BFCNs coupling their firing with cortical activation on the performance of the animal during auditory conditioning. We correlated the distinct BFCN subgroups' firing to the timing and the outcome of a behavioral event. For this purpose, we correlated behavioral outcomes (Hit, False Alarm, Correct Reject, Miss) with STAs measuring the synchrony between the cortex and BFCNs' spikes.

4. METHODS

4.1. Development of the measuring setup

The current section (4.1) summarizes the methodological developments which was described at the Solari et al. paper (Solari et al., 2018). These methodological improvements were not only indispensable for the cholinergic experiments described in this essay, but it provided a flexible, generally applicable, open source solution for behavioral studies with electrophysiological measurements and optogenetics. We provided not only the setup design and the codebase necessary for carrying out experiments but all the control measurements to assess the delays and the limitations of the system. My personal contribution to this work was primarily the delay measurements with Nicola Solari and the building of the sound attenuated enclosure with Katalin Sviatkó.

4.1.1. Sound Attenuated Enclosure

We used sound absorbing foams (Hanno Sealing and Insulation Systems) designed for machine and commercial vehicle industries. In these foams the sound absorbing element is a combination of an open-cell polyurethane foam and a 25 μm surface skin coated with black synthetic fiber (Hanno Protecto product line, Techfoam)(Figure 16).

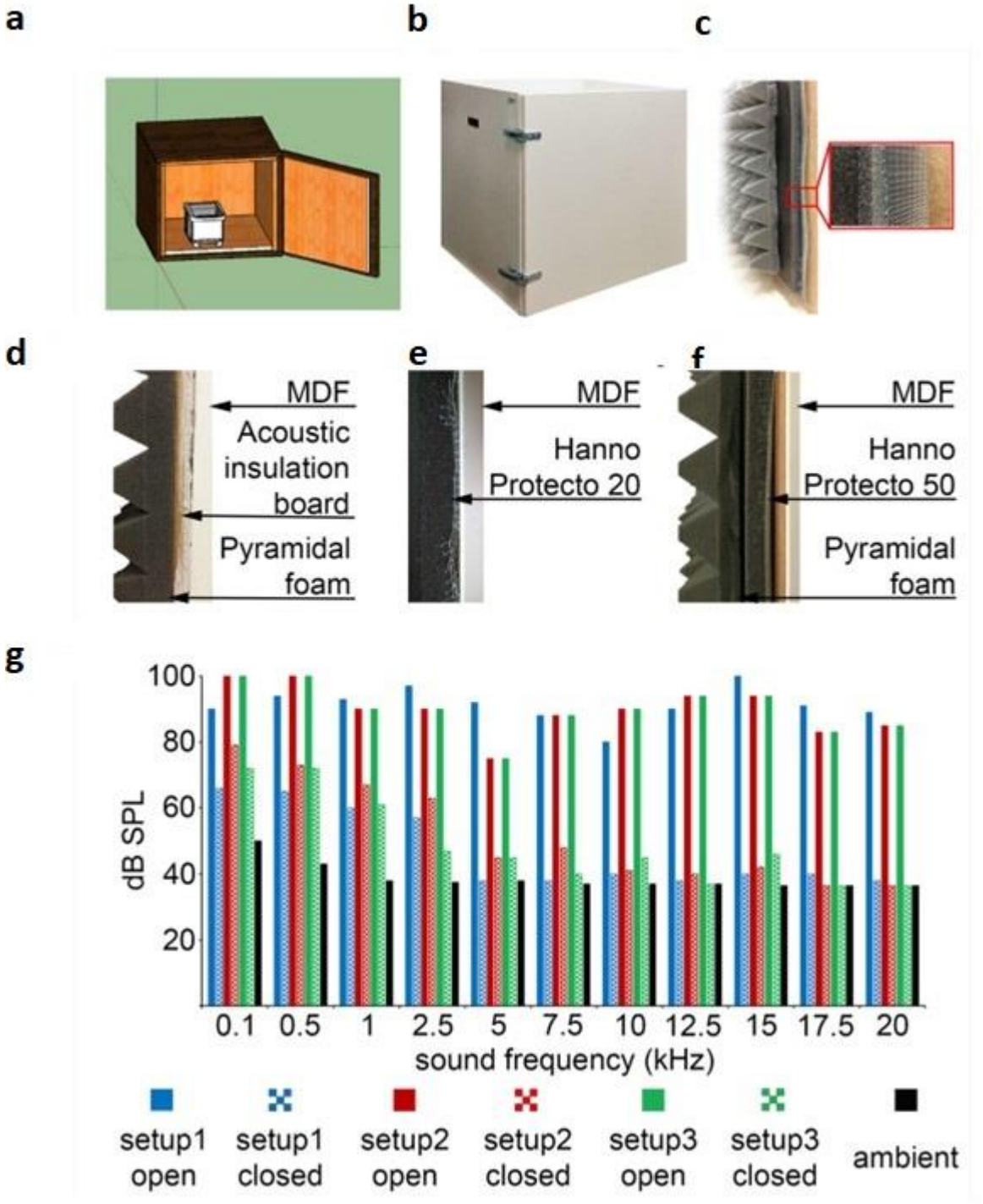

FIGURE 16 | Custom-made sound-attenuated enclosures. (a) A 50-by-50-by-50 cm sound attenuated box designed in the freely available 3D modeling software SketchUp. (b) Picture of the sound attenuated chamber. (c) Cross-section of the box: from left to right, pyramidal foam, sound absorbing foam, stainless steel mesh and medium-density fiberboard (MDF). (d) Configuration #1: sound attenuation by acoustic insulation board

with quartz sand filling and pyramidal foam. (e) Configuration #2: Hanno Protecto 20 foam. (f) Configuration #3: Hanno Protecto 50 foam combined with pyramidal foam. (g) Sound attenuation measurements: pure tones of different pitch were played from speakers outside the enclosure and the dB SPL was measured by a microphone placed inside with the door open or closed. (Solari et al., 2018)

These foams were optimized for airborne sound absorption by converting sound energy to heat as a consequence of friction in the polyurethane cell framework. In our experience, these foams are pliable, easy to cut, handle and mount on vertical surfaces aided by self-adhesive coating. Sound absorbing foams were compared to a 15 mm acoustic insulation board (15 mm Acoustic Board, PhoneStar) used for sound insulating floors, walls and ceilings in the construction industry. The acoustic insulation board consists of a fluted cardboard shell and compacted quartz sand filling. The oscillation of loose sand grains converts acoustic energy into kinetic energy. According to specifications, the acoustic insulation board reduces airborne sound by 36 dB and impact sound by 21 dB. However, the boards are relatively heavy (18 kg/m^2) and there is some sand leakage after cutting to size. We found that while sound absorbing foams and the acoustic insulation board provided comparable levels of sound attenuation, the foam was easier to work with. Although only tested in the 1–20 kHz range, based on our measurements and the industrial specifications we extrapolate that similar sound attenuation levels might be achieved in higher frequency ranges relevant for rodent ultrasonic communication. In addition, we used a 70 mm open-cell pyramid foam borrowed from the music studio and stage equipment industry (215894, Muziker) that absorbs higher frequencies and efficiently reduces resonance and echoes (Figure 20). Design file available at https://github.com/hangyabalazs/Rodent_behavior_setup/sound_attenuated_box.skp. (Solari et al., 2018)

4.1.2. Head-Fixed Setup

The setup was assembled from a combination of Thorlabs and custom parts. A 3D-printed lick port housing a light-emitting diode (LED), an infrared photodiode and corresponding infrared photosensor (https://sanworks.io/shop/viewproduct?productID=1010) was mounted on an xyz stage (DT12XYZ/M, Thorlabs). The mouse was placed on a 3D-printed (https://github.com/hangyabalazs/Rodent_behavior_setup/;

https://github.com/hangyabalazs/Rodent_behavior_setup/blob/master/stage_rect.skp) rectangular, walled stage mounted on a lab jack (S63081, Fisher). Water delivery for reward and facial air puff were controlled by fast solenoid valves (LHDA0531115H, Lee Company). We used the open source Bpod behavioral control system (Sanworks, https://sanworks.io/shop/viewproduct?productID=1014) for real-time behavioral control and monitored the animals through infrared cameras (FL3-U3-13S2M-CS, Point Grey) using Bonsai open source computer vision software (http://www.open-ephys.org/bonsai/)(Lopes et al., 2015) (Figure 17). (Solari et al., 2018)

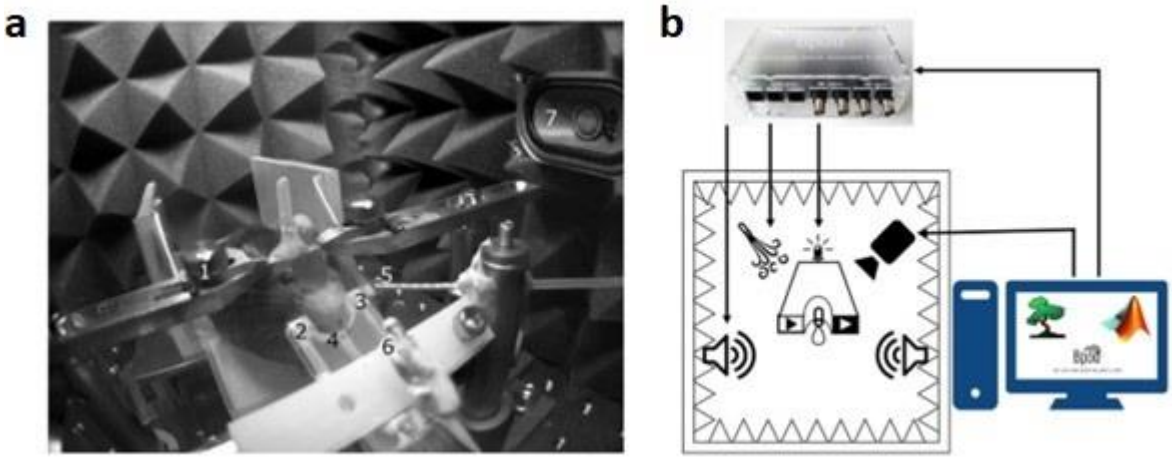

FIGURE 17 | Head-fixed setup. (a) The animal was held by an implanted head bar with a pair of metal holders (1), facing a custom-made lick port hosting an IR emitter and an IR receiver (2, 3) for lick detection and a plastic water spout (4). Air-puff was delivered via a cannula placed near the animal's face (5). Visual and auditory cues were delivered by a central LED (6) and lateral speakers (7). (b) Schematic diagram of the behavior setup. Cue and reinforcement delivery were controlled by Bpod. Motion was monitored with a camera using Bonsai open software. (Solari et al., 2018)

4.1.3. Sound Calibration

Pure tones were generated in Matlab (Mathworks) as sine waves. The tones were uploaded as .wav files to a USB-based microcontroller development system Teensy 3.2 and its audio adaptor board (TEENSY32 and TEENSY3_AUDIO, PJRC) using the Bpod r0.5 behavior control system (Sanworks LLC, www.sanworks.io). The uploaded tracks were played applying Bpod commands controlled by custom-written Matlab code

(https://github.com/hangyabalazs/Rodent_behavior_setup/tree/master/sound_calibration. The Teensy adaptor board's jack output was connected to an Adafruit audio amplifier Stereo 20w Class D (MAX9744, Adafruit) attached to 8 ohm magnetic speakers (668-1447-ND, Digikey) positioned on the left and right side of the behavioral chamber. A calibrated precision electret condenser microphone (EMM-6, Daytonaudio) was connected to a preamplifier digital converter (AudioBox iOne, PreSonus) and placed in the behavioral enclosure to model the position of the animal's head in a head-fixed configuration. The sound pressure level (dB SPL) values registered by the microphone were read using the free version of TrueRTA software, a commercial audio analysis software package (TrueRTA, True Audio), and fed back to the custom developed calibration software (Figure 18 a,b).

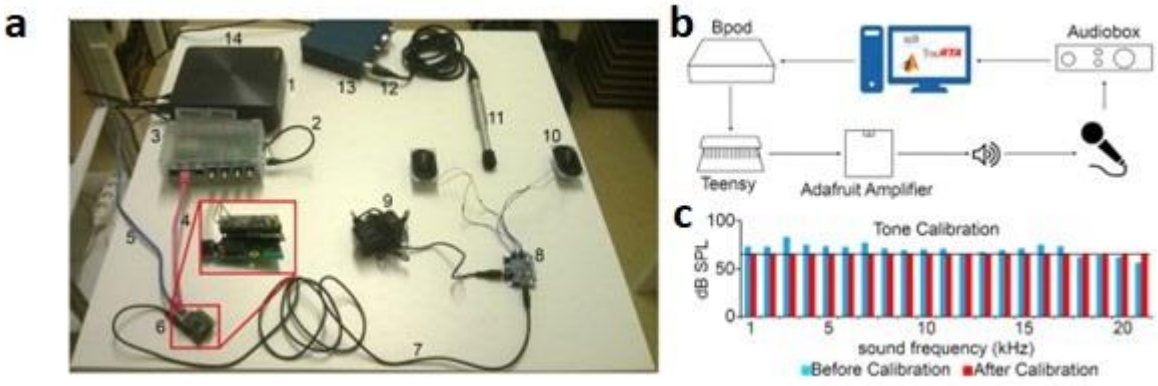

FIGURE 18 | Sound calibration and delivery. (a) Components: computer (1), mini-USB-USB A cable (2), Bpod (3), RJ45 cable (4), miniUSB-USB A cable (5), Audio Adaptor Board for Teensy + Teensy USB Development Board + SD card (6), 3.5 mm stereo jack to jack cable (7), Adafruit Audio Amplifier (8), 12V power supply (9), Digi-key 8 Ohm Magnetic Speakers (10), EMM-6 Electret Measurement Microphone (11), Male–Female three-pin XLR cable (12), AudioBox iOne (13), USB B -USB A cable (14). (b) Schematic of the setup. A sine wave is generated in Matlab and sent to Bpod, which loads it to the Teensy apparatus as a. wav file. When played by the speakers, the sound is detected by the microphone, delivered to the computer and the dB SPL is read using the TrueRTA software. (c) The dB SPL levels at each frequency before (blue) and after (red) the calibration process. Solid black line indicates the calibration target volume (60 dB SPL). (Solari et al., 2018)

4.1.4. Measuring the Delay of Visual Cues

LEDs were used for visual stimuli. These were controlled by the Bpod behavioral control system through an open source printed circuit board ('port interface board', https://sanworks.io/shop/viewproduct?productID=1008). Stimulus intensity can be directly modulated from Bpod on a 1 to 255 scale. All delays were measured by sending command signals from Bpod on two different outputs: the BNC output port and the RJ45 connector for communication with the port interface board. First, we measured the 'internal' delay in addressing these two ports, i.e., the average minimal temporal difference between sending signals on these connectors by Bpod (Figure 19A). The time difference between the two signals was of 0.045 ± 0.001 ms (mean ± SD, n = 180 repeats; see Figure 18A for distribution). This 45 ms delay adds only negligible noise to our delay measurements that are on the millisecond order; therefore, we refer to the two signals as 'concurrent' hereinafter. To determine the temporal delay between the command- and the voltage signal sent directly to the LED, a PC oscilloscope (PicoScope 2204A, Pico Technology) was connected to the LED output wire terminal of the port interface board (Figure 19B). Concurrent with the command signal to the board, a TTL pulse was sent to the oscilloscope from the Bpod BNC output terminal. We determined the distribution of temporal differences between the above two signals using oscilloscope measurements (n = 180 repeats). (Solari et al., 2018)

4.1.5. Measuring the Delay of Sound Delivery

Sounds were delivered using an audio adaptor board (Audio Adaptor Board for Teensy 3, PJRC) and a microcontroller development system (Teensy USB Development Board 3.2, PJRC) connected to Bpod. To measure the time delay between the command signal and the digital sound signal, the PC oscilloscope was connected to the line out pins of the Audio Adaptor Board (Figure 19C). Whenever a tone was triggered, the signal was detected by the oscilloscope. A BNC cable connected the Bpod module BNC output channel directly to the oscilloscope: the commands for triggering a sound and for sending a TTL pulse were elicited simultaneously and the time difference between the board output and the Bpod TTL was measured as the sound delivery delay (n = 180 repeats). (Solari et al., 2018)

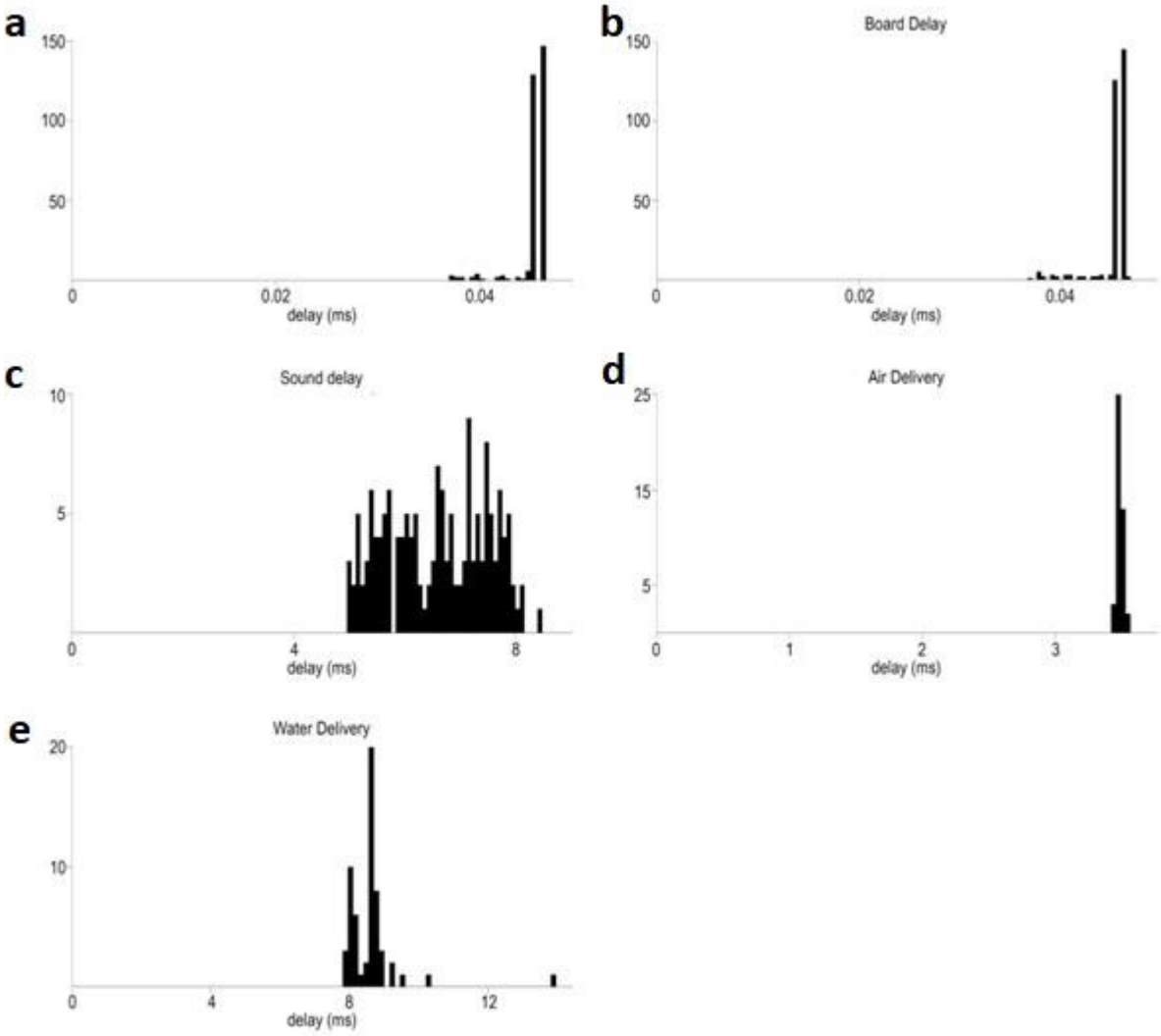

FIGURE 19 | Temporally precise delivery of stimuli and feedback. (a) Distribution of minimal elapsed time between sending signals to the BNC and RJ45 output of Bpod (mean ± SD, 0.045 ± 0.001 ms). (b) Board delay: distribution of delays between the signals from the BNC output port and the LED output wire terminal of the port interface board (mean ± SD, 0.047 ± 0.003 ms) (c) Delay distribution of sound delivery, between the signals from the BNC output port and the Teensy board (mean ± SD, 6.59 ± 0.9 ms). (d) Delay distribution of air puff delivery (mean ± SD, 3.48 ± 0.02 ms). (e) Delay distribution of water delivery (mean ± SD, 8.61 ± 0.81 ms). (Solari et al., 2018)

4.1.6. Measuring the Delay of Reinforcement Delivery

Air was supplied from a pressurized tank adjusted by an air pressure reducing valve. Water was delivered by gravity from a reservoir placed atop the cage. Reinforcer delivery

was controlled by 12V solenoid valves (LHDA0531115H, The Lee Company) connected to the Bpod port interface board. The air and water reservoirs were connected to the valves by Nalgene 180 Clear Plastic PVC Metric Tubing (ID, 2 mm; OD, 4 mm; Thermo Scientific 8001-0204); the same tubing was used between the valves and the lick port. The lick port was equipped with small pieces of polyethylene tubing (ID, 1.14 mm; OD, 1.57 mm; Warner Instruments 64-0755/PE-160) on the output side. The PC oscilloscope was connected to the LED output wire terminal of the port interface board, but the circuit was kept open leaving a small gap (less than 1 mm) between the wire from the port interface board and the one connected to the oscilloscope input. The end of the water delivery tubing was placed directly to the gap. Power output was constantly provided to the LED terminal, so upon water outflow the circuit closed and a voltage change could be detected (Figure 20D).

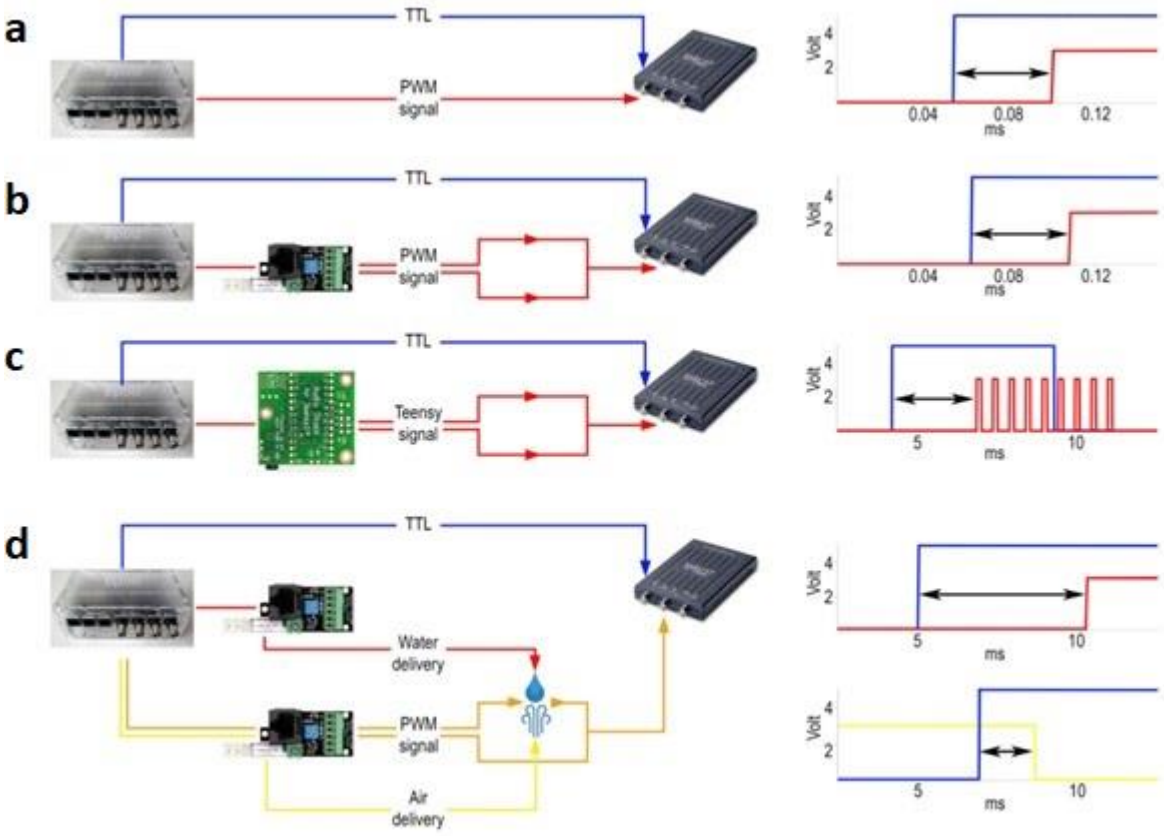

FIGURE 20 | Delay measurements. (a) Internal delay. Left, signals were sent from the BNC output port (blue) and the RJ45 output connector for communication with the port interface board (red) directly to the oscilloscope. Right, example signals detected by the oscilloscope. Arrow, measured delay. (b) Delay of visual cue. Left, signals were sent from

Bpod to the oscilloscope both directly (blue) and via the port interface board (red). Right, example of the signals detected by the oscilloscope. (c) Delay of sound delivery. Left, signals were sent directly (blue) or via the Teensy board (red). The oscilloscope receives the latter signal from the line out pins of the Teensy slave board. Right, example of the signals detected by the oscilloscope. (d) Delay of reinforcement delivery. Left, signals were sent from the BNC output port (blue) directly to the oscilloscope and to two port interface boards. One port was receiving commands to open and close the water valve (red), while the other was receiving similar input for controlling the air valve (yellow) along with a constant PWM signal (orange). The latter was sent to the oscilloscope throughout a circuit that water or air could close or break, respectively, changing the oscilloscope voltage input. Top right, example of the signals detected by the oscilloscope for water delay measurement. Bottom right, example of the signals detected by the oscilloscope for air delay measurement. (Solari et al., 2018)

To measure the water delivery delay, a TTL pulse was sent to the oscilloscope from the Bpod BNC output terminal in parallel with the logic pulse to the port interface board. The delay was the difference between the signal caused by closing the circuit via the LED terminal and the TTL sent from the Bpod BNC output. The delay of air puff delivery was measured similarly but the circuit through the LED terminal of the port interface board was closed by a small drop of water before measurement and the outflow of air disconnected this circuit. Delay was measured as the time difference between the drop of the signal through the port interface board and the rising edge of the TTL from the Bpod BNC output (n = 60 repeats for each reinforcer). (Solari et al., 2018)

4.1.7. Animals and Surgery for the delay measurements

Electrophysiology and optogenetic stimulation data in this study was obtained from three adult male mice (2 ChAT-IRES-Cre, B6129F1 and 1 PV-IRES-Cre, FVB/AntFx) and behavioral data was presented from an adult male ChAT-IRES-Cre mouse. For virus injection and microdrive and headbar implantation, mice were anesthetized with an intraperitoneal injection of ketamine-xylazine (0.166 and 0.006 mg/kg, respectively) after a brief induction with isoflurane. After shaving and disinfecting the scalp (Betadine), the skin was infiltrated with Lidocaine and the eyes were protected with eye ointment (Laboratoires Thea). The mouse was placed in a stereotaxic frame and its skull was leveled along both the lateral and the anteroposterior axes. The skin, connective tissues and

periosteum were removed from the skull and a cranial window was drilled above the ventral pallidum/substantia innominata/horizontal diagonal band region of the basal forebrain (VP/SI/HDB, antero-posterior 0.75 mm, lateral 0.6 mm). Cre-dependent Adeno-associated virus [AAV 2/5. EF1a.Dio.hChR2(H134R)-eYFP.WPRE.hGH] was injected into the VP/SI/HDB at 5 and 4.7 mm depth from skull surface. Two additional holes were drilled above the parietal cortex for ground and reference. After the virus injection a custom-built microdrive (Hangya et al., 2015; Kvitsiani et al., 2013) was implanted into the VP/SI/HDB using a cannula holder on the stereotactic arm. The microdrive and headbar were fixed with dental cement (LangDental acrylic powder and liquid resin). (Solari et al., 2018)

4.1.8. Electrophysiological Measurement and Optogenetic Manipulation

During the surgery, eight tetrode electrodes (PX000004, Sandvik) were implanted into the VP/SI/HDB along with an optic fiber. Data acquisition was conducted with an Open Ephys board, digitized at 30 kHz. Behavioral data was collected using Bpod and synchronized with the neural data using Open Ephys sync board. For optogenetic stimulation of Channelrhodopsin-expressing neurons in the VP/SI/HDB, we used 1 ms blue laser pulses (Sanctity Laser, SSL – 473 – 0100 – 10TM – D – LED) at 20 Hz frequency with a 2 s on 3 s off duty cycle triggered by PulsePal (1102, Sanworks). (Solari et al., 2018)

4.2. Experimental methods

4.2.1. Animals for Cholinergic studies.

Adult (age >2months) ChAT-Cre (n=15, 14/15 male (Higley et al., 2011)), ChAT-ChR2 (n=3, 3/3 male) and PV-Cre (n=4, 4/4 male(Zhao et al., 2011)) mice were used for behavioral recording experiments under the protocol approved by the Cold Spring Harbor Laboratory Institutional Animal Care and Use Committee in accordance with the National Institutes of Health regulations. ChAT-Cre mice (male, n=3, age >2months) were used for *in vivo* and ChAT-Cre mice (n=12, 7/12 males, P50-150) were used for *in vitro* recordings according to the regulations of the European Community's Council Directive of 24 November 1986 (86/609/EEC); experimental procedures were reviewed and approved by the Animal Welfare Committee of the Institute of Experimental Medicine, Budapest

and the Committee for Scientific Ethics of Animal Research of the National Food Chain Safety Office. See also Nature Research Reporting Summary.

4.2.2. In vivo electrophysiology and optogenetic tagging experiments.

Surgical procedures, viral injection, microdrive construction and implantation, recording, optogenetic tagging and histology have been described previously (Hangya et al., 2015). Mice were trained on one of two versions of an auditory head-fixed detection task. In the operant version, mice had to detect pure tones in a go/no-go paradigm as described in (Hangya et al., 2015). In the Pavlovian version, mice responded to reward- and punishment-predicting pure tones with anticipatory licking. In this version, air-puff punishment was delivered in a fixed proportion of trials in each trial type, irrespective of the anticipatory lick response of mice (Solari et al., 2018).

4.2.3. Analysis of *in vivo* experiments.

Spike sorting was carried out using MClust (A.D. Redish). Only neurons with isolation distance >20 and L-ratio (a cluster quality measure based on Mahalanobis distance; see ref. (Schmitzer-Torbert et al., 2005)) <0.15 were included. Optogenetic tagging was verified using the SALT (detailed in (Hangya et al., 2015)). Putative cholinergic neurons were selected based on hierarchical cluster analysis of punishment response properties (response magnitude, PETH correlation with identified cholinergic neurons and PETH similarity scores with templates derived from groups of all unidentified cells and unidentified cells suppressed after punishment). These analyses have been described in detail previously (Hangya et al., 2015). ACGs were calculated at 0.5ms resolution. ACG graphs were smoothed by a 5-point (2.5ms) moving average for plotting. When plotting all or average ACGs per group, individual ACGs were mean normalized and sorted using burst index (Burst-BFCNs) or refractory period (Reg-BFCNs). The burst index was calculated inspired by the algorithm introduced by the Buzsaki lab (Royer et al., 2012): the difference between the maximum ACG for lags of 0–10ms and the mean ACG for lags of 180–200ms was normalized by the larger of the two numbers, yielding an index between −1 and 1. The selectivity index for bursts and single spikes was calculated as the burst or single spike number in 20–50 ms relative to 100–250 ms post-event windows. It was not

calculated for neurons that did not have bursts/single spikes in these windows due to an insufficient quantity of data. The theta index was calculated as the normalized difference between the mean ACG for a ±25-ms window around the peak between lags of 100 and 200ms (corresponding to a 5- to 10-Hz theta band) and the mean ACG for lags of 225–275 and 65–85ms. Normalization was performed similar to that for the burst index. The relative refractory period was defined as a low spiking probability after an AP had been fired, and was calculated by estimating the central gap in the ACG (Royer et al., 2012). To estimate the range of delays after an AP at which spiking happened with lower probability, we calculated the maximal bin count of the ACG smoothed by a 10-ms moving average, and took the delay value at which the smoothed ACG first reached half of this value (width at half-height). We note that this definition captures low spike probability and not biophysical partial repolarization, as also used by Royer et al. (Royer et al., 2012). As this algorithm allows APs in the 'refractory period', we used the term 'relative refractory period' (lower probability of firing). Nevertheless, this property captured the distinction between regular rhythmic and bursting neurons well (see Figure 21). Cross-correlations (CCGs) were calculated at 1-ms resolution. Segments (±100ms) around reinforcement events were excluded to avoid trivial event-driven correlations; 0-ms lag (middle) values were excluded to avoid potential contamination from spike sorting artifacts. When plotting all or average CCGs, individual CCGs were Z-scored and smoothed by a 15-point moving average. Co-activation was considered significant if raw CCGs crossed the 95% confidence limits, calculated by the shift predictor method, for at least two consecutive bins. PETHs were averaged from binned spike rasters and smoothed by a moving average. For comparisons of bursts and single spikes, PETHs were divided by (1 + average baseline PETH). All PETHs were baseline subtracted for visual comparison. LFP recordings were carried out in the primary auditory cortex (A1) simultaneously with the tetrode recordings using platinum–iridium stereotrodes. LFP traces were Z-scored and averaged in windows centered on the APs of interest for STAs. Positive-deflecting STA traces were inverted before averaging for coherence because the depth of recording was not precisely controlled; therefore, we could not draw conclusions from absolute delta phases. Wavelet calculations were performed using the Morlet wavelet and STSs were calculated from the wavelet power and phase spectra. Individual frequencies were

normalized by their averages to give equal weight to spectral components and visualized on a decibel scale. Note that this normalization method may introduce negative STS values.

4.2.4. In vitro recordings.

Mice were decapitated under deep isoflurane anesthesia. The brain was removed and placed into an ice-cold cutting solution, which had been bubbled with 95% O_2–5% CO_2 (carbogen gas) for at least 30min before use. The cutting solution contained the following (in mM): 205 sucrose, 2.5 KCl, 26 $NaHCO_3$, 0.5 $CaCl_2$, 5 $MgCl_2$, 1.25 NaH_2PO_4, 10 glucose. Coronal slices of 300-µm thickness were cut using a Vibratome (Leica VT1000S). After acute slice preparation, slices were placed into an interface-type holding chamber for recovery. This chamber contained standard ACSF solution at 35 °C which gradually cooled down to room temperature. The ACSF solution contained the following (in mM): 126 NaCl, 2.5 KCl, 26 $NaHCO_3$, 2 $CaCl_2$, 2 $MgCl_2$, 1.25 NaH_2PO_4, 10 glucose, saturated with 95% O_2–5% CO_2. Recordings were performed under visual guidance using differential interference contrast microscopy (Nikon FN-1) and a 40× water-dipping objective. Cholinergic neurons expressing ChR2-mCherry were visualized with the aid of a mercury arc lamp and detected with a CCD camera (Hamamatsu Photonics). Patch pipettes were pulled from borosilicate capillaries (with inner filament, thin-walled, outer diameter (OD) 1.5) with a PC-10 puller (Narishige). The composition of the intracellular pipette solution was as follows (in mM): 110 potassium gluconate, 4 NaCl, 20 4-(2-hydroxyethyl)- 1-piperazine-ethanesulfonic acid, 0.1 (ethylenebis(oxonitrilo))tetra-acetate, 10 phosphocreatine, 2 ATP, 0.3 GTP, 3mg ml^{-1} of biocytin adjusted to pH 7.3–7.35 using KOH (285–295mosmol l^{-1}). Recordings were performed with a Multiclamp 700B amplifier (Molecular Devices), low-pass filtered at 3 kHz, digitized at 10–20 kHz with NI USB-6353, X Series DAQ, and recorded with an in-house data acquisition and stimulus software (courtesy of Attila Gulyás, Institute of Experimental Medicine, Budapest, Hungary). For *in vitro* light illumination, we used a blue laser diode (447nm, Roithner LaserTechnik GmbH) attached to a single optic fiber (Thorlabs) positioned above the slice.

4.2.5. Analysis of *in vitro* experiments.

All *in vitro* data were processed and analyzed off-line using self-developed programs written in Python v.2.7.0 and Delphi v.6.0 by A.I.G. and D.S. Spike delay was defined as the time between the start of the 1-s-long positive current injection step and the peak time of the first following AP. Burst frequency was calculated from the following three ISIs. The membrane potential in Figure 25f,g was calculated as the average membrane potential of a 1-s-long period preceding the positive current injection step. ACGs for each cell were calculated on spikes evoked by step protocols (see Figure 25b) and were smoothed by a 5-ms moving average. In the case of Figure 25n, step protocols form each cell were classified into three groups (see Figure 25n, inset). Burst indices were calculated in a similar way to the *in vivo* recordings: the difference between the maximum ACG for lags of 0–15ms and the mean ACG for lags of 50–300ms was normalized by the larger of the two numbers, yielding an index between −1 and 1. The average burst index as a function of AP distance from bregma was calculated as a three-section moving average (pink line in Figure 35e).

4.2.6. Statistics.

No statistical methods were used to predetermine sample sizes, but our sample sizes are similar to those reported in previous publications (Guo et al., 2019; Hangya et al., 2015). The present study did not involve separate experimental groups; therefore, randomization and blinding across groups were not relevant. Behavioral trials were presented in randomized order. Data analysis was automated, irrespective of neuron identity. Putative single neurons with isolation distance >20 and L-ratio <0.15 were included in the *in vivo* analysis. These criteria were pre-established based on recommendations and standards of the field (Schmitzer-Torbert et al., 2005). In addition, the selectivity index could not be calculated for neurons that did not show any bursts or single spikes in the analyzed data window. If the number of recorded spikes exceeded 50,000, ACGs, CCGs, STAs and STS analyses were restricted to 50,000 spikes to avoid out-of-memory errors. We used non-parametric tests (Figures 1 and 2, and also Figure S4 in ref. 17), therefore these neurons were pooled and resulted in a dataset of 78 BFCNs. Previous *in vitro* studies suggested that cholinergic neurons may exhibit heterogeneous firing patterns, however, this has not been tested *in vivo* and the potential diversity of BFCNs is unexplored in awake animals. We noticed that some cholinergic neurons were capable of firing bursts of action

potentials *in vivo* with short, <10ms interspike intervals (ISIs), whereas others exhibited a markedly different pattern of regular rhythmic firing dominated by long ISIs (Figure 21b–d). To quantify this, we defined relative refractory periods of basal forebrain cholinergic neurons for comparing central tendencies of two distributions, because normal distribution of the underlying data could not be determined unequivocally. For unpaired samples, the two-sided Mann–Whitney U-test was applied. For paired samples, we used the two-sided Wilcoxon's signed-rank test. Correlations were calculated using Pearson's correlation and tested using the one-sided F-test. Distributions over categorical variables were compared using the $\chi 2$ test for homogeneity. We tested the significance of optogenetic tagging using the SALT, which is a bootstrap test based on the Jensen– Shannon divergence (Dominik M. Endres & Johannes E. Schindelin, 2003) of spike time distributions with or without stimulation. A full description of the test is provided in ref. (Kvitsiani et al., 2013).

5. RESULTS

5.1. Distinct firing patterns of cholinergic neurons *in vivo.*

We performed extracellular tetrode recordings from the BF of awake mice (Figure 21a; see also Methods). Cholinergic neurons were identified using an optogenetic tagging approach. Neurons responding with statistically significant short latency firing (stimulus-associated spike latency test (SALT): $P<0.01$) to blue laser light in transgenic mice expressing the photosensitive channelrhodopsin (ChAT-Cre infected by AAV-DIO-EF1a-ChETA, n = 15 or by AAV-DIO-EF1a-hChR2(H134R), n = 3; or ChAT-ChR2, n = 3 mice) were considered to be optogenetically identified cholinergic neurons (n = 56). In addition, neurons that fell in the same cluster by hierarchical clustering of response properties were considered to be putative cholinergic neurons (n = 22; the algorithm was detailed in ref. (Hangya et al., 2015)). We detected no systematic differences between optogenetically identified and putative cholinergic neurons (Figures 22 and 23, and also Figure S4 in ref. (Hangya et al., 2015)), therefore these neurons were pooled and resulted in a dataset of 78 BFCNs. Previous *in vitro* studies suggested that cholinergic neurons may exhibit heterogeneous firing patterns (Khateb et al., 1992; Simon et al., 2006; Zaborszky, Unal, et al., 2012) however, this has not been tested *in vivo* and the potential diversity of BFCNs is unexplored in awake animals. We noticed that some cholinergic neurons were capable of firing bursts of action potentials *in vivo* with short, <10ms interspike intervals (ISIs), whereas others exhibited a markedly different pattern of regular rhythmic firing dominated by long ISIs (Figure 21b–d). To quantify this, we defined relative refractory periods of basal forebrain cholinergic neurons based on their auto-correlograms, characterized by low probability of firing (inspired by (Royer et al., 2012); see Methods). The distribution of the relative refractory period duration covered a broad range (1–137 ms) and showed a bimodal distribution with two distinct, approximately log-normal modes (Buzsáki & Mizuseki, 2014) (Figure 21e–h). This was confirmed by a model selection approach based on Akaike and Bayesian information criteria (Figure 23c). This demonstrated the existence of a separate, short-refractory, burst-firing and long-refractory, regular-firing group of cholinergic neurons. Therefore, we called these cholinergic neurons Burst-BFCNs and Reg-BFCNs, respectively. We further analyzed the burst-firing properties of Burst-BFCNs and found considerable heterogeneity based on their spike autocorrelations (ACGs). Many short-refractory neurons exhibited strongly bursting patterns

with classic ‘burst shoulders’ (Royer et al., 2012) in their auto-correlograms (Burst-BFCN-SBs, strongly bursting), whereas others showed irregular patterns of ISIs, resembling a Poisson process (Burst-BFCN-PLs, ‘Poisson like’; Figure 21f). Of note, the lack of a central peak in the autocorrelation did not preclude the occasional presence of bursts (Figure 21c). These firing patterns were, on average, distinct (Figure 21h); however, this separation was less evident than the bimodal relative refractory distribution, and a few neurons could have been categorized in either group (Figure 21i). We note that the long-refractory neurons exhibited strong rhythmicity in the theta frequency band (5–10 Hz; Figure 21j,k). The strength of rhythmic firing, quantified based on autocorrelation peaks in the theta band (theta index, see Methods), correlated with the length of the relative refractory period (Pearson’s correlation, $P = 0.0007$, one-tailed F-test). Next, we analyzed the firing patterns of a large dataset of untagged BF neurons. Burst firing has been shown for GABAergic BF neurons before (Lee et al., 2005; Lin & Nicolelis, 2008) in agreement with this, we found that many (SB: n=559, PL: 692) noncholinergic cells were capable of burst firing (Figure 24a,b). Surprisingly, however, only a small proportion of untagged BF neurons showed regular rhythmic firing with a long refractory period (n = 17; Figure 24c–g). These neurons were similar to those that we had characterized as cholinergic (n = 12; Figure 21h). This suggests that at least about 40% of regular rhythmic BF neurons are cholinergic, and may provide the means to identify this subgroup of putative cholinergic neurons based on firing rate and regular rhythmic activity pattern, when their response to air-puffs is not available (Figure 24h).

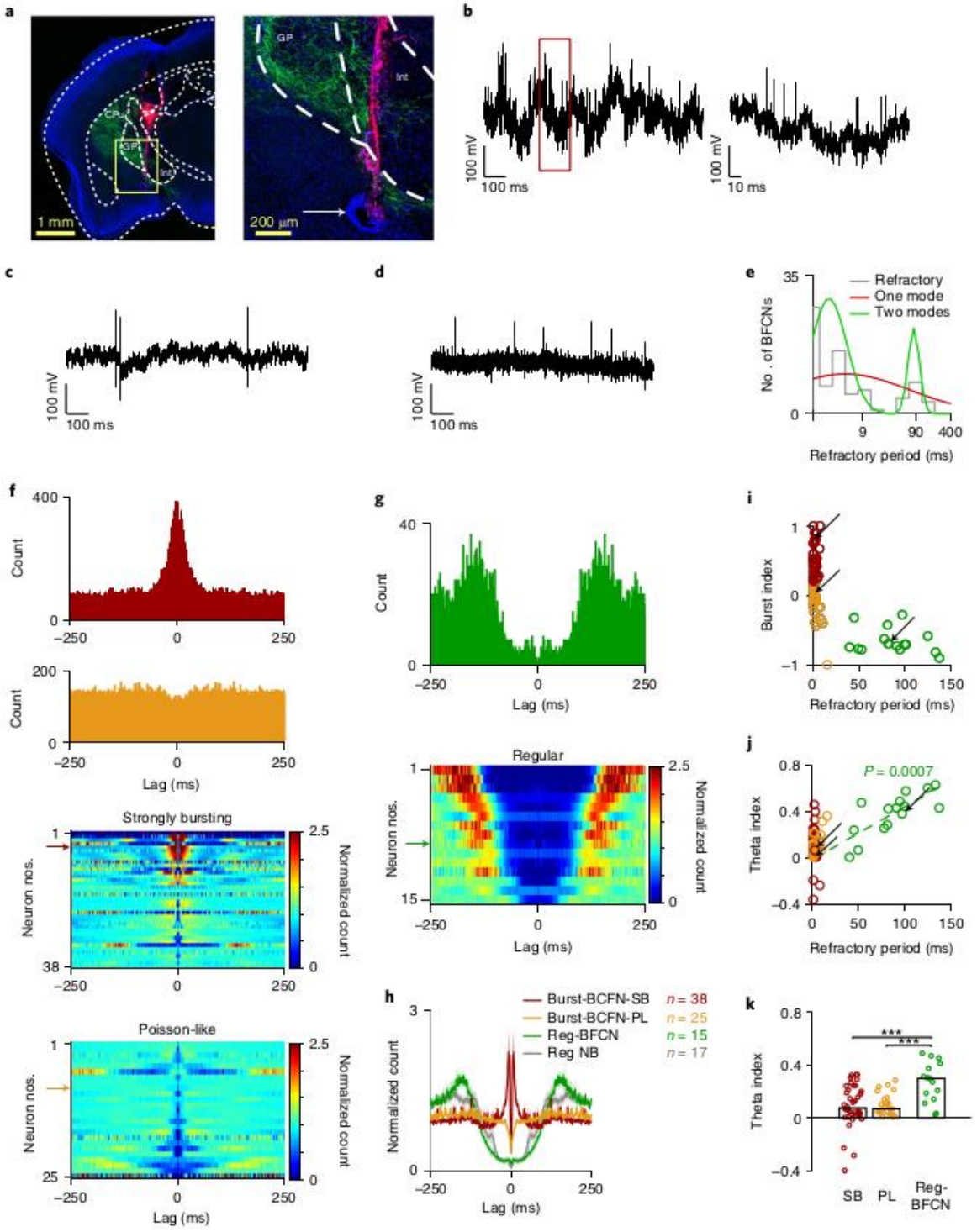

FIGURE 21 | *In vivo* recordings revealed two types of central cholinergic neurons, Burst-BFCNs and Reg-BFCNs. (a) Coronal section with the tetrode tracks (red, DiI) and the electrolytic lesion (arrow) (green, ChAT-ChR2-eYFP; blue, nuclear staining (DAPI)). (b) Left: example of a raw trace of a Burst-BFCN; right: burst enlarged. (c) Example short ISI of a Burst-BFCN-PL. (d) Example raw trace of a Reg-BFCN. (e) Distribution of

relative refractory periods (n = 78 BFCNs). The log(refractory) values (gray bars) were fitted with one (red) or two (green) modes. (f) Top: example ACGs of a Burst-BFCN-SB (red) and a Burst-BFCN-PL (orange); bottom: all neurons as individual rows. (g) Top: example ACG of a Reg-BFCN (green); bottom: all neurons as individual rows. (h) Average ACGs. Unidentified regular firing neurons (Reg NB, gray) are few and resemble Reg-BFCN (green) based on their auto-correlograms (solid lines, mean; shading, s.e.m.). (i) Scatter plot showing the burst index and relative refractory period. (j) Pearson's correlation between relative refractory period and theta index (P = 0.0007 for n = 15 Reg-BFCNs, one-sided F-test, F(1,13) = 19.67). (k) Median theta index. ***P < 0.001; Burst-BFCN-SBs versus Reg-BFCNs, P = 1.91×10^{-5}; Burst-BFCN-PLs versus Reg-BFCNs, P = 5.1×10^{-5}; Burst-BFCN-SBs versus Burst-BFCN-PLs, P = 0.63; two-sided Mann–Whitney U-test; n = 38 Burst-BFCN-SBs (red), n = 25 Burst-BFCN-PLs (orange), n = 15 Reg-BFCNs (green). Arrows in (f–j) indicate example cells shown in (f) and (g).

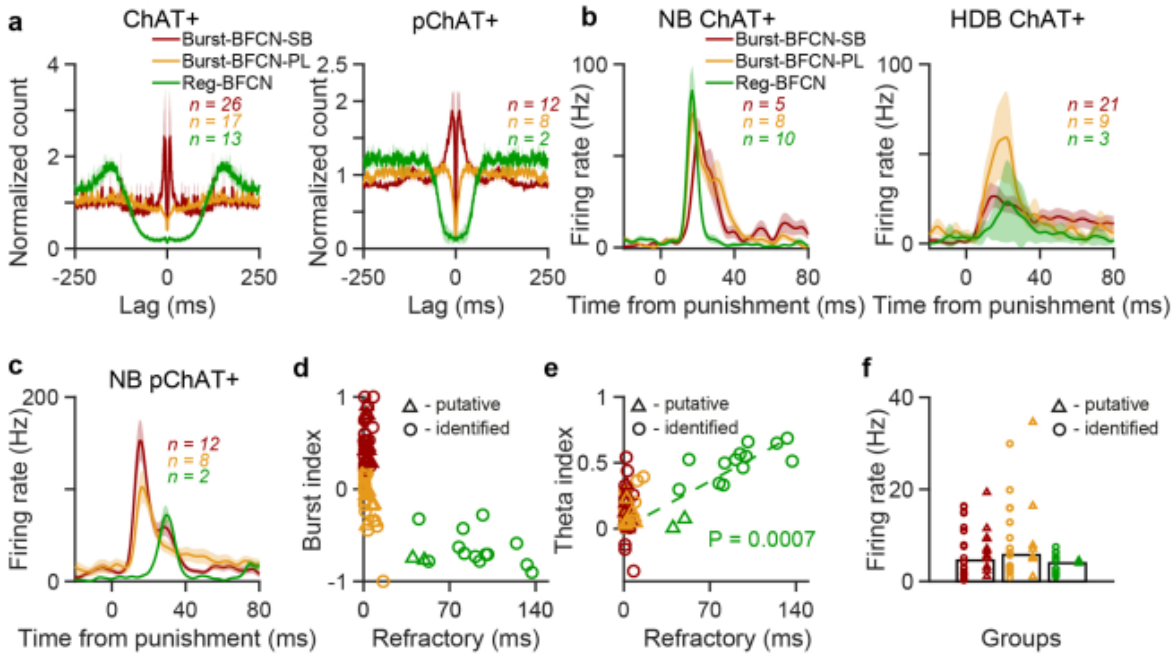

FIGURE 22 | Optogenetically identified and putative cholinergic neurons behave similarly. (a) Average auto-correlogram of Burst-BFCN-SBs (red), Burst-BFCN-PLs (orange) and Reg-BFCNs (green). Left, optogenetically identified; right, putative. While nominal normalized magnitudes may differ due to varying noise levels and moderate sample sizes, the auto-correlation curves are qualitatively similar. Solid lines, mean; shading, s.e.m. (b) Response to punishment of identified cholinergic neurons (left, identified

NB; right, identified HDB). Solid lines, mean; shading, s.e.m. (c) Response to punishment of putative cholinergic neurons. HDB neurons showed somewhat slower and more variable responses. Note also the longer response latencies of two regular pChAT neurons. Solid lines, mean; shading, s.e.m. (d) Burst index vs. relative refractory period for identified (circle; red, n = 26 Burst-BFCN-SBs; orange, n = 17 Burst-BFCN-PLs; green, n = 13 Reg-BFCNs) and putative (triangle; red, n = 12 Burst-BFCN-SBs; orange, n = 8 Burst-BFCN-PLs; green, n = 2 Reg-BFCNs) cholinergic neurons. (e) Pearson's correlation between theta index and relative refractory period. No systematic difference between identified (circle; red, n = 26 Burst-BFCN-SBs; orange, n = 17 Burst-BFCN-PLs; green, n = 13 Reg-BFCNs) and putative (triangle; red, n = 12 Burst-BFCN-SBs; orange, n = 8 Burst-BFCN-PLs; green, n = 2 Reg- BFCNs) cholinergic neurons were detected ($p = 0.0007$ for n = 15 Reg-BFCNs, one-sided F-test, $F(1,13) = 19.67$). (f) Baseline firing rate did not show systematic differences between identified (circle; red, n = 26 Burst-BFCN-SBs; orange, n = 17 Burst-BFCN-PLs; green, n = 13 Reg-BFCNs) and putative (triangle; red, n = 12 Burst-BFCN-SBs; orange, n = 8 Burst-BFCN-PLs; green, n = 2 Reg-BFCNs) cholinergic neurons.

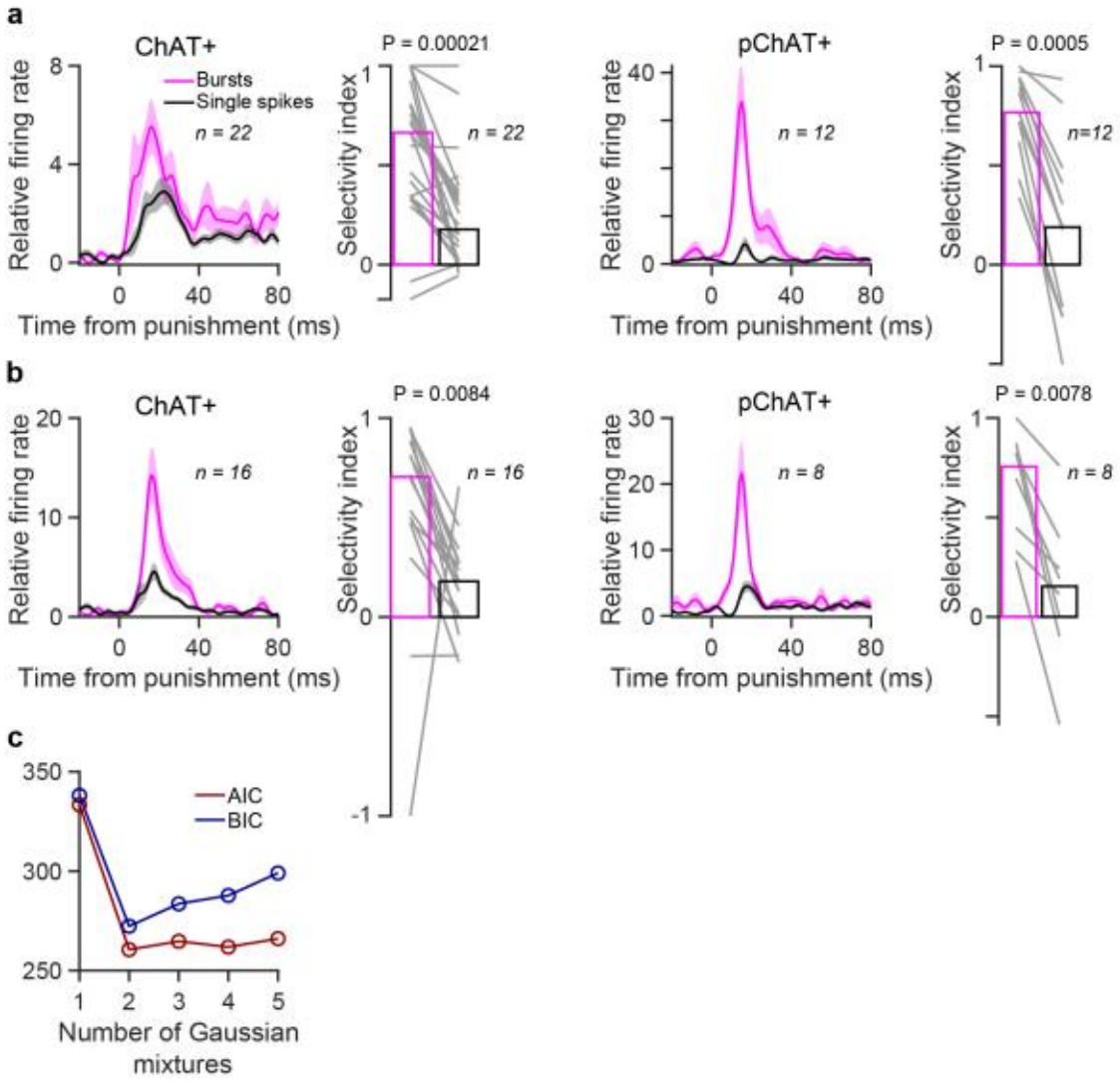

FIGURE 23 | Burst selectivity and model fitting. (a) Identified (left, p = 0.00021, two-sided Wilcoxon signed rank test) and putative (right, p = 0.0005, two-sided Wilcoxon signed rank test) Burst-BFCN-SBs exhibited similar burst selectivity. Solid lines, mean; shading, s.e.m.; bars, median. (b) The same for Burst-BFCN-PLs (left, identified, p = 0.0084, two-sided Wilcoxon signed rank test; right, putative, p = 0.0078, two-sided Wilcoxon signed rank test). Solid lines, mean; shading, s.e.m.; bars, median. (c) A mixture of Gaussian distributions from 1 to 5 modes were fitted on the logarithm of refractory period distribution. Refractory period of BFCNs (n = 78) showed bimodal distribution, confirmed by AIC (red) and BIC (blue) model selection measures (lowest value corresponds to best fit model).

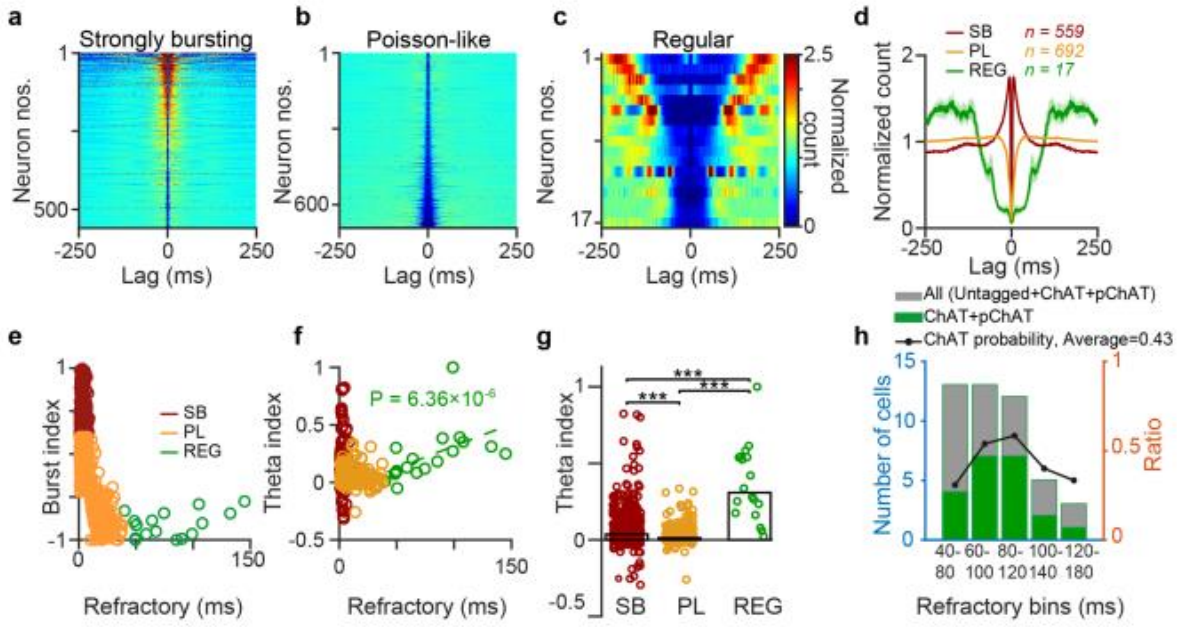

FIGURE 24 | Many regular rhythmic basal forebrain neurons are cholinergic. (a-c) Auto-correlations of untagged bursting (a), Poisson-like (b), and regular rhythmic (c) NB neurons. (d) Average auto-correlations (red, n = 559 untagged strongly bursting; orange, n = 692 Poisson-like; green, n = 17 regular rhythmic basal forebrain neurons). Solid lines, mean; shading, s.e.m. (e) Scatter plot showing burst index and refractory period of the same neurons. (f) Pearson's correlation between refractory period and theta index ($p = 6.36 \times 10^{-6}$ for n = 17 regular rhythmic basal forebrain neurons (green), one-sided F-test, $F(1,15) = 45.77$; red, n = 559 untagged strongly bursting; orange, n = 692 Poisson-like basal forebrain neurons). (g) Median theta index (red, n = 559 untagged strongly bursting; orange, n = 692 Poisson-like; green, n = 17 regular rhythmic basal forebrain neurons; ***, $p < 0.001$; strongly bursting vs. Poisson-like, $p = 1.99 \times 10^{-24}$; strongly bursting vs. regular rhythmic, $p = 4.41 \times 10^{-8}$; Poisson-like vs. regular rhythmic, 6.04×10^{-11}; two-sided Mann-Whitney U-test). Bars, median. (h) Predictive value of regular rhythmic firing pattern for cholinergic identity as a function of relative refractory period. Black line and right y-axis correspond to the ratio of (identified or putative) cholinergic neurons to all neurons in the bin.

5.2. In vitro recordings confirmed two types of cholinergic neurons.

We wondered whether the different cholinergic firing patterns observed in our *in vivo* recordings reflect intrinsic properties produced by distinct cell types. Alternatively,

distinct firing patterns may be determined by the current state of the network or variations in the input strength of individual cells. To answer this, we turned to *in vitro* preparations, where the membrane potential of the neuron and the strength of activation are precisely controlled and monitored. We performed whole-cell patch clamp recordings from n=60 cholinergic neurons from the BF in acute slices. Cholinergic neurons were identified by their red epifluorescence in n=12 mice injected with AAV2/5-EF1a-DIO-hChR2(H134R)-mCherry-WPRE-HGHpA (Figure 25a).

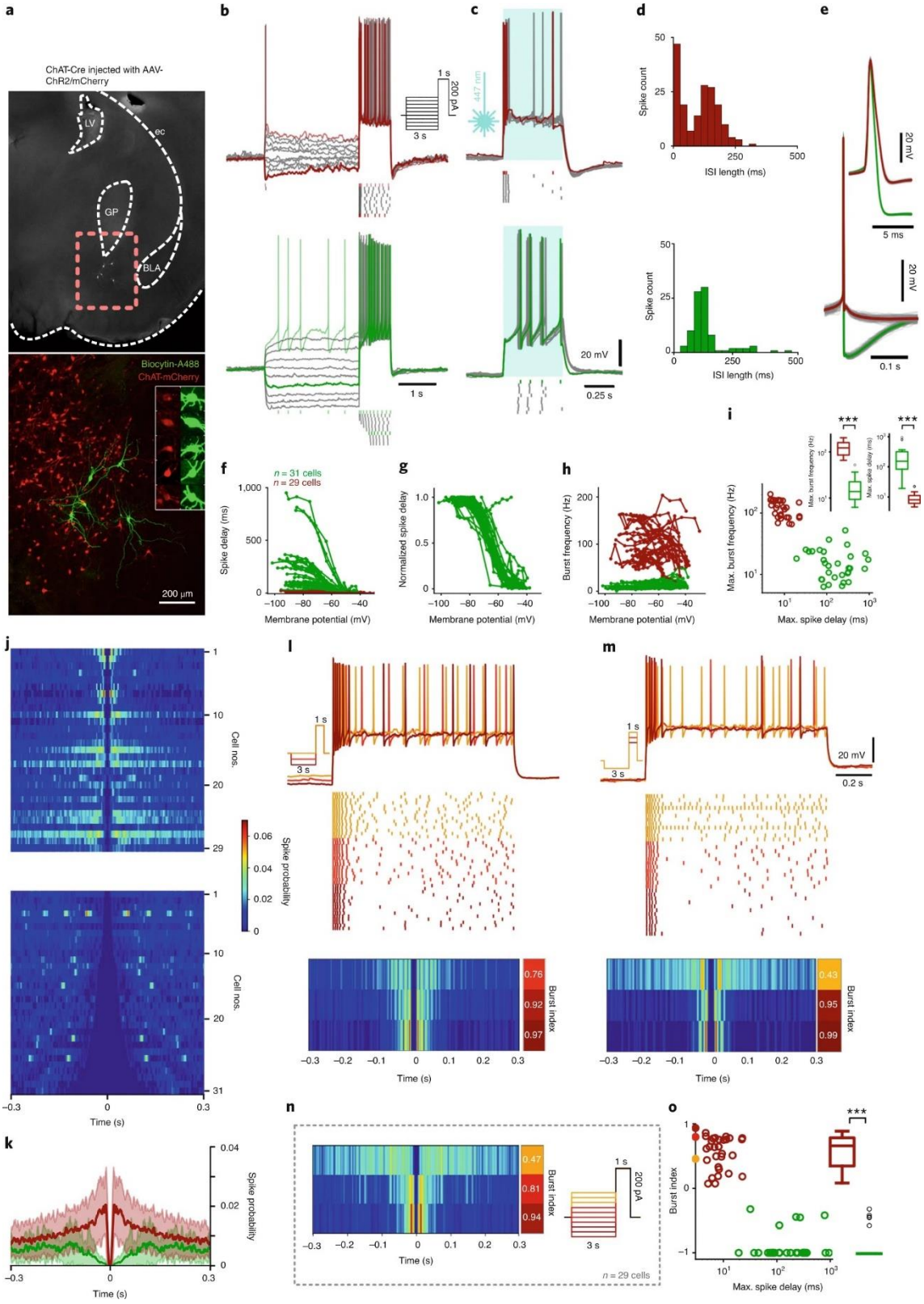

FIGURE 25 | *In vitro* recordings confirmed two types of central cholinergic neurons. (a) Representative confocal image of recorded and biocytin-filled cholinergic cells expressing ChR2 in the nucleus basalis of the BF. (b) Top: firing pattern of an early-firing cell,

showing short spike delay and high-frequency spike clusters on positive current injections. Bottom: firing pattern of a representative late-firing cholinergic cell, showing low maximal firing rate and prominent spike delay when driven from hyperpolarized membrane states. (c) The same cells show similar responses on photostimulation (0.5 s). (d) ISI histograms of the same cells show bimodal (early-firing) or unimodal (late-firing) distributions. (e) Average AP shape from an example early-firing (red) and late-firing (green) cholinergic cell (100 APs per cell in gray, average in color). (f) Spike delay depended on the membrane potential (n = 31 for late-firing and n = 29 for early-firing cholinergic cells). (g) Normalized spike delay showed stereotypical behavior in late-firing cholinergic neurons (n = 31). (h) Maximal burst frequency as a function of the membrane potential (n = 31 late-firing and n = 29 early-firing cholinergic cells). (i) Maximal burst frequency plotted against maximal spike delay in all recorded cells (n = 31 late-firing and n = 29 early-firing cholinergic cells). ***$P < 0.001$; maximal spike delay, $P = 2.08 \times 10^{-11}$; maximal burst frequency, $P = 1.54 \times 10^{-11}$; two-sided Mann–Whitney U-test. Box-and-whisker plots show median, interquartile range, nonoutlier range and outliers. (j) Spike auto-correlograms during somatic current injection protocols for all cells (top: n = 29 early-firing cholinergic cells; bottom: n = 31 late-firing cholinergic cells). (k) Average auto-correlograms of early-firing (red, n = 29) and late-firing (green, n = 31) cholinergic cells (solid lines, mean; shading, s.e.m.). (l) Firing pattern of an early-firing cell in response to three current injection protocols, with different current magnitude applied before the depolarization step. The protocol was designed to model the internal state (membrane potential) dependence of the spiking pattern in response to a uniform input. Raster plot represents 20 trials with each protocol (deeper red, more hyperpolarized states). Bottom: corresponding auto-correlograms and burst indices. (m) Firing pattern of the same cell in response to current injection protocols with different depolarization step magnitudes. The protocol was designed to mimic input strength dependence of the spiking pattern. Raster plot shows 20 trials for each protocol, with a deeper red corresponding to smaller injected currents. (n) Average ACGs and corresponding burst indices of early-firing cells (n = 29) driven from depolarized (top) and hyperpolarized (bottom) states. Three groups were formed from all early-firing cells based on the 3-s-long prepolarization magnitude (right inset).(o) Burst index plotted against maximal spike delay (n = 31 late-firing and n = 29 early-firing cholinergic cells). Dots overlaid on the y axis correspond to

the burst indices presented in n. Burst indices: ***P < 0.001, P = 2.11 × 10^{-12}; two-sided Mann–Whitney U-test. Box-and-whisker plots show median, interquartile range, nonoutlier range and outliers.

We applied a somatic current injection protocol (Figure 25b) containing a 3-s-long, incremental 'prepolarization' step followed by a positive square pulse (1 s), to elicit spiking starting from different membrane potentials. We found two distinct behaviors on current injection (Figure 25b–i) using similar testing conditions (Figure 26a). Cholinergic cells from the first group (red, n=29) displayed a short spike delay (8.05±0.74ms, median±s.e. of median) and bimodal ISI distribution (Figure 25d, top) with short ISIs corresponding to high-frequency 'burst' firing (maximum, 122.69±18.99Hz; Figure 25h,i). The second group (green, n=31) displayed low maximal firing rate (13.81±2.32Hz, P=1.54×10^{-11}, two-sided Mann–Whitney U-test), unimodal ISI distribution (Figure 25d, bottom) and a prominent spike delay (maximum spike delay, 153.05±55.59ms, 2.08×10^{-11} compared with the first group; two-sided Mann–Whitney U-test) which depended on the membrane potential before spiking (Figure 25f,g). Importantly, depolarized late-firing cells responded to suprathreshold current injections with a short spike delay as opposed to the hyperpolarized state where late firing was prominent (Figure 26b).

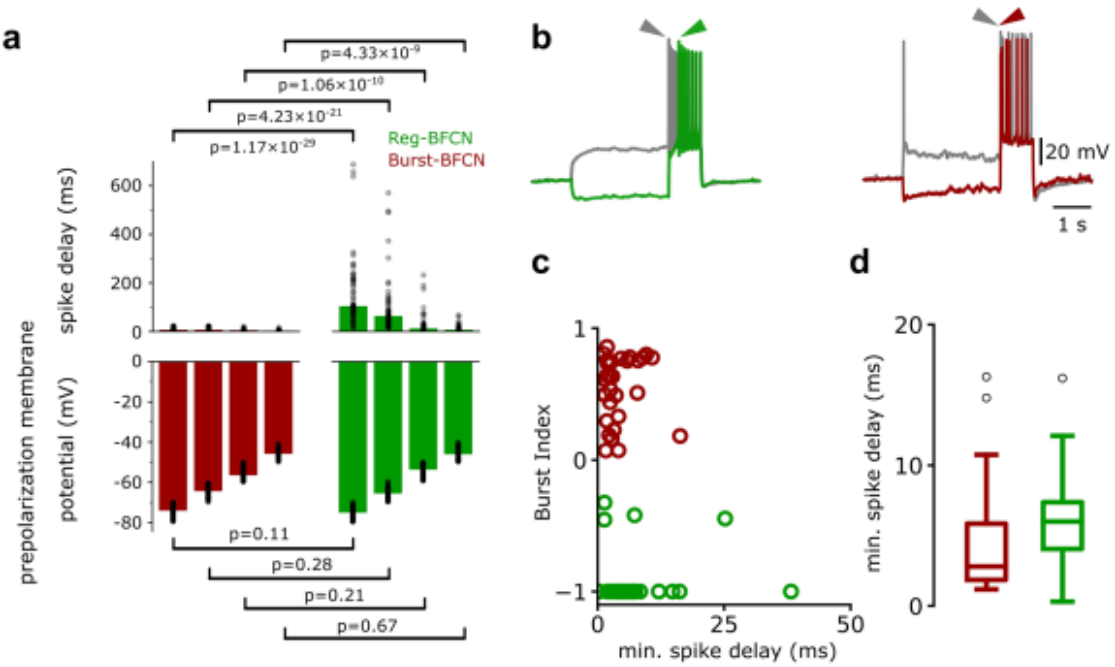

FIGURE 26 | Similar testing conditions resulted in robust spike delay difference between

Burst-BFCNs and Reg-BFCNs, while spike delays were comparable at depolarized membrane potentials. (a) Statistical comparison of spike delay as function of pre-polarization membrane potential. To confirm that late spiking property of Reg-BFCNs was not due to different testing conditions, we compared pre-polarization membrane potentials between groups (n = 31 late-firing and n = 29 early firing cholinergic cells, two-sample, two-sided Kolmogorov-Smirnov test). Bars show median. (b) Example traces of a Reg-BFCN (left) and Burst-BFCN (right) spike response at hyperpolarized and depolarized membrane potentials. Note that the late-firing property of Reg-BFCNs is characteristic to hyperpolarized membrane potentials.(c) Minimum spike delay of each recorded cell vs. burst index (green, Reg-BFCNs; red, Burst-BFCNs). (d) Minimum spike delay group statistics (n = 31 late-firing and n = 29 early firing cholinergic cells). Box-whisker plots show median, interquartile range, non-outlier range and outliers.

These distinct early responding/burst-firing or late responding/nonbursting modes were also reliably elicited by optogenetic depolarization (Figure 25c). Spontaneous action potentials revealed shorter spikes and large-amplitude, slowly decaying afterhyperpolarization in late-firing compared with early-firing (bursting) cells (Figure 25e). To compare *in vivo* and *in vitro* firing patterns, we calculated ACGs and burst indices (early-firing, 0.64±0.08; late-firing,−1.0±0, 2.11×10^{-12}, two-sided Mann–Whitney U-test) from spike trains during the current injection protocol (Figure 25j,k). Early and late-firing neurons *in vitro* matched Burst-BFCNs and Reg-BFCNs *in vivo*, suggesting that these groups are the same. Next, we tested whether the different *in vivo* firing modes of bursting cholinergic neurons (Burst-BFCN-SBs versus Burst-BFCN-Pls) could be explained by variations in the membrane potential and input strength. To investigate this possibility, we applied somatic current injection protocols designed to test input and state dependency of the degree of bursting. Indeed, we found that the same Burst-BFCNs were capable of producing both strongly bursting and Poisson-like firing patterns. This property depended on both the membrane potential of the neuron (Figure 25l–o) and the strength of the activation (Figure 25m), with Poisson-like firing occurring more frequently in more depolarized states and in response to stronger depolarizing inputs. In summary, we identified two types of BFCNs.

Reg-BFCNs showed regular theta-rhythmic firing *in vivo* and late, regular responses to current injections *in vitro*; Burst-BFCNs exhibited burst firing both *in vivo* and *in vitro*, where the strength of bursting was determined by the level of excitation.

5.3. Cholinergic bursts transmit phasic information about reinforcers.

Cholinergic neurons act at different timescales regulating different aspects of cognition, from slow sleep–wake and arousal processes to fast subsecond or even millisecond timescales of reinforcement learning and plasticity (Hangya et al., 2015; Sarter et al., 2009; Teles-Grilo Ruivo et al., 2017). Based on *in vitro* studies it was hypothesized that bursting specifically represents fast 'phasic' information transfer (Zaborszky, Unal, et al., 2012); however, this has not been tested. Therefore, we analyzed the activity of basal forebrain cholinergic neurons after reward and punishment in mice performing auditory conditioning (Hangya et al., 2015)(Figure 27a).

We defined a burst as a series of action potentials starting with an ISI <10ms and subsequent ISI durations of <15ms to allow for typical ISI accommodation patterns (Royer et al., 2012). As expected, Burst-BFCNs, categorized based on auto-correlograms, showed a high percentage of burst firing: 28% for Burst-BFCN-SBs and 20% for Burst-BFCN-PLs, whereas little burst activity was detected in Reg-BFCNs (3%; Figure 27b).

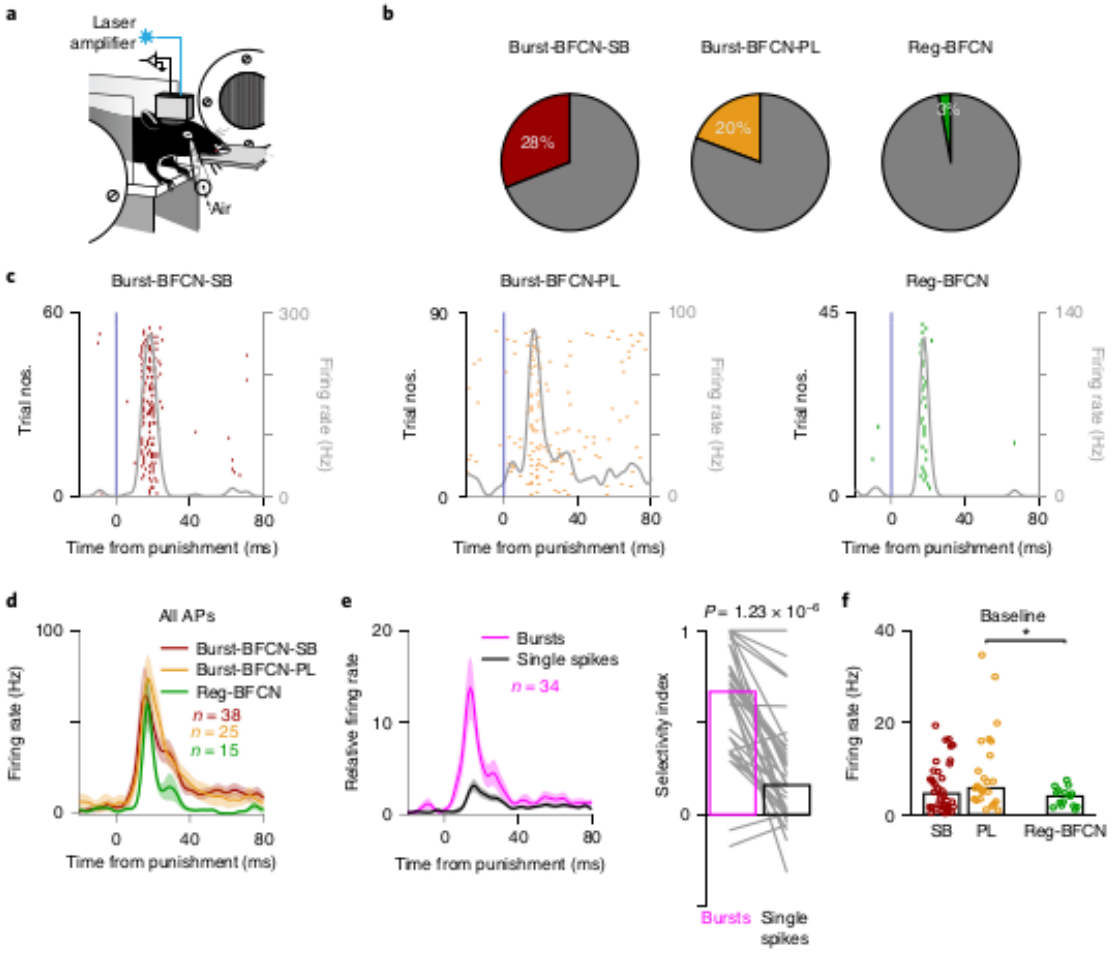

FIGURE 27 | Cholinergic bursts transmit phasic information about reinforcers. (a) Mice were trained to lick for cue stimuli of pure tones. Hits were rewarded with a drop of water, whereas false alarms were punished by an air-puff (modified from ref. (Hangya et al., 2015)). (b) Percentage of intraburst aPs (n = 38 Burst-BFCN-SBs, red; n = 25 Burst-BFCN-PLs, orange; n = 15 Reg-BFCNs, green).(c) Example raster plots of phasic responses to punishment by Burst-BFCN-SB (left), Burst-BFCN-PL (middle) and Reg-BFCN (right). PETHs smoothed by moving average are overlaid in gray. (d) Average response of cholinergic neurons to punishment (n = 38 Burst-BFCN-SBs, red; n = 25 Burst-BFCN-PLs, orange; n = 15 Reg-BFCNs, green) (solid lines, mean; shading, s.e.m.). (e) Left: occurrence of bursts and single spikes in Burst-BFCN-SBs normalized to the baseline (solid lines, mean; shading, s.e.m.). Right: median selectivity index calculated as spike number in 20–50 ms relative to 100–250 ms post-event windows. Bursts of Burst-BFCN-SBs (n = 34) are more concentrated after punishment compared with single spikes ($P = 1.23 \times 10^{-6}$, two-sided Wilcoxon's signed-rank test). (f) Median baseline firing rate

(red, n = 38 Burst-BFCN-SBs; orange, n = 25 Burst-BFCN-PLs; green, n = 15 Reg-BFCNs). *P < 0.05, P = 0.0236, two-sided Mann–Whitney U-test.

We have shown previously that the strongest response of cholinergic neurons occurred after air-puff punishments (Hangya et al., 2015): BFCNs responded phasically with short latency (18±1.9ms, median±s.e. of median), low jitter (5.7±0.1ms) and high reliability (81.7±2.6%). In the present study, we compared bursting and regular rhythmic cholinergic neurons, and found that both types showed strong response to air-puff punishment (Figure 27c,d). Contrary to previous hypotheses, Reg-BFCNs were also capable of surprisingly fast and precise phasic firing, emitting a precisely timed single action potential, typically followed by a pause and then a reset of their intrinsic theta oscillation (Figure 27c,d, and Figure 28a). This clearly distinguished them from tonically active striatal interneurons, which did not show such responses (Figure 28b–d).

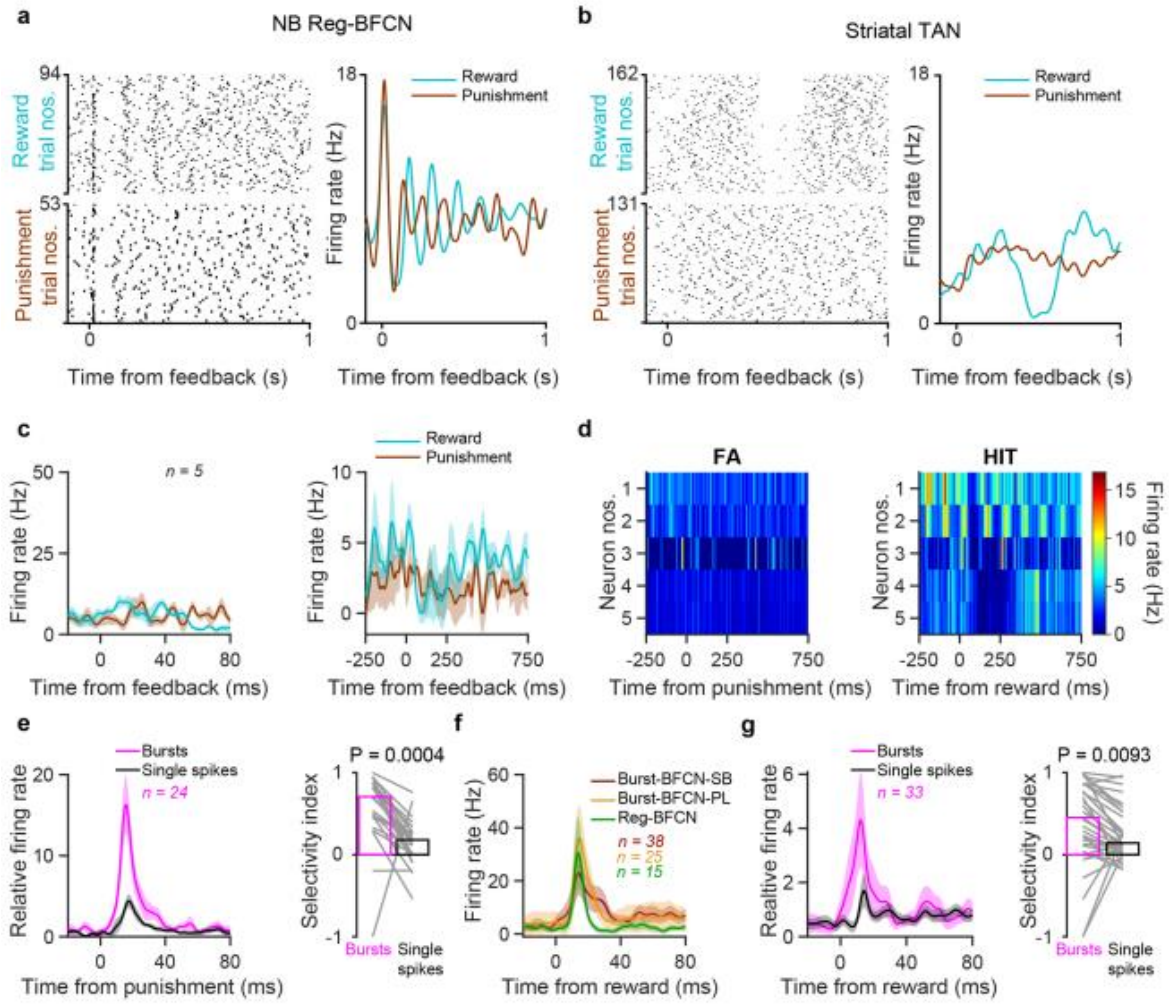

FIGURE 28 | Cholinergic bursts transmit phasic information about reinforcers. (a) Raster plots (left) and corresponding peri-event time histograms (PETH, right) aligned to reward (blue) and punishment (brown) of a Reg-BFCN. After the precise phasic response, the intrinsic theta oscillation resumes. (b) Raster plots (left) and corresponding PETHs (right) aligned to reward (blue) and punishment (brown) of an optogenetically identified tonically active cholinergic interneuron (TAN) recorded from the nucleus accumbens. Note the lack of precisely timed action potentials after reinforcement. Instead, TANs show well-characterized so-called 'pause-burst' responses after reward.(c) Average PETH aligned to reward (blue) and punishment (brown) at two different time scales of n = 5 optogenetically identified TANs from caudate putamen (n = 3) and nucleus accumbens (n = 2) Solid lines, mean; shading, s.e.m. (d) PETHs aligned to punishment (left) and reward (right) for all recorder TANs. (e) Burst-BFCN-PLs showed similar burst selectivity after punishment as Burst-BFCN-SBs (p = 0.0004, two-sided Wilcoxon signed rank

test). Solid lines, mean; shading, s.e.m.; bars, median. (f) BFCNs responded phasically to reward (red, n = 38 Burst-BFCN-SBs; orange, n = 25 Burst-BFCN-PLs; green, n = 15 Reg-BFCNs). Solid lines, mean; shading, s.e.m. (g) Bursts of Burst-BFCN-SBs (n = 33) appeared selectively after reward (p = 0.0093, two-sided Wilcoxon signed rank test). Solid lines, mean; shading, s.e.m.; bars, median.

Burst-BFCNs are capable of emitting both bursts of action potentials and single spikes. Therefore, we wondered whether bursts and single spikes represent salient events such as air-puffs differently, in which case this should be reflected in a difference in peri-event time histograms (PETHs) of bursts versus single APs aligned to punishment events. We found that bursts of Burst-BFCNs significantly concentrated after punishment compared with single spikes in most neurons ($P=1.23\times10^{-6}$, two-sided Wilcoxon's signed-rank test; Figure 27e and Figure 28e). We observed similar concentration of bursts after reward, but not cue stimuli or trial start signals (Figure 28f,g), suggesting that bursts represent external events differently compared with single spikes (Zeldenrust et al., 2018). *In vitro* studies also predicted that tonically active neurons would be more important in controlling slow tonic changes in acetylcholine levels, which could potentially be reflected in higher baseline firing rates of Reg-BFCNs. However, we found that baseline firing rates were largely similar across cholinergic cell types and firing patterns (median±s.e.: Burst-BFCN-SBs, 4.55±1.26; Burst-BFCN-PLs, 5.74±1.39; Reg-BFCNs, 3.96±1.0), with slightly faster firing in Burst-BFCN-PLs, consistent with the more depolarized membrane potentials and stronger excitatory inputs suggested by our *in vitro* recordings in Figure 25l–o (Burst-BFCN-SBs versus Burst-BFCN-PLs, P=0.11; Burst-BFCN-SBs versus Reg-BFCNs, P=0.41; Burst-BFCN-PLs versus Reg-BFCNs; P=0.0236; two-sided Mann–Whitney U-test; Figure 27f). Bursting cholinergic neurons show synchronous activity. Bursts of cholinergic neurons were found to precisely align to reinforcement (Figure 27c–e), generating a strong synchronous activation of the cholinergic system after reward and punishment. Is synchronous firing specific to these unique behaviorally relevant events or do they occur at other times as well? Synchronous versus asynchronous activation of subcortical inputs has a fundamentally different impact on cortical computations. However, although there is a lot known about synchrony in cortical circuits both within and across cell types, there is little information on synchronous firing in subcortical nuclei.

Specifically, no recordings of multiple identified cholinergic neurons have been performed. In some cases, we recorded 2 (n=15) or 3 (n=3) cholinergic neurons simultaneously, resulting in 24 pairs of concurrent cholinergic recordings. By calculating pairwise cross-correlations, we found that Burst-BFCNs, especially Burst-BFCN-SBs, showed strong zero-phase synchrony with each other (6/6 pairs of two Burst-BFCN-SBs and 5/11 pairs containing Burst-BFCN-Sbs and -PLs showed significant co-activation, $P<0.05$). Reg-BFCNs showed little synchrony with other BFCNs (2/7 pairs that contained at least one Reg-BFCN were significantly co-activated, $P<0.05$, bootstrap test; Figure 30a,b and Figure 29).

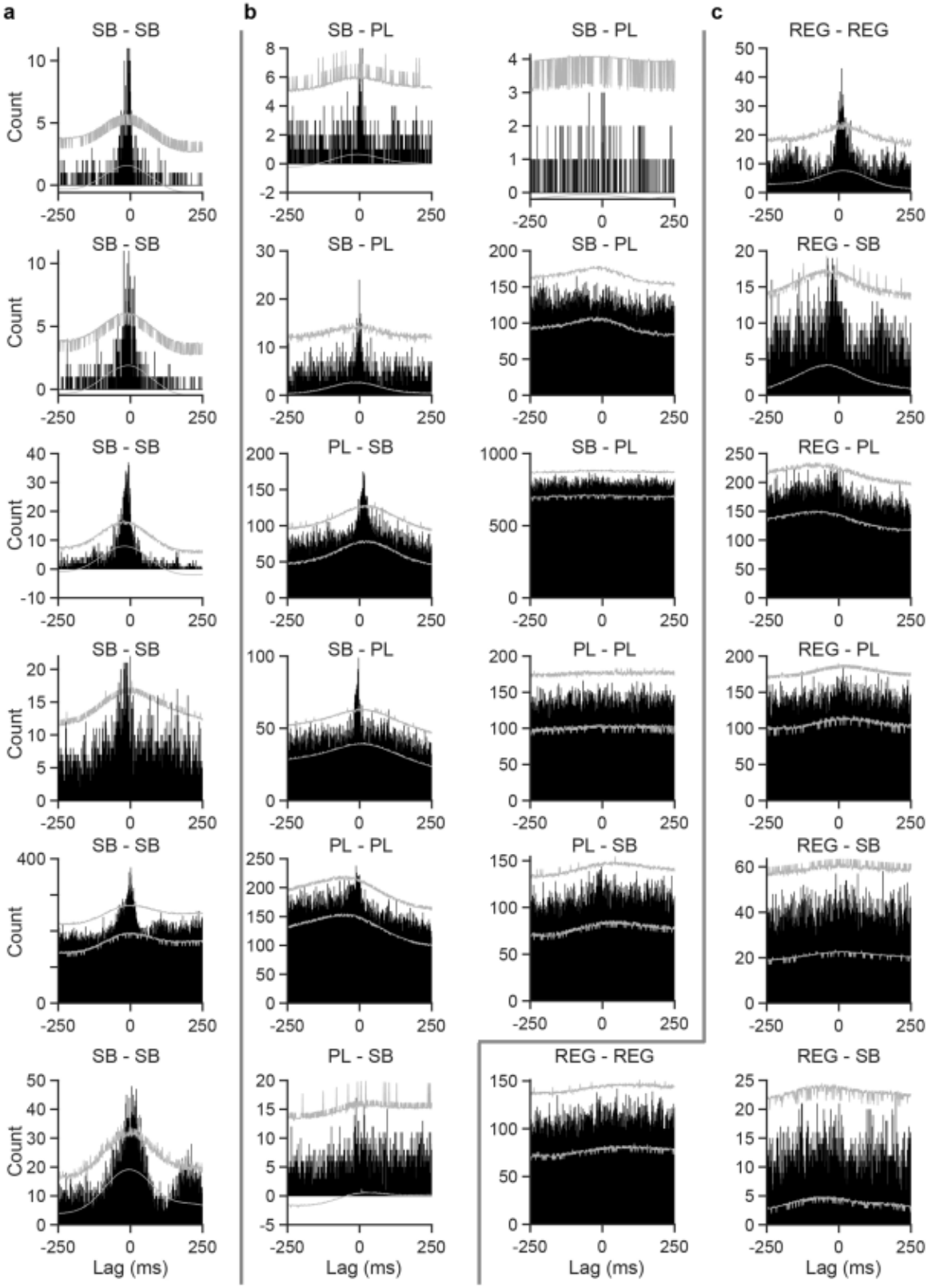

FIGURE 29 | Individual cross-correlations for all BFCN pairs. (a) Pairs of Burst-BFCN-SBs. (b) Pairs containing Burst-BFCN-PLs and Burst-BFCN-SBs.(c) Pairs containing

Reg-BFCNs. Grey lines indicate 95% bootstrap confidence intervals calculated with the shift predictor method.

Co-activation of Burst-BFCNs typically spanned ±25ms (27.22±5.37, mean±s.e.m.; maximum 42ms) and was not restricted to the bursts themselves, because single action potentials of bursting neurons showed similar synchrony (Figure 30c); thus Burst-BFCNs may share a synchronizing input that differentiates them from other BFCNs, possibly contributing to the bursting phenotype itself.

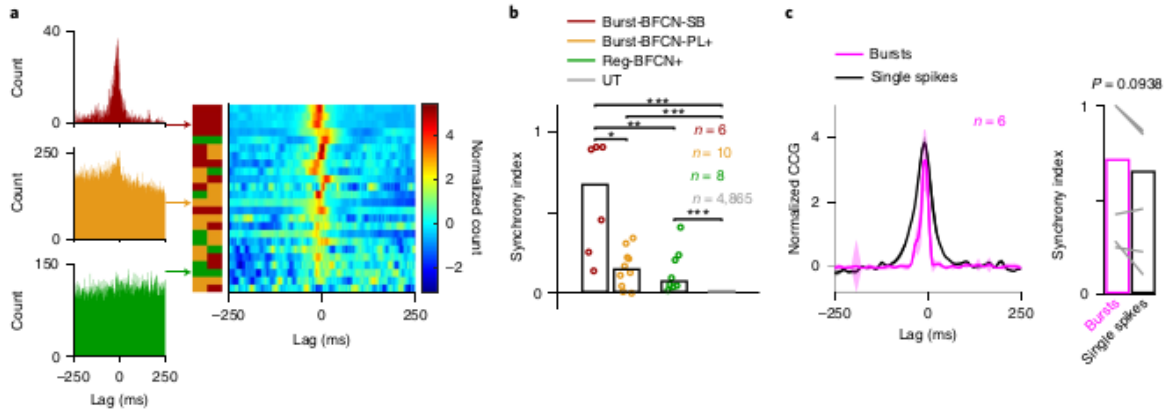

FIGURE 30 | Bursting cholinergic neurons show synchronous activity. (a) Cross-correlations of pairs of cholinergic neurons. Left: examples (red, Burst-BFCN-SB; orange Burst-BFCN-PL; green, Reg-BFCN). Right: all pairs; left: color bar indicates the firing mode of the two neurons that form the pair. Please note, that, in some cases, the Z-score normalization necessary to show all CCG pairs can magnify central peaks that are otherwise small relative to baseline; therefore, all individual CCG pairs are shown in Figure 28 without normalization. (b) Pairs of Burst-BFCN-SBs show stronger synchrony than pairs that contain Burst-BFCN-PLs or Reg-BFCNs. The synchrony index calculated as average cross-correlation in −30 to +30ms windows normalized to 100–250 ms baseline period (bars, median) (n = 6 Burst-BFCN-SB pairs (red); n = 10 Burst-BFCN pairs containing PL, denoted by PL+ (orange); n = 8 pairs continaing Reg-BFCN, denoted by Reg-BFCN+ (green); n = 4,865 untagged (UT, gray) cholinergic cell pairs). *P < 0.05; **P < 0.01; ***P < 0.001. Burst-BFCN-SB versus Burst-BFCN-PL+, P = 0.011; Burst-BFCN-SB versus Reg-BFCN+, P = 0.008; Burst-BFCN-SB versus UT, P = 2.7×10^{-5}; Burst-BFCN-PL+ versus UT, P = 3.02×10^{-4}; Reg-BFCN+ versus UT neurons, P = 9.81×10^{-5};

two-sided Mann–Whitney U-test.(c) Both bursts and single spikes of Burst-BFCN-SBs (n = 6) showed zero-lag synchrony. Left: solid lines, mean; shading s.e.m. Right: bars show median. P = 0.0938, two-sided Wilcoxon's signed-rank test.

5.4. Cholinergic bursts are coupled to cortical activity.

Cholinergic neurons send dense innervation to the cortex, including projections from the nucleus basalis (NB) to auditory cortices (Saper, 1985; Zaborszky, van den Pol, et al., 2012). These inputs can potently activate cortical circuits, leading to desynchronization and gamma oscillations (Buzsaki et al., 1988; Pinto et al., 2013) which we confirmed by optogenetic stimulation of NB cholinergic neurons that elicited broad-band activity in the auditory cortical LFPs (Figure 32a). We reasoned that bursts of cholinergic firing might lead to stronger cortical activation, whereas synchronous activation of ensembles of cholinergic neurons may further increase this effect, providing a finely graded control over cortical activation and thus arousal by the ascending cholinergic system. At the same time, the BF receives cortical feedback (Do et al., 2016; Gielow & Zaborszky, 2017; Zaborszky, van den Pol, et al., 2012) that may be capable of entraining cholinergic neurons, thus establishing an ongoing synchrony between cortical and BF activity, a hypothesis largely under-explored (but see refs. (Lee et al., 2005; Tingley et al., 2015; Yang, Thankachan, et al., 2017)). To test these possibilities, we calculated spike-triggered LFP averages and spike-triggered spectrogram averages of auditory cortical LFPs aligned to the action potentials of BFCNs recorded during auditory operant conditioning. We used spike-triggered averages (STAs) to identify synchronization between BFCN spiking and cortical oscillations, because LFP changes not phase locked with BFCN spikes cancel out (Lee et al., 2005). Individual STAs aligned to cholinergic spikes showed prominent oscillations in the theta band (4–12Hz), suggesting that NB cholinergic activity can synchronize to cortical theta oscillations (Figure 32b,c). In addition, we often observed strong deflections in cortical LFPs after cholinergic spikes (Figure 31; peak latency, 36.0±13.0ms; median±s.e. of median), which may be a signature of cortical activation by cholinergic input.

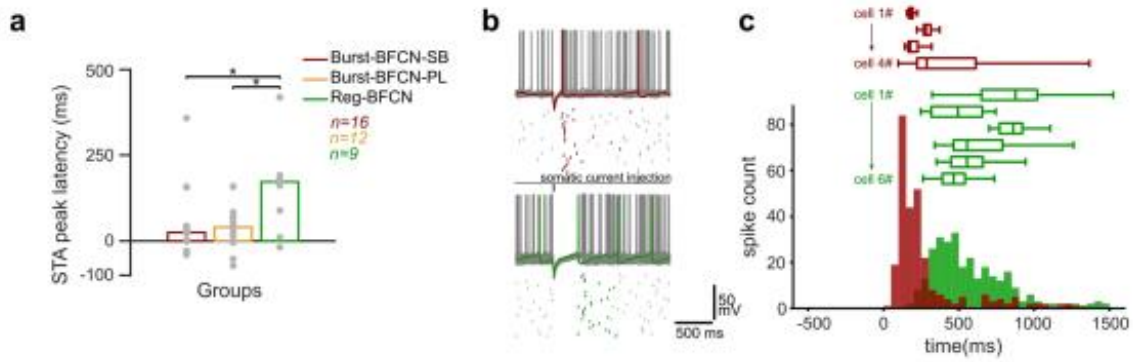

FIGURE 31| Bursting and regular rhythmic cholinergic neurons respond differently to hyperpolarization *in vitro*. (a) Peak latency statistics of auditory LFP average triggered on BF spikes *in vivo* (see Figure 32b-c; red, n = 16 Burst-BFCN-SBs; orange, n = 12 Burst-BFCN-PLs; green, n = 9 Reg-BFCNs; *, $p < 0.05$; Burst-BFCN-SBs vs. Burst-BFCN-PLs, $p = 0.546$; Burst-BFCN-SBs vs. Reg-BFCNs, $p = 0.014$; Burst-BFCN-PLs vs. Reg-BFCNs, $p = 0.017$; two-sided Mann-Whitney U-test). Bars, median. (b) Representative responses of a Burst-BFCN (top, red) and Reg-BFCN (bottom, green) upon short (20 ms) hyperpolarizing somatic current injection *in vitro*. Spike rasters of 30 consecutive current injection sessions are displayed below.(c) Distribution of the first spike latencies following hyperpolarization. Individual cells (horizontal bar plots) are shown above summary histogram (red, n = 4 Burst-BFCNs, green, n = 6 Reg-BFCNs, $p = 6.47 \times 10^{-44}$, two-sided Mann-Whitney U-test; box plots show median, interquartile range and non-outlier range). To assess this, we used spike-triggered spectrograms (STSs) to identify evoked responses that are not phase coupled. STS analysis showed high-frequency beta/gamma-band activity after cholinergic spiking (Figure 32c). Importantly, bursts of BFCNs were associated with stronger LFP responses compared with single spikes (Figure 32d–f).

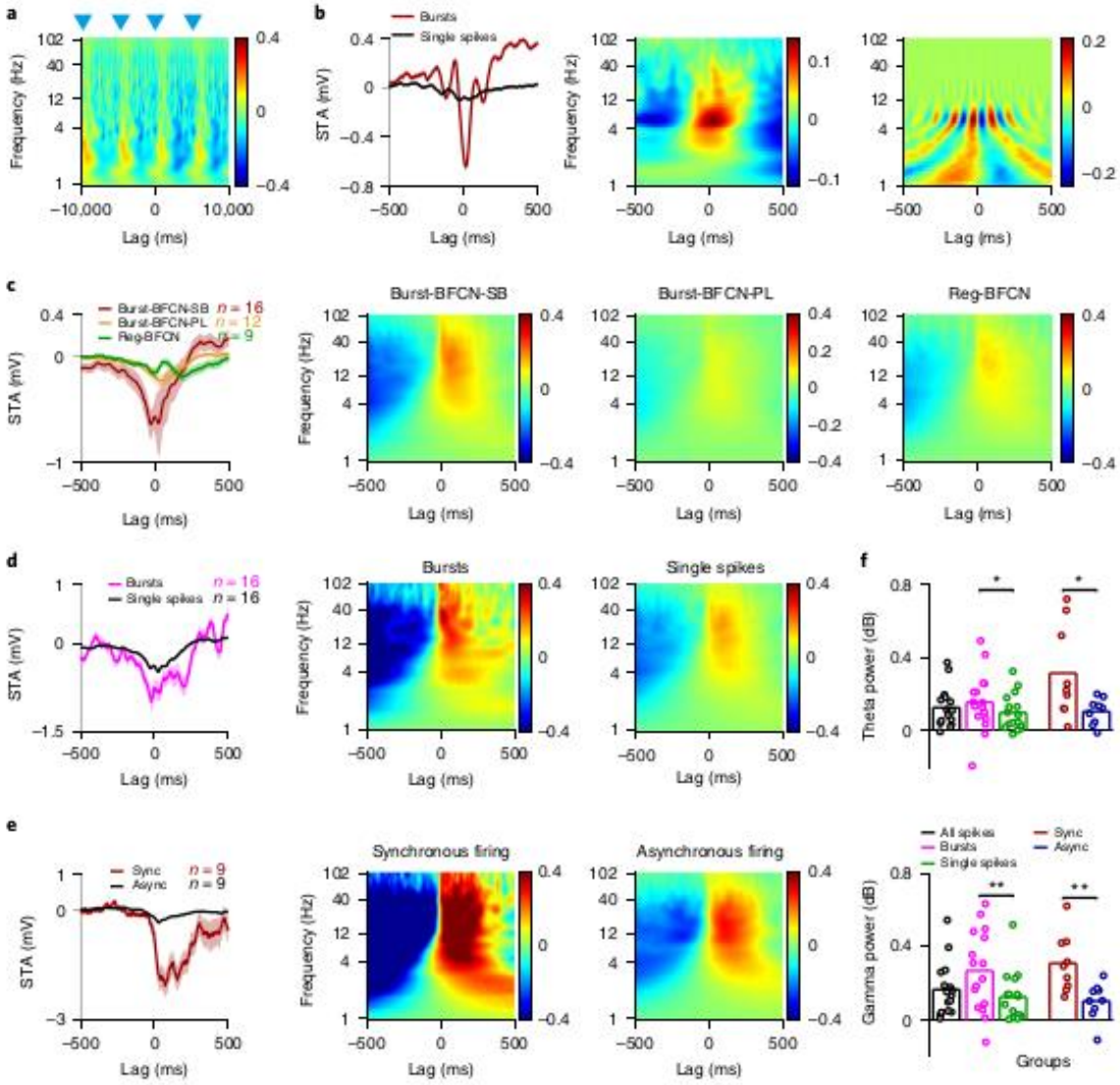

FIGURE 32 | Cholinergic bursts are coupled to cortical activity. (a) Photostimulation of BFCNs (n = 37) activates the auditory cortex; stimulus-triggered average spectrogram aligned to photostimulation (blue triangles). Color code represents spectral power (dB). (b) Example of a Burst-BFCN-SB (n = 16,680 bursts and 50,996 single spikes) strongly synchronized to cortical theta. Left: STAs based on all spikes (solid lines, mean; shading, s.e.m.); middle: STS; right, STS phase demonstrates phase locking in the theta band.(c) From left to right: average STA for BFCN groups (solid lines, mean; shading, s.e.m.); average STS for Burst-BFCN-SBs, Burst-BFCN-PLs and Reg-BFCNs. (d) Bursts elicit stronger cortical activation. Left: average STA (solid lines, mean; shading, s.e.m.); middle: average STS for bursts; right: average STS for single spikes. (e) Synchronous firing elicits stronger cortical activation. Left: average STA (solid lines, mean; shading, s.e.m.); middle: average STS for synchronous (Sync) firing; right: average STS for asynchronous

(Async) firing. (f) Mean spectral power in the theta (top) and gamma band (bottom: black, all spikes, n = 16; pink, bursts, n = 16; green, single spikes, n = 16; dark red, synchronous firing, n = 9; blue, asynchronous firing, n = 9; *P < 0.05, **P < 0.01; theta band, bursts versus single spikes, P = 0.0437; synchronous versus asynchronous firing, P = 0.0391; gamma-band, bursts versus single spikes, P = 0.006; synchronous versus asynchronous firing, P = 0.008; two-sided Wilcoxon's signed-rank test). We note that a small number of single neurons recorded on the stereotrodes implanted in the auditory cortex showed phase locking to local theta, indicating that oscillations recorded in the auditory cortex were at least partially locally generated (Figure 33).

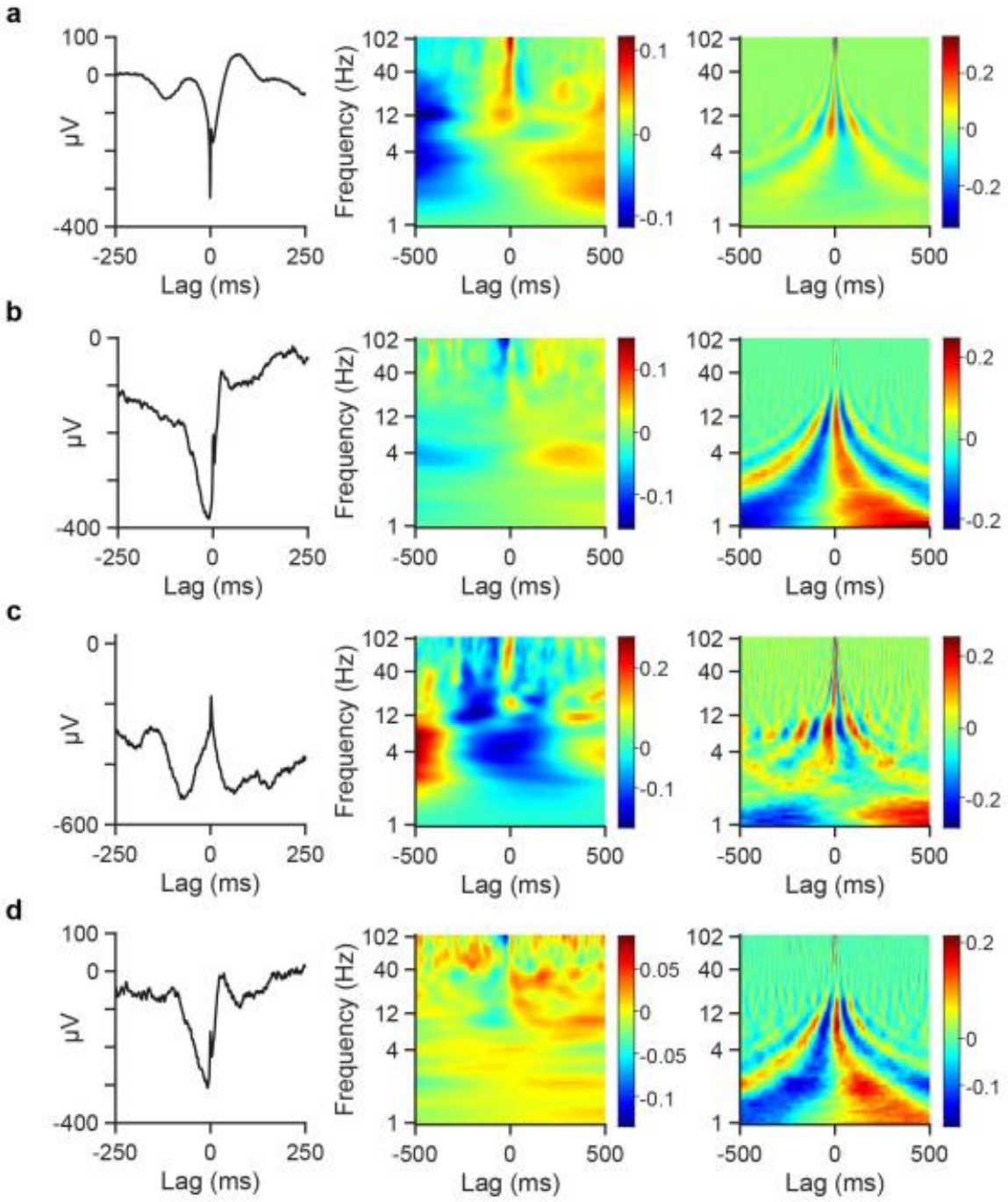

FIGURE 33 | Some auditory cortical neurons are synchronous with local LFP. (a-d) Example cortical neurons that show synchrony with local LFP. Left, STA; middle, STS power; right, STS phase (a, n = 50000 spikes; (b) n = 21765 spikes;(c) n = 4083 spikes; (d) n = 7834 spikes). Solid line, mean; shading, s.e.m.

We confirmed that artificial synchrony of BFCNs imposed by optogenetic or electrical stimulation induced cortical desynchronization (Figure 32a), as shown previously (Buzsaki et al., 1988; Pinto et al., 2013). As we have found that synchronous activation of BFCNs also occurred in a physiological setting (see Figure 30), this raises the question of whether such synchrony indeed leads to stronger cortical impact. To test this, we focused our analysis on the synchronous firing of cholinergic pairs. We found that synchronous events defined by two Burst-BFCNs firing within 10ms was associated with strong cortical activation compared with asynchronous firing, confirming our prediction that NB signatures of enhanced cholinergic release represent a stronger impact on cortical population activity (Figure 32e,f). We observed that bursting cholinergic neurons often showed synchronization to cortical theta-band oscillations (Figure 32b, left). The presence of high values in the theta band in the average spectral phase (phase domain of STSs; Figure 32b, right) confirmed this, because it reflects phase locking to LFP oscillations. We reasoned that differential activation of cholinergic cell types by their inputs might underlie differences in synchronizing with cortical oscillations. It is known that frontal cortical projections to the BF synapse on GABAergic neurons (Zaborszky, van den Pol, et al., 2012), likely providing indirect hyperpolarizing input to cholinergic neurons (Yang, Thankachan, et al., 2017). To model the impact of this circuit on BFCNs, we tested whether Burst-BFCNs and Reg-BFCNs show differential responses to hyperpolarizing current injections *in vitro*. We found that Burst-BFCNs recovered their spikes with shorter and less variable latency (n=4, 172.3±9.95ms, median±s.e. of median than Reg-BFCNs (n=6, 561.25±23.77ms; 6.47×10−44, two-sided Mann–Whitney U-test; Figure 31b,c). This supports the hypothesis that cortically driven indirect inhibition of BFCNs may contribute to their differential coupling to cortical activity.

5.5. Synchrony of BFCN spiking with cortical activity predicts behavior during auditory detection.

We have demonstrated that bursting and regular rhythmic cholinergic neurons are differentially coupled with the auditory cortex. However, the functional significance of this connection remains unclear. Therefore, we tested whether synchrony between BFCNs and the auditory cortex predicted behavioral performance during auditory conditioning (Figure 27a). Specifically, we restricted our analysis to 1-s-long windows around auditory

cue presentation during the operant auditory detection task (Hangya et al., 2015). We found that Burst-BFCNs, especially Burst-BFCN-SBs, showed larger STA deflections during hit and false-alarm trials compared with miss and correct-rejection trials (Figure 34a–c).

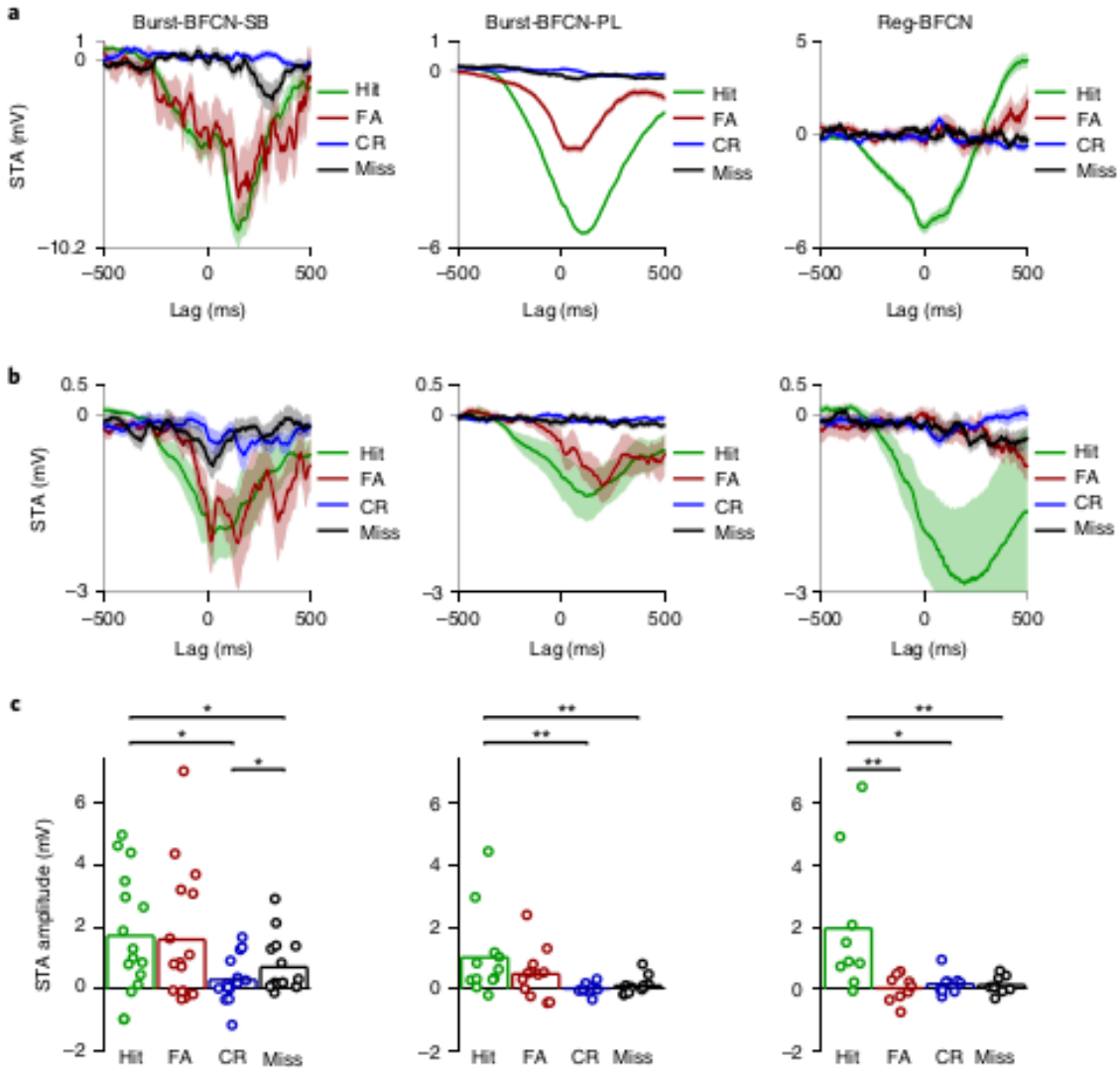

FIGURE 34 | Cortex–BFCN synchrony predicts behavior in an auditory detection task. (a) Example STAs calculated for spikes of a Burst-BFCN-SB (left), a Burst-BFCN-PL (middle) and a Reg-BFCN (right) restricted to a 1-s-long window around cue tone presentations during auditory detection, separated based on trial outcome. FA, false alarm; CR, correct rejection. Solid lines, mean; shading, s.e.m. (b) Average STAs calculated for spikes in a 1-s window centered on cue presentations for the Burst BFCN-SB (left, n = 16), Burst-BFCN-PL (middle, n = 12) and Reg-BFCN (right, n = 9) groups (solid lines, mean; shading, s.e.m.). (c) Mean absolute STA deflections (*P < 0.05, **P < 0.01; left:

n = 16 Burst BFCN-SB neurons; hit versus FA, P = 0.163; hit versus CR, P = 0.02; hit versus miss, P = 0.03; FA versus CR, P = 0.063; FA versus miss, P = 0.109; CR versus miss, P = 0.049; middle: n = 12 Burst-BFCN-PLs0 hit versus FA, P = 0.11, hit versus CR, P = 0.009; hit versus miss, P = 0.009; FA versus CR, P = 0.077; FA versus miss, P = 0.11; CR versus miss, P = 0.622; right: n = 9 Reg-BFCNs; hit versus FA, P = 0.008; hit versus CR; P = 0.012; hit versus miss, P = 0.008; FA versus CR, P = 1; FA versus miss, P = 0.734; CR versus miss, P = 0.82; two-sided Wilcoxon's signed-rank test).

Therefore, synchronization of Burst-BFCNs with cortical networks predicts mouse responses but not their accuracy, because correct and incorrect responses showed similar STAs. In contrast, we found that large STA deflections for Reg-BFCNs specifically predicted hits; thus, synchronization of Reg-BFCNs and the auditory cortex predicted performance. We did not find similar predictive activity in a 1-s window before the cues, suggesting that predictive synchronization of the BF and auditory cortex was evoked by the cue tones. In summary, we found a behavioral dissociation between the two cholinergic cell types; while cortical coupling of Burst-BFCNs preceded all responses of the animals regardless of performance, Reg-BFCNs specifically predicted correct responses.

5.6. The horizontal diagonal band contains few regular cholinergic neurons.

We wondered whether the uncovered diversity of cell types is uniform across the basal forebrain; alternatively, differences in the distribution of bursting and regular rhythmic cholinergic neurons may suggest that dedicated cortical areas are differentially regulated by BF cholinergic afferents. The cholinergic neurons we recorded were distributed in the NB (see Figure 21a) and in the more anterior horizontal limb of the diagonal band of Broca (HDB; Figure 35a), spanning almost 2mm rostrocaudal distance. This allowed us to investigate whether BFCN types are differentially distributed along the anteroposterior axis of the BF. In our *in vivo* recordings, 27% (n=12/45) of the NB neurons belonged to the regular rhythmic type, whereas this was only 9% (n=3/33) for the HDB (Figure 35b).

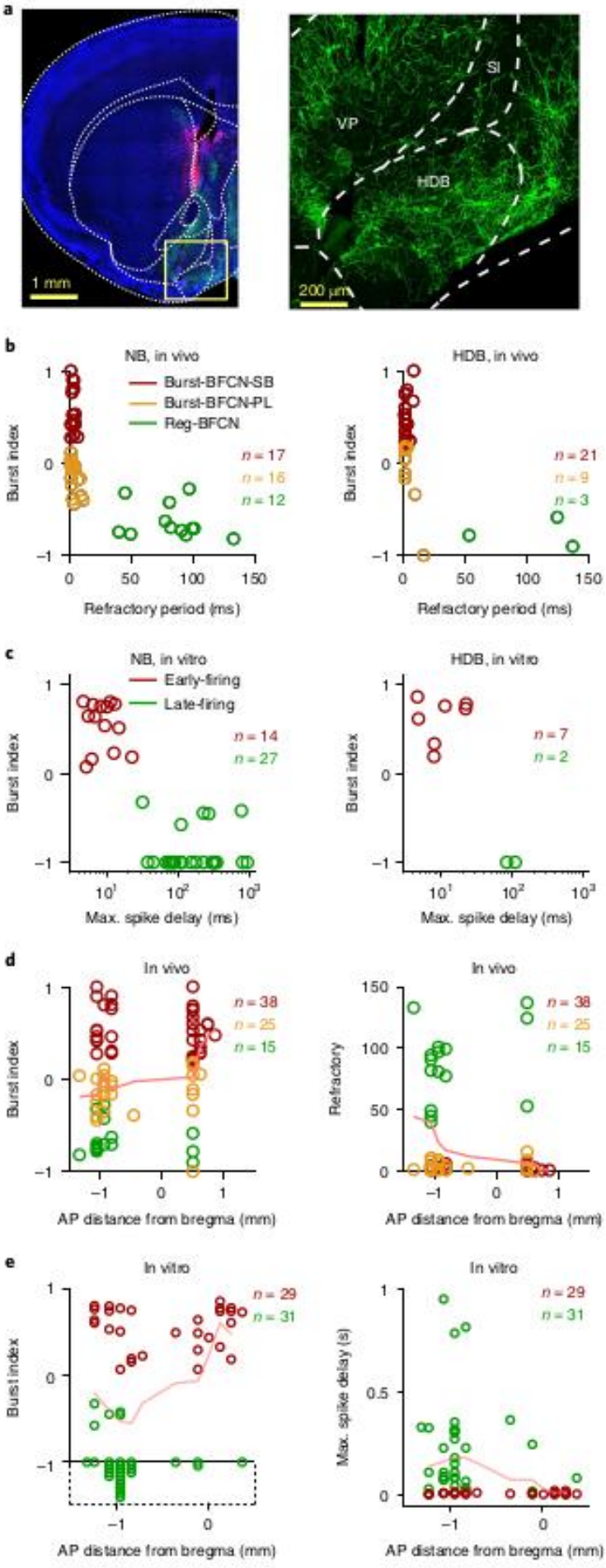
a
1 mm
SI
VP
HDB
200 µm
b
NB, in vivo
Burst-BFCN-SB
Burst-BFCN-PL
Reg-BFCN
n = 17
n = 16
n = 12
Burst index
Refractory period (ms)
HDB, in vivo
n = 21
n = 9
n = 3
Burst index
Refractory period (ms)
c
NB, in vitro
Early-firing
Late-firing
n = 14
n = 27
Burst index
Max. spike delay (ms)
HDB, in vitro
n = 7
n = 2
Burst index
Max. spike delay (ms)
d
In vivo
n = 38
n = 25
n = 15
Burst index
AP distance from bregma (mm)
In vivo
n = 38
n = 25
n = 15
Refractory
AP distance from bregma (mm)
e
In vitro
n = 29
n = 31
Burst index
AP distance from bregma (mm)
In vitro
n = 29
n = 31
Max. spike delay (s)
AP distance from bregma (mm)

FIGURE 35 | The horizontal diagonal band contains few regular firing cholinergic neurons. (a) Coronal section showing ChR2 expression (green, eYFP) and tetrode tracks (red, DiI) in the HDB (blue, DAPI staining) (modified from ref. (Hangya et al., 2015)). (b) Burst index versus relative refractory period for cholinergic neurons recorded *in vivo* from the NB (left: red, n = 17 Burst-BFCN-SBs; orange, n = 16 Burst-BFCN-PLs; green, n = 12 Reg-BFCNs) and HDB (right: red, n = 21 Burst-BFCN-SBs; orange, n = 9 Burst-BFCN-PLs; green, n = 3 Reg-BFCNs). (c) Burst index versus maximal spike delay for cholinergic neurons recorded *in vitro* from the NB (left) and the HDB (right). (d) Burst index (left) and relative refractory period (right) as a function of anteroposterior (AP) localization *in vivo* (n = 38 Burst-BFCN-SBs, n = 25 Burst-BFCN-PLs, n = 15 Reg-BFCNs neurons; pink lines, median as a function of the anteroposterior localization, smoothed with a three-point moving average). (e) Burst index (left) and maximal spike delay (right) as a function of the anteroposterior localization *in vitro* (n = 31 late-firing (green), n = 29 early-firing (red) cholinergic cells; pink lines, median as a function of the anteroposterior localization, smoothed with a three-point moving average; cells with burst indices of −1 were dispersed along the y axis to avoid overlapping, marked by the dotted box).

When we recorded NB neurons *in vitro*, 66% (n=27/41) were Reg-BFCNs, whereas only 22% (2/9) Reg-BFCNs were found in the HDB (Figure 35c). The higher proportion of Burst-BFCNs in our *in vivo* recordings could be due to better cluster separation because of their somewhat higher firing rates (Figure 27f) and distinct spike shape (Figure 25e). Nevertheless, we found that the NB contained three times more regular rhythmic cholinergic neurons both *in vivo* and *in vitro* compared with the HDB, which mostly contained the bursting type ($P=0.0007$, $\chi 2=11.37$, $\chi 2$ test). In line with these, the burst index and relative refractory period of cholinergic neurons changed systematically along the anteroposterior axis of the BF (Figure 35d,e), suggesting that different brain areas may receive different combinations of cholinergic inputs. Turning to untagged HDB neurons that we recorded *in vivo*, we found that only 12 of 560 HDB neurons were characterized as regular firing (Figure 36), which confirms both the lack of Reg-BFCNs in the HDB (Figure 35) and the connection between regular rhythmic phenotype and cholinergic identity (Figure 21h and Figure 24h).

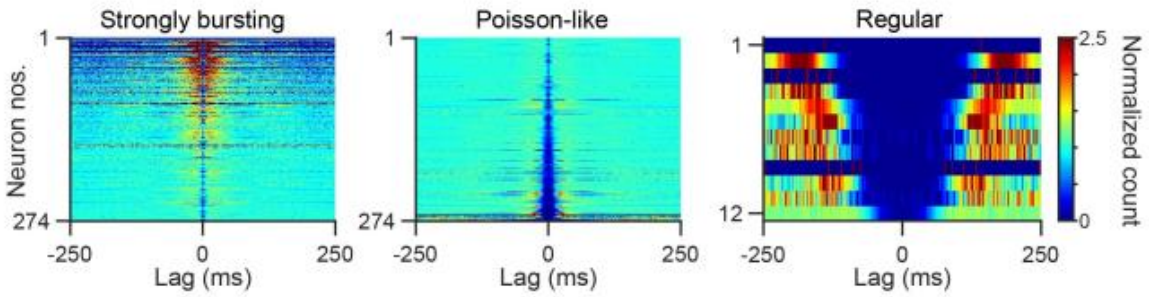

FIGURE 36 | HDB contains few regular rhythmic neurons. Auto-correlograms of all unidentified HDB neurons (left, bursting, n = 274; middle, Poisson-like, n = 274; right, regular rhythmic, n = 12). HDB had only 12/560 regular rhythmic neurons.

6. DISCUSSION

The main findings of my PhD thesis are as follows: (1) The cholinergic basal forebrain contains two distinct functional cell types characterized by either burst-firing or rhythmic, non-bursting firing patterns. (2) Burst-BFCNs showed strong synchrony with each other and cortical oscillations, suggesting that they may have a strong impact on cortical processing. (3) Synchrony between Burst-BFCNs and the auditory cortex at stimulus presentation predicted response timing. (4) Coupling between Reg-BFCNs and the auditory cortex was strongest before mice made successful hits, thus predicting behavioral performance.

6.1. Technical considerations

Previous studies focusing on temporal coding mainly used commercial measuring systems for delivering sensory stimuli and reinforcers while monitoring the animal's behavior. Such currently available measuring systems are well-designed for millisecond precision but the flexibility of the system for various behavioral measuring scenarios is very limited. These commercial setups often also lack delay measurement specifications which is crucial to appropriate reinforcement delivery. To overcome this problem, we designed a microcontroller-based behavior control system (Solari et al., 2018) combined with a sound delivery system for playing complex acoustic stimuli, fast solenoid valves for precisely timed reinforcement delivery and a custom-built sound attenuated chamber using high-end industrial insulation materials. Together this setup provides a physical environment to train head-fixed animals, enables calibrated sound stimuli and precisely timed fluid and air puff presentation as reinforcers. We provide latency measurements for stimulus and reinforcement delivery and an algorithm to perform such measurements on other behavior control systems. Combined with electrophysiology and optogenetic manipulations, the millisecond timing accuracy will help interpret temporally precise neural signals and behavioral changes. Additionally, since software and hardware provided here can be readily customized to achieve a large variety of paradigms, these solutions enable an unusually flexible design of rodent behavioral experiments.

6.2. The cholinergic basal forebrain contains two distinct functional cell types

What makes the basal forebrain cholinergic system capable of modulating a wide variety of cortical processes in distinct cortical target regions and at different timescales? To answer this question, we had to start with the investigation of BFCNs' cellular properties. Previous *in vitro* (Zaborszky, Unal, et al., 2012) and *in vivo* (Lee et al., 2005) studies suggested that basal forebrain cholinergic neurons exhibit heterogeneous firing properties either by artificially evoked current injection protocols or in *in vivo* experiments during different sleep-wake stages showing specific functional correlation with cortical EEG. Our group conducted *in vitro* and *in vivo* experiments to find out if the differences in the firing properties among the BFCNs is a result of distinct BFCN subgroups with different cellular properties or identical BFCNs produce different firing outputs as a result of receiving different cellular inputs.

Our data provided evidence (Laszlovszky et al., 2020), that BFCNs can be separated into two distinct subgroups based on their firing patterns (Figure 37). Burst-BFCN cells were capable of firing bursts of action potentials whereas Reg-BFCN cells responded rhythmically with single action potentials. Regular firing BFCNs were unable to produce bursts, even in response to *in vitro* current injections. This also held for the *in vivo* recorded BFCNs, demonstrating a clear separation between the bursting and the regular firing ones. Burst-BFCNs were further separated into the strongly bursting (Burst-BFCN-SB) and to the Poisson-like (Burst-BFCN-PL) bursting groups. Burst-BFCN-SB cells responded with classical bursts of action potentials with relatively uniform ISIs (with a linear increase between the action potentials towards the end of the burst), whereas Poisson-like cells showed diverse ISIs from short to long intervals which resembled a Poisson process (Figures 21e–i and 25b–k). *In vitro* experiments were carried out to test the difference between the Burst-BFCN-SB and Burst-BFCN-PL firing patterns and concluded that the same neurons could exhibit the two firing modes based on their membrane potential and synaptic input properties. The position of the cells firing pattern between the strongly bursting and the Poisson-like ends of the scale could be assessed by calculating the burst index for the cells.

Another metric that we used was the refractory number capturing the length of the refractory period of the cells. Refractoriness showed a strong correlation with rhythmic firing of the BFCNs. Regular firing BFCNs exhibited refractory periods in the theta range; however, they did not show synchronous firing in their cross-correlograms. Their asynchronous firing and their theta preference could be a result of cell intrinsic properties rather than a similar input to the regular BFCNs; however, this needs to be experimentally tested. Intrinsic theta preference is not a unique phenomenon showed only by BFCNs, since striatal cholinergic interneurons showed similar theta rhythmicity (Tanimura et al., 2019).

In addition to the discovered functional differences among BFCNs, we reconstructed the topology of the BFCNs recorded in the *in vivo* experiments. Reg-BFCNs added up to around half of the recorded cholinergic cells in the NB (one-third to two-thirds) showing a balanced output between the bursting and regular BFCNs to cortical target regions. This ratio markedly differed in case of the cells recorded from the HDB. Cholinergic neurons in the HDB were predominantly Burst-BFCNs (80-90%) (see Figure 35), showing a shift towards a mostly bursting type output of cholinergic cells in the more anterior BF regions. Functional differences between the NB and the HDB cholinergic cells combined with their distinct cortical innervation pattern suggests a more complex cholinergic modulation on a brain-wide level.

Summarizing the cellular level discoveries, we provided proof for the existence of distinct cholinergic subgroups with different innervation patterns, which we further investigated by testing how they synchronize with each other and with cortical oscillations (Figure 37). In the following chapter we discuss the importance of these newly discovered cellular and network level properties exhibited by the basal forebrain cholinergic neurons.

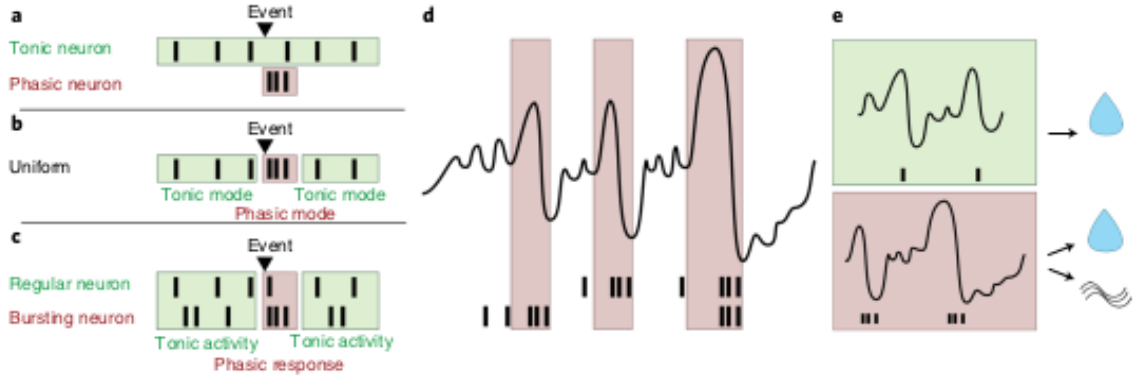

FIGURE 37 | Tonic and phasic cholinergic effects. (a) Based on heterogeneity found *in vitro*, it was hypothesized that tonic and phasic responses are mediated by different cell types. Green shading, tonic effects; pink shading, phasic effects through all panels. (b) Based on homogeneity found *in vivo*, it was suggested that different firing modes of a uniform cell type mediate tonic and phasic effects. (c) We found that phasic responses to behaviorally significant events are mediated by phasic single spike and burst firing of Reg-BFCNs and Burst-BFCNs, respectively. (d) Bursts of BFCNs synchronize with cortical LFPs. Synchronous bursting of Burst-BFCNs is characterized by stronger BF–cortex synchrony. (e) Synchronization of Reg-BFCNs to cortical LFPs predicts correct detections. Cortical synchronization of Burst-BFCNs precedes both correct and incorrect responses.

6.3 Burst-BFCNs showed strong synchrony with each other and cortical oscillations

We proved that Burst-BFCNs and Reg-BFCNs were two separate cholinergic cell types; however, the relationship between their firing modes and their effects on cortical oscillations had to be tested.

Cross-correlations were calculated among and between the distinct BFCN groups to identify synchronous activations of the cells. Rhythmic Reg-BFCNs showed the least synchrony with each other and with the Burst-BFCNs (Figure 30).

While Reg-BFCNs showed asynchronous firing properties, Burst-BFCNs showed a robust synchronous activation on the cross-correlograms suggesting that they synchronize their activation to each other, making them an ideal candidate for conveying a strong synchronized phasic activation signal towards their cortical postsynaptic targets. Whether they are synchronized by a common excitatory sensory input or indirectly by GABAergic

inhibitory neurons in the BF through inhibition-triggered rebound mechanism is still (Zaborszky, van den Pol, et al., 2012).

It seems self-explanatory that Burst-BFCNs are responsible for fast, while Reg-BFCNs are responsible for slow cholinergic modulation controlling markedly different cortical processes.

Our results suggested that single spikes of Reg-BFCNs are also contributing to fast phasic modulation with high precision spike timing (Figure 27c), which was already suggested by (Hangya et al., 2015). However, during this fast activation Burst-BFCNs are capable of responding with firing either single spikes or burst packages; therefore, we tested the correlation of their single APs compared to the correlation of their bursts with salient events (Figure 27). To test if bursts are selectively coupling to these salient events, we correlated bursts compared to single spikes of the same cells with cortical oscillations and, as expected, bursts of Burst-BFCNs were more selective to these salient events and they were followed by stronger desynchronizations in the cortex and predicted an elevation of beta-gamma band activity compared with single spikes. Furthermore, the strongest cortical desynchronizations were observed after synchronous firing of BFCNs, suggesting that cholinergic activation on a network level can create a strong modulatory signal towards the cortex.

6.4 synchrony between Burst-BFCNs and the auditory cortex at stimulus presentation predicted response timing.

We correlated BFCNs' firing with the ongoing oscillations in the auditory cortex and their relationship to behaviorally salient events. We discovered that bursts appeared with a higher percentage after reinforcement, both in case of positive and negative outcomes. To compare Reg-BFCNs with Burst-BFCNs, we calculated bursts as a single event (counted them as a single unit of information) aligned to the first spike of the burst. Bursts showed specificity for reinforcement signals compared to single action potentials, and they showed elevated synchrony with the auditory cortex at stimulus presentation. Their synchronous activation was predictive for response timing but not the outcome of the current trial (see Figures 30, 32, 34). The lack of synchronous activation among Reg-BFCNs and no sign of elevated synchrony with the auditory cortex suggests that Burst-BFCNs receive a different input signal which entrains them to send a robust activation signal towards the

cortex, but this has to be further tested. The information that Burst-BFCNs convey does not carry specific information about outcome of the current behavioral event; however, they are selectively firing due to sensory activation, wakefulness of the animal, or the amount of engagement of the animal in the current trial.

6.5 coupling between Reg-BFCNs and the auditory cortex was strongest before mice made successful hits, thus predicting behavioral performance.

Reg-BFCNs did not carry rapid activation signals as the synchronous burst firing of the Burst-BFCNs; however, they showed a specific activation pattern which predicted not the timing but the performance of the animal. As mentioned earlier, they tended to fire asynchronously with regular ISIs in the theta range during baseline activity. However, in case of a common synchronizing signal received by Reg-BFCN cells, they can hypothetically reset their internal clocks resulting a theta-rhythmic synchronous activation. Our data showed that Reg-BFCNs activation in correlation with the activation of the auditory cortex conveys information about the outcome of the current trial. As seen in Figure 34, STAs calculated between Reg-BFCN spikes and cortical activity showed an outcome specific elevation after cue presentation. We called a successful hit those case when the animal performed correctly the task. In cases of hits coupling between Reg-BFCNs and the auditory cortex showed significant elevation. The increased correlation between the firing of the tonic cells and population activity in the auditory cortex has a predictive power about the outcome of the current trial. This phenomenon added another layer of complexity to the BF cholinergic modulation. In the current study we provided proof that distinct BFCN subgroups exhibit functionally different firing patterns. There is a topological difference in the distribution of the subgroups throughout the BF along the antero-posterior axis. The behavior relevant specific activation of Reg-BFCNs could predict the mouse performance. Returning to our initial question whether generalist or specialist BFCNs are responsible for the complex modulatory control of the cholinergic system, outcome-specific activation of Reg-BFCNs support the idea of specialist subgroups are responsible for functionally different modulation.

For deeper understanding of the different cortical effects evoked by distinct BF cholinergic subgroups it is necessary to measure the evoked responses in their target cells. The

effects on the target side evoked by synaptic versus nonsynaptic release (Sarter et al., 2009) and muscarinergic versus nicotinergic effects (Arroyo et al., 2014; Gu & Yakel, 2011; Urban-Ciecko et al., 2018; Yang, Thankachan, et al., 2017) further complicates the understanding of cholinergic modulation.

6.6 General discussion

Although an earlier *in vitro* study (Zaborszky, Unal, et al., 2012) already hypothesized the existence of distinct BF cholinergic subgroups and that their synchronous activation can result in a strong cortical activation in the target regions (Buzsaki et al., 1988; Pinto et al., 2013; Rye et al., 1984), our results are providing the first comprehensive proof for this long unsolved question about cholinergic modulation. Our *in vitro* (n=60) dataset describes the cellular background of the hypothesized BF cholinergic functional differences resolving the unanswered questions about the early- and late-firing cholinergic cells by the Zaborszky group.

In case of former *in vivo* results the literature is even more incomplete and their initial conclusions are sometimes contradictory to each other. Comparing only by size our large *in vivo* (n=78) dataset with previous juxtacellular labeling experiments (recorded cholinergic neurons n=5, (Lee et al., 2005)), or anesthesized rat measurements (two separate studies with n=3-3 labeled cholinergic neurons, (Duque et al., 2000; Simon et al., 2006) we were able to analyze specific cholinergic effects with a statistically robust pool of data. These studies described cholinergic effects which – in some cases – were contradictory to each other as it was summarized in our paper (Laszlovszky et al., 2020).

7. CONCLUSIONS

The main conclusions of my doctoral dissertation are the following:

(1) The cholinergic basal forebrain contains two distinct functional cell types characterized by either burst-firing or rhythmic, non-bursting firing patterns.

(2) Reg-BFCNs constitute about half (one-third to two-thirds) of BFCNs in the NB, whereas the more anterior HDB cholinergic neurons were mostly (80–90%) of the Burst-BFCN type.

(3) Regular firing cholinergic cells are incapable of firing bursts even in *in vitro* current injection experiments.

(4) Burst-BFCNs showed strong synchrony with each other and cortical oscillations, suggesting that they may have a strong impact on cortical processing.

(5) Synchrony between Burst-BFCNs and the auditory cortex at stimulus presentation predicted response timing.

(6) Coupling between Reg-BFCNs and the auditory cortex was strongest before mice made successful hits, thus predicting behavioral performance.

8. SUMMARY

The basal forebrain cholinergic system has long been considered as a main component in the neuromodulation of synaptic plasticity, learning, and memory, as well as in the modulation of sleep-wake cycle, brain states and oscillations. The regulation of these cortical functions strongly depend on the afferents targeting the BFCNs, their internal connections and synchronization patterns within the BF, and their topographic efferents sending projections to distinct cortical targets. The complexity of the cholinergic modulation is not only a result of the complex anatomical connections but it also comes from the different timescales that these cortical processes are regulated. Cholinergic modulation span broad timescales ranging from milliseconds to seconds or hours resulting either in fast switches of sensory information processing or in slow changes of the sleep-wake cycle by setting cortical acetylcholine levels. Despite these cortical processes were described by a large body of research, the cellular and network effects of BF specific cholinergic modulation in behaviorally relevant conditions remained unexplained.

To address these questions, we analyzed a large dataset of *in vitro* and *in vivo* measurements of BFCNs. BFCNs' intracellular properties were probed by precisely controlled *in vitro* experiments characterizing the electrical properties of the BFCNs by controlling their input parameters while testing their output firing patterns. BFCNs' firing were correlated with behaviorally relevant events, their synchronization with each other were tested by measuring multiple cholinergic single-unit's activity simultaneously with cortical local field potential (LFP).

Our data revealed that the cholinergic basal forebrain contains two distinct functional cell types characterized by either burst-firing or rhythmic, non-bursting firing patterns. These two BFCN subgroups showed topographic organization differences along the BF anteroposterior axis. Furthermore, the cross-correlations and STA analysis revealed that Burst-BFCNs showed strong synchrony with each other and cortical oscillations, which was predictive of response timing in the current behavioral trial. On the other hand coupling between Reg-BFCNs and the auditory cortex was strongest before mice made successful hits, thus predicting behavioral performance.

9. ÖSSZEFOGLALÁS

A bazális előagyi (BF) kolinerg rendszerről régóta ismert, hogy az egyik fő neuromodulációs szerepet tölti be a szinaptikus plaszticitás, tanulás, memóriaraktározás, illetve az alvás-ébrenléti ciklus és az agyi állapotok, oszcillációk szabályozásának a terén. Ezeknek a magassabbrendű folyamatoknak a bazális előagyi kolinerg sejtek (BFCN) általi szabályozása függ a rájuk érkező afferensektől, a kolinerg sejtek bazális előagyon belüli kapcsolatrendszerétől, a BFCN tüzelésének szinkronizációjától, illetve a topografikusan eltérő efferenseik különböző kérgi területekre küldött beidegzéseitől. Továbbá a kolinerg moduláció időskálája a milliszekundumostól a másodpercekig vagy akár órákig is terjedhet melyek eredménye gyors állapotváltozásokat a szenzoros információfeldolgozásban vagy az alvás-ébrenléti ciklusok lassú változáa a kérgi acetilkolin szint szabályozása révén. Annak ellenére, hogy ezen kérgi folyamatokról jelentős mennyiségű kutatási eredmény született a BF specifikus szabályozási funkcióinak sejtszintű, illetve hálózati hatásai viselkedési szempontból releváns körülmények között feltáratlanok maradtak.

Ezen kérdések megválaszolásához a BFCN-ek *in vitro* és *in vivo* méréseikből származó igen jelentős méretű adathalmazait elemeztük. A BFCN-ek intracelluláris tulajdonságait precízen kontrollált *in vitro* kísérletekkel vizsgáltuk, melyek a BFCN-ek elektromos tulajdonságait jellemezték a sejtek bemeneti paramétereinek szabályozásával, miközben teszteltük a sejtek kimeneti tüzelését. A BFCN-ek tüzelését viselkedési szempontból releváns eseményekkel korreláltuk, illetve egymással való szinkronizázációjukat több kolinerg sejt egyedi aktivitásának mérésével teszteltük egyidejűleg a kérgi lokális mezőpotenciál (LFP) rögzítésével.

Adataink alapján a kolinerg BF két funkcionálisan elkülönölő sejttípust tartalmaz, amelyekre vagy burstölő tüzelésű, vagy ritmikus, egyedülálló akciópotenciálokat tartalmazó minták jellemzőek. Ez a két BFCN alcsoport topográfiai szerveződési különbségeket mutatott a BF antero-posterior tengelye mentén. Ezenkívül a keresztkorrelációk és az STA elemzés feltárta, hogy a Burst-BFCN-ek erős szinkronizációt mutattak egymással és a kérgi oszcillációkkal, ami előre jelezte a válaszidőzítést a jelenlegi viselkedési vizsgálatban. Másrészt a Reg-BFCN-ek és a hallókéreg közötti kapcsolódás az egerek sikeres találata előtt volt a legerősebb, így előre jelezve a viselkedési teljesítményt.

10. REFERENCES

Alonso, A., Faure, M. P., & Beaudet, A. (1994). Neurotensin promotes oscillatory bursting behavior and is internalized in basal forebrain cholinergic neurons. *Journal of Neuroscience*, *14*(10), 5778–5792. https://doi.org/10.1523/jneurosci.14-10-05778.1994

Alonso, A., Khateb, A., Fort, P., Jones, B. E., & Mühlethaler, M. (1996). Differential oscillatory properties of cholinergic and non-cholinergic nucleus basalis neurons in guinea pig brain slice. *European Journal of Neuroscience*, *8*(1), 169–182. https://doi.org/10.1111/j.1460-9568.1996.tb01178.x

Anaclet, C., Pedersen, N. P., Ferrari, L. L., Venner, A., Bass, C. E., Arrigoni, E., & Fuller, P. M. (2015). Basal forebrain control of wakefulness and cortical rhythms. *Nature Communications*, *6*, 1–14. https://doi.org/10.1038/ncomms9744

Armstrong, D. M., Saper, C. B., Levey, A. I., Wainer, B. H., & Terry, R. D. (1983). Distribution of cholinergic neurons in rat brain: Demonstrated by the immunocytochemical localization of choline acetyltransferase. *Journal of Comparative Neurology*, *216*(1), 53–68. https://doi.org/10.1002/cne.902160106

Arroyo, S., Bennett, C., & Hestrin, S. (2014). Nicotinic modulation of cortical circuits. *Frontiers in Neural Circuits*, *8*(MAR), 1–6. https://doi.org/10.3389/fncir.2014.00030

Baxter, M. G., Bucci, D. J., Gorman, L. K., Wiley, R. G., & Gallagher, M. (2013). Selective immunotoxic lesions of basal forebrain cholinergic cells: Effects on learning and memory in rats. *Behavioral Neuroscience*, *127*(5), 619–627. https://doi.org/10.1037/a0033939

Baxter, M. G., & Chiba, A. A. (1999). Cognitive functions of the basal forebrain Baxter and Chiba 179. *Current Opinion in Neurobiology*, 178–183.

Boskovic, Z., Milne, M. R., Qian, L., Clifton, H. D., McGovern, A. E., Turnbull, M. T., Mazzone, S. B., & Coulson, E. J. (2018). Cholinergic basal forebrain neurons regulate fear extinction consolidation through p75 neurotrophin receptor signaling. *Translational Psychiatry*, *8*(1). https://doi.org/10.1038/s41398-018-0248-x

Brown, R. E., & McKenna, J. T. (2015). Turning a negative into a positive: Ascending GABAergic control of cortical activation and arousal. *Frontiers in Neurology*, *6*(MAY). https://doi.org/10.3389/fneur.2015.00135

Buzsaki, G., Bickford, R. G., Ponomareff, G., Thal, L. J., Mandel, R., & Gage, F. H. (1988). Nucleus basalis and thalamic control of neocortical activity in the freely moving rat. *Journal of Neuroscience*, *8*(11), 4007–4026. https://doi.org/10.1523/jneurosci.08-11-04007.1988

Buzsáki, G., & Mizuseki, K. (2014). The log-dynamic brain: How skewed distributions affect network operations. *Nature Reviews Neuroscience*, *15*(4), 264–278. https://doi.org/10.1038/nrn3687

Chen, L., Yin, D., Wang, T. X., Guo, W., Dong, H., Xu, Q., Luo, Y. J., Cherasse, Y., Lazarus, M., Qiu, Z. L., Lu, J., Qu, W. M., & Huang, Z. L. (2016). Basal Forebrain Cholinergic Neurons Primarily Contribute to Inhibition of Electroencephalogram Delta Activity, Rather Than Inducing Behavioral Wakefulness in Mice. *Neuropsychopharmacology*, *41*(8), 2133–2146. https://doi.org/10.1038/npp.2016.13

Chubykin, A. A., Roach, E. B., Bear, M. F., & Shuler, M. G. H. (2013). A Cholinergic Mechanism for Reward Timing within Primary Visual Cortex. *Neuron*, *77*(4), 723–735. https://doi.org/10.1016/j.neuron.2012.12.039

Counts, S. E., Perez, S. E., Ginsberg, S. D., & Mufson, E. J. (2010). Neuroprotective role for galanin in Alzheimer's disease. *Exs*, *102*, 143–162. https://doi.org/10.1007/978-3-0346-0228-0_11

Damborsky, J. C., Smith, K. G., Jensen, P., & Yakel, J. L. (2017). Local cholinergic-GABAergic circuitry within the basal forebrain is modulated by galanin. *Brain Structure and Function*, *222*(3), 1385–1400. https://doi.org/10.1007/s00429-016-1283-0

Détári, L., Rasmusson, D. D., & Semba, K. (1999). The role of basal forebrain neurons in tonic and phasic activation of the cerebral cortex. *Progress in Neurobiology*, *58*(3), 249–277. https://doi.org/10.1016/S0301-0082(98)00084-7

Disney, A. A., Aoki, C., & Hawken, M. J. (2007). Gain Modulation by Nicotine in Macaque V1. *Neuron*, *56*(4), 701–713. https://doi.org/10.1016/j.neuron.2007.09.034

Do, J. P., Xu, M., Lee, S. H., Chang, W. C., Zhang, S., Chung, S., Yung, T. J., Fan, J. L., Miyamichi, K., Luo, L., & Dan, Y. (2016). Cell type-specific long-range connections of basal forebrain circuit. *ELife*, *5*(September), 1–18. https://doi.org/10.7554/eLife.13214

Dominik M. Endres, & Johannes E. Schindelin. (2003). A New metric for probability distributions. *Ieee Transactions on Information Theory*, *49*(7), 1858–1860.

Duque, A., Balatoni, B., Detari, L., & Zaborszky, L. (2000). EEG correlation of the discharge properties of identified neurons in the basal forebrain. *Journal of Neurophysiology*, *84*(3), 1627–1635. https://doi.org/10.1152/jn.2000.84.3.1627

Everitt, B. J., & Robbins, T. W. (1997). Central cholinergic systems and cognition. *Annual Review of Psychology*, *48*, 649–684. https://doi.org/10.1146/annurev.psych.48.1.649

Froemke, R. C., Merzenich, M. M., & Schreiner, C. E. (2007). A synaptic memory trace for cortical receptive field plasticity. *Nature*, *450*(7168), 425–429. https://doi.org/10.1038/nature06289

Fuhrmann, F., Justus, D., Sosulina, L., Kaneko, H., Beutel, T., Friedrichs, D., Schoch, S., Schwarz, M. K., Fuhrmann, M., & Remy, S. (2015). Locomotion, Theta Oscillations, and the Speed-Correlated Firing of Hippocampal Neurons Are Controlled by a Medial Septal Glutamatergic Circuit. *Neuron*, *86*(5), 1253–1264. https://doi.org/10.1016/j.neuron.2015.05.001

Furuta, T., Koyano, K., Tomioka, R., Yanagawa, Y., & Kaneko, T. (2004). GABAergic Basal Forebrain Neurons That Express Receptor for Neurokinin B and Send Axons to the Cerebral Cortex. *Journal of Comparative Neurology*, *473*(1), 43–58. https://doi.org/10.1002/cne.20087

Gielow, M. R., & Zaborszky, L. (2017). The Input-Output Relationship of the Cholinergic Basal Forebrain. *Cell Reports*, *18*(7), 1817–1830. https://doi.org/10.1016/j.celrep.2017.01.060

Gritti, I., Henny, P., Galloni, F., Mainville, L., Mariotti, M., & Jones, B. E. (2006). Stereological estimates of the basal forebrain cell population in the rat, including neurons containing choline acetyltransferase, glutamic acid decarboxylase or phosphate-activated glutaminase and colocalizing vesicular glutamate transporters. *Neuroscience*, *143*(4), 1051–1064. https://doi.org/10.1016/j.neuroscience.2006.09.024

Gritti, I., Mainville, L., Mancia, M., & Jones, B. E. (1997). GABAergic and other noncholinergic basal forebrain neurons, together with cholinergic neurons, project to the mesocortex and isocortex in the rat. *Journal of Comparative Neurology*,

383(2), 163–177. https://doi.org/10.1002/(SICI)1096-9861(19970630)383:2<163::AID-CNE4>3.0.CO;2-Z

Gritti, I., Manns, I. D., Mainville, L., & Jones, B. E. (2003). Parvalbumin, calbindin, or calretinin in cortically projecting and GABAergic, cholinergic, or glutamatergic basal forebrain neurons of the rat. *Journal of Comparative Neurology*, *458*(1), 11–31. https://doi.org/10.1002/cne.10505

Gritton, H. J., Howe, W. M., Mallory, C. S., Hetrick, V. L., Berke, J. D., & Sarter, M. (2016). Cortical cholinergic signaling controls the detection of cues. *Proceedings of the National Academy of Sciences of the United States of America*, *113*(8), E1089–E1097. https://doi.org/10.1073/pnas.1516134113

Gu, Z., & Yakel, J. L. (2011). Timing-Dependent Septal Cholinergic Induction of Dynamic Hippocampal Synaptic Plasticity. *Neuron*, *71*(1), 155–165. https://doi.org/10.1016/j.neuron.2011.04.026

Guo, W., Robert, B., & Polley, D. B. (2019). The Cholinergic Basal Forebrain Links Auditory Stimuli with Delayed Reinforcement to Support Learning. *Neuron*, *103*(6), 1164-1177.e6. https://doi.org/10.1016/j.neuron.2019.06.024

Gyengesi, E., Andrews, Z. B., Paxinos, G., & Zaborszky, L. (2013). Distribution of secretagogin-containing neurons in the basal forebrain of mice, with special reference to the cholinergic corticopetal system. *Brain Research Bulletin*, *94*, 1–8. https://doi.org/10.1016/j.brainresbull.2013.01.009

Halassa, M. M., Florian, C., Fellin, T., Munoz, J. R., Lee, S. Y., Abel, T., Haydon, P. G., & Frank, M. G. (2009). Astrocytic Modulation of Sleep Homeostasis and Cognitive Consequences of Sleep Loss. *Neuron*, *61*(2), 213–219. https://doi.org/10.1016/j.neuron.2008.11.024

Han, Y., Shi, Y. F., Xi, W., Zhou, R., Tan, Z. B., Wang, H., Li, X. M., Chen, Z., Feng, G., Luo, M., Huang, Z. L., Duan, S., & Yu, Y. Q. (2014). Selective activation of cholinergic basal forebrain neurons induces immediate sleep-wake transitions. *Current Biology*, *24*(6), 693–698. https://doi.org/10.1016/j.cub.2014.02.011

Hangya, B., Ranade, S. P., Lorenc, M., & Kepecs, A. (2015). Central Cholinergic Neurons Are Rapidly Recruited by Reinforcement Feedback. *Cell*, *162*(5), 1155–1168. https://doi.org/10.1016/j.cell.2015.07.057

Harrison, T. C., Pinto, L., Brock, J. R., & Dan, Y. (2016). Calcium imaging of basal forebrain activity during innate and learned behaviors. *Frontiers in Neural Circuits*, *10*(MAY), 1–12. https://doi.org/10.3389/fncir.2016.00036

Hassani, O. K., Lee, M. G., Henny, P., & Jones, B. E. (2009). Discharge profiles of identified GABAergic in comparison to cholinergic and putative glutamatergic basal forebrain neurons across the sleep-wake cycle. *Journal of Neuroscience*, *29*(38), 11828–11840. https://doi.org/10.1523/JNEUROSCI.1259-09.2009

Hasselmo, M. E., & Sarter, M. (2011). Modes and models of forebrain cholinergic neuromodulation of cognition. *Neuropsychopharmacology*, *36*(1), 52–73. https://doi.org/10.1038/npp.2010.104

Hawryluk, J. M., Ferrari, L. L., Keating, S. A., & Arrigoni, E. (2012). Adenosine inhibits glutamatergic input to basal forebrain cholinergic neurons. *Journal of Neurophysiology*, *107*(10), 2769–2781. https://doi.org/10.1152/jn.00528.2011

Hermanstyne, T. O., Kihira, Y., Misono, K., Deitchler, A., Yanagawa, Y., & Misonou, H. (2010). Immunolocalization of the voltage-gated potassium channel Kv2.2 in GABAergic neurons in the basal forebrain of rats and mice. *Journal of Comparative Neurology*, *518*(21), 4298–4310. https://doi.org/10.1002/cne.22457

Hermanstyne, T. O., Subedi, K., Le, W. W., Hoffman, G. E., Meredith, A. L., Mong, J. A., & Misonou, H. (2013). Kv2.2: A novel molecular target to study the role of basal forebrain GABAergic neurons in the sleep-wake cycle. *Sleep*, *36*(12), 1839–1848. https://doi.org/10.5665/sleep.3212

Higley, M. J., Gittis, A. H., Oldenburg, I. A., Balthasar, N., Seal, R. P., Edwards, R. H., Lowell, B. B., Kreitzer, A. C., & Sabatini, B. L. (2011). Cholinergic interneurons mediate fast VGluT3-dependent glutamatergic transmission in the striatum. *PLoS ONE*, *6*(4). https://doi.org/10.1371/journal.pone.0019155

Hur, E. E., & Zaborszky, L. (2005). Vglut2 afferents to the medial prefrontal and primary somatosensory cortices: A combined retrograde tracing in situ hybridization. *Journal of Comparative Neurology*, *483*(3), 351–373. https://doi.org/10.1002/cne.20444

Jonakait, G. M., Pratt, L., Acevedo, G., & Ni, L. (2012). Microglial regulation of cholinergic differentiation in the basal forebrain. *Developmental Neurobiology*, *72*(6), 857–864. https://doi.org/10.1002/dneu.20969

Jones, B. E. (2004). Activity, modulation and role of basal forebrain cholinergic neurons innervating the cerebral cortex. *Progress in Brain Research*, *145*, 157–169. https://doi.org/10.1016/S0079-6123(03)45011-5

Kalinchuk, A. v., McCarley, R. W., Stenberg, D., Porkka-Heiskanen, T., & Basheer, R. (2008). The role of cholinergic basal forebrain neurons in adenosine-mediated homeostatic control of sleep: Lessons from 192 IgG-saporin lesions. *Neuroscience*, *157*(1), 238–253. https://doi.org/10.1016/j.neuroscience.2008.08.040

Khateb, A., Mühlethaler, M., Alons, A., Serafin, M., Mainville, L., & Jones, B. E. (1992). Cholinergic nucleus basalis neurons display the capacity for rhythmic bursting activity mediated by low-threshold calcium spikes. *Neuroscience*, *51*(3), 489–494. https://doi.org/10.1016/0306-4522(92)90289-E

Kilgard, M. P., & Merzenich, M. M. (1998). Cortical map reorganization enabled by nucleus basalis activity. *Science*, *279*(5357), 1714–1718. https://doi.org/10.1126/science.279.5357.1714

Kim, T., Ramesh, V., Dworak, M., Choi, D. S., McCarley, R. W., Kalinchuk, A. v., & Basheer, R. (2015). Disrupted sleep-wake regulation in type 1 equilibrative nucleoside transporter knockout mice. *Neuroscience*, *303*, 211–219. https://doi.org/10.1016/j.neuroscience.2015.06.037

Kim, T., Thankachan, S., McKenna, J. T., McNally, J. M., Yang, C., Choi, J. H., Chen, L., Kocsis, B., Deisseroth, K., Strecker, R. E., Basheer, R., Brown, R. E., & McCarley, R. W. (2015). Cortically projecting basal forebrain parvalbumin neurons regulate cortical gamma band oscillations. *Proceedings of the National Academy of Sciences of the United States of America*, *112*(11), 3535–3540. https://doi.org/10.1073/pnas.1413625112

Kvitsiani, D., Ranade, S., Hangya, B., Taniguchi, H., Huang, J. Z., & Kepecs, A. (2013). Distinct behavioural and network correlates of two interneuron types in prefrontal cortex. *Nature*, *498*(7454), 363–366. https://doi.org/10.1038/nature12176

Laszlovszky, T., Schlingloff, D., Hegedüs, P., Freund, T. F., Gulyás, A., Kepecs, A., & Hangya, B. (2020). Distinct synchronization, cortical coupling and behavioral function of two basal forebrain cholinergic neuron types. *Nature Neuroscience*, *23*(8), 992–1003. https://doi.org/10.1038/s41593-020-0648-0

Lee, M. G., Hassani, O. K., Alonso, A., & Jones, B. E. (2005). Cholinergic basal forebrain neurons burst with theta during waking and paradoxical sleep. *Journal of Neuroscience*, *25*(17), 4365–4369. https://doi.org/10.1523/JNEUROSCI.0178-05.2005

Li, X., Yu, B., Sun, Q., Zhang, Y., Ren, M., Zhang, X., Li, A., Yuan, J., Madisen, L., Luo, Q., Zeng, H., Gong, H., & Qiu, Z. (2017). Generation of a whole-brain atlas for the cholinergic system and mesoscopic projectome analysis of basal forebrain cholinergic neurons. *Proceedings of the National Academy of Sciences of the United States of America*, *115*(2), 415–420. https://doi.org/10.1073/pnas.1703601115

Lin, S. C., Brown, R. E., Shuler, M. G. H., Petersen, C. C. H., & Kepecs, A. (2015). Optogenetic dissection of the basal forebrain neuromodulatory control of cortical activation, plasticity, and cognition. *Journal of Neuroscience*, *35*(41), 13896–13903. https://doi.org/10.1523/JNEUROSCI.2590-15.2015

Lin, S. C., Gervasoni, D., & Nicolelis, M. A. L. (2006). Fast modulation of prefrontal cortex activity by basal forebrain noncholinergic neuronal ensembles. *Journal of Neurophysiology*, *96*(6), 3209–3219. https://doi.org/10.1152/jn.00524.2006

Lin, S. C., & Nicolelis, M. A. L. (2008). Neuronal Ensemble Bursting in the Basal Forebrain Encodes Salience Irrespective of Valence. *Neuron*, *59*(1), 138–149. https://doi.org/10.1016/j.neuron.2008.04.031

Lopes, G., Bonacchi, N., Frazão, J., Neto, J. P., Atallah, B. v., Soares, S., Moreira, L., Matias, S., Itskov, P. M., Correia, P. A., Medina, R. E., Calcaterra, L., Dreosti, E., Paton, J. J., & Kampff, A. R. (2015). Bonsai: An event-based framework for processing and controlling data streams. *Frontiers in Neuroinformatics*, *9*(APR), 1–14. https://doi.org/10.3389/fninf.2015.00007

McGaughy, J., Everitt, B. J., Robbins, T. W., & Sarter, M. (2000). The role of cortical cholinergic afferent projections in cognition: Impact of new selective immunotoxins. *Behavioural Brain Research*, *115*(2), 251–263. https://doi.org/10.1016/S0166-4328(00)00262-X

Mckenna, J. T., Yang, C., Franciosi, S., Winston, S., Abarr, K. K., Rigby, M. S., Yanagawa, Y., Mccarley, R. W., & Brown, R. E. (2013). Distribution and intrinsic membrane properties of basal forebrain GABAergic and parvalbumin neurons in

the mouse. *Journal of Comparative Neurology*, *521*(6), 1225–1250. https://doi.org/10.1002/cne.23290

Mesulam, M. M., & van Hoesen, G. W. (1976). Acetylcholinesterase-rich projections from the basal forebrain of the rhesus monkey to neocortex. *Brain Research*, *109*(1), 152–157. https://doi.org/10.1016/0006-8993(76)90385-1

Mesulam, M. -Marsel, Mufson, E. J., Levey, A. I., & Wainer, B. H. (1983). Cholinergic innervation of cortex by the basal forebrain: Cytochemistry and cortical connections of the septal area, diagonal band nuclei, nucleus basalis (Substantia innominata), and hypothalamus in the rhesus monkey. *Journal of Comparative Neurology*, *214*(2), 170–197. https://doi.org/10.1002/cne.902140206

Metherate, R., Cox, C. L., & Ashe, J. H. (1992). Cellular bases of neocortical activation: Modulation of neural oscillations by the nucleus basalis and endogenous acetylcholine. *Journal of Neuroscience*, *12*(12), 4701–4711. https://doi.org/10.1523/jneurosci.12-12-04701.1992

Mitchell, S. J., Richardson, R. T., Baker, F. H., & DeLong, M. R. (1987). The primate nucleus basalis of Meynert: neuronal activity related to a visuomotor tracking task. *Experimental Brain Research*, *68*(3), 506–515. https://doi.org/10.1007/BF00249794

Nickerson Poulin, A., Guerci, A., el Mestikawy, S., & Semba, K. (2006). Vesicular glutamate transporter 3 immunoreactivity is present in cholinergic basal forebrain neurons projecting to the basolateral amygdala in rat. *The Journal of Comparative Neurology*, *498*(5), 690–711. https://doi.org/https://doi.org/10.1002/cne.21081

O. von Bohlen und Halbach, R. D. (2006). Neurotransmitters and Neuromodulators. In *Neurotransmitters and neuromodulators: Handbook of receptors and biological effects (2nd ed.).* (2nd ed.). Wiley-VCH Verlag.

Ozen Irmak, S., & de Lecea, L. (2014). Basal forebrain cholinergic modulation of sleep transitions. *Sleep*, *37*(12), 1941–1951. https://doi.org/10.5665/sleep.4246

Parikh, V., Kozak, R., Martinez, V., & Sarter, M. (2007). Prefrontal Acetylcholine Release Controls Cue Detection on Multiple Timescales. *Neuron*, *56*(1), 141–154. https://doi.org/10.1016/j.neuron.2007.08.025

Pinto, L., Goard, M. J., Estandian, D., Xu, M., Kwan, A. C., Lee, S. H., Harrison, T. C., Feng, G., & Dan, Y. (2013). Fast modulation of visual perception by basal

forebrain cholinergic neurons. *Nature Neuroscience*, *16*(12), 1857–1863. https://doi.org/10.1038/nn.3552

Riascos, D., Nicholas, A., Samaeekia, R., Yukhananov, R., Mesulam, M. M., Bigio, E. H., Weintraub, S., Guo, L., & Geula, C. (2014). Alterations of Ca2+-responsive proteins within cholinergic neurons in aging and Alzheimer's disease. *Neurobiology of Aging*, *35*(6), 1325–1333. https://doi.org/10.1016/j.neurobiolaging.2013.12.017

Richardson, R. T., & DeLong, M. R. (1986). Nucleus basalis of Meynert neuronal activity during a delayed response task in monkey. *Brain Research*, *399*(2), 364–368. https://doi.org/10.1016/0006-8993(86)91529-5

Robinson, J., Manseau, F., Ducharme, G., Amilhon, B., Vigneault, E., el Mestikawy, S., & Williams, S. (2016). Optogenetic activation of septal glutamatergic neurons drive hippocampal theta rhythms. *Journal of Neuroscience*, *36*(10), 3016–3023. https://doi.org/10.1523/JNEUROSCI.2141-15.2016

Royer, S., Zemelman, B. v., Losonczy, A., Kim, J., Chance, F., Magee, J. C., & Buzsáki, G. (2012). Control of timing, rate and bursts of hippocampal place cells by dendritic and somatic inhibition. *Nature Neuroscience*, *15*(5), 769–775. https://doi.org/10.1038/nn.3077

Rye, D. B., Wainer, B. H., Mesulam, M. M., Mufson, E. J., & Saper, C. B. (1984). Cortical projections arising from the basal forebrain: A study of cholinergic and noncholinergic components employing combined retrograde tracing and immunohistochemical localization of choline acetyltransferase. *Neuroscience*, *13*(3), 627–643. https://doi.org/10.1016/0306-4522(84)90083-6

Saper, C. B. (1985). Organization of cerebral cortical afferent systems in the rat. II. Hypothalamocortical projections. *Journal of Comparative Neurology*, *237*(1), 21–46. https://doi.org/10.1002/cne.902370103

Sarter, M., Parikh, V., & Howe, W. M. (2009). Phasic Ach release and volume transmission. *Nature Reviews Neuroscience*, *10*(may), 383–390.

Saunders, A., Granger, A. J., & Sabatini, B. L. (2015). Corelease of acetylcholine and GABA from cholinergic forebrain neurons. *ELife*, *2015*(4), 1–13. https://doi.org/10.7554/eLife.06412

Schmitzer-Torbert, N., Jackson, J., Henze, D., Harris, K., & Redish, A. D. (2005). Quantitative measures of cluster quality for use in extracellular recordings. *Neuroscience*, *131*(1), 1–11. https://doi.org/10.1016/j.neuroscience.2004.09.066

Shi, Y. F., Han, Y., Su, Y. T., Yang, J. H., & Yu, Y. Q. (2015). Silencing of cholinergic basal forebrain neurons using archaerhodopsin prolongs slow-wave sleep in mice. *PLoS ONE*, *10*(7), 1–18. https://doi.org/10.1371/journal.pone.0130130

Simon, A. P., Poindessous-Jazat, F., Dutar, P., Epelbaum, J., & Bassant, M. H. (2006). Firing properties of anatomically identified neurons in the medial septum of anesthetized and unanesthetized restrained rats. *Journal of Neuroscience*, *26*(35), 9038–9046. https://doi.org/10.1523/JNEUROSCI.1401-06.2006

Solari, N., Sviatkó, K., Laszlovszky, T., Hegedüs, P., & Hangya, B. (2018). Open source tools for temporally controlled rodent behavior suitable for electrophysiology and optogenetic manipulations. *Frontiers in Systems Neuroscience*, *12*(May), 1–14. https://doi.org/10.3389/fnsys.2018.00018

Takács, V. T., Cserép, C., Schlingloff, D., Pósfai, B., Szőnyi, A., Sos, K. E., Környei, Z., Dénes, Á., Gulyás, A. I., Freund, T. F., & Nyiri, G. (2018). Co-transmission of acetylcholine and GABA regulates hippocampal states. *Nature Communications*, *9*(1). https://doi.org/10.1038/s41467-018-05136-1

Tanimura, A., Pancani, T., Lim, S. A. O., Tubert, C., Alexandra, E., Shen, W., & Surmeier, D. J. (2019). Striatal cholinergic interneurons and Parkinson's disease. *European Journal of Neuroscience*, *47*(10), 1148–1158. https://doi.org/10.1111/ejn.13638.Striatal

Teles-Grilo Ruivo, L. M., Baker, K. L., Conway, M. W., Kinsley, P. J., Gilmour, G., Phillips, K. G., Isaac, J. T. R., Lowry, J. P., & Mellor, J. R. (2017). Coordinated Acetylcholine Release in Prefrontal Cortex and Hippocampus Is Associated with Arousal and Reward on Distinct Timescales. *Cell Reports*, *18*(4), 905–917. https://doi.org/10.1016/j.celrep.2016.12.085

Tingley, D., Alexander, A. S., Quinn, L. K., Chiba, A. A., & Nitz, D. A. (2015). Cell assemblies of the basal forebrain. *Journal of Neuroscience*, *35*(7), 2992–3000. https://doi.org/10.1523/JNEUROSCI.4432-14.2015

Unal, C. T., Pare, D., & Zaborszky, L. (2015). Impact of basal forebrain cholinergic inputs on basolateral amygdala neurons. *Journal of Neuroscience*, *35*(2), 853–863. https://doi.org/10.1523/JNEUROSCI.2706-14.2015

Urban-Ciecko, J., Jouhanneau, J. S., Myal, S. E., Poulet, J. F. A., & Barth, A. L. (2018). Precisely Timed Nicotinic Activation Drives SST Inhibition in Neocortical Circuits. *Neuron*, *97*(3), 611-625.e5. https://doi.org/10.1016/j.neuron.2018.01.037

Verhoog, M. B., Obermayer, J., Kortleven, C. A., Wilbers, R., Wester, J., Baayen, J. C., de Kock, C. P. J., Meredith, R. M., & Mansvelder, H. D. (2016). Layer-specific cholinergic control of human and mouse cortical synaptic plasticity. *Nature Communications*, *7*, 1–13. https://doi.org/10.1038/ncomms12826

Wu, M., Dumalska, I., Morozova, E., van den Pol, A. N., & Alreja, M. (2009). Gonadotropin inhibitory hormone inhibits basal forebrain vGluT2-gonadotropin-releasing hormone neurons via a direct postsynaptic mechanism. *Journal of Physiology*, *587*(7), 1401–1411. https://doi.org/10.1113/jphysiol.2008.166447

Xu, M., Chung, S., Zhang, S., Zhong, P., Ma, C., Chang, W. C., Weissbourd, B., Sakai, N., Luo, L., Nishino, S., & Dan, Y. (2015). Basal forebrain circuit for sleep-wake control. *Nature Neuroscience*, *18*(11), 1641–1647. https://doi.org/10.1038/nn.4143

Yang, C., McKenna, J. T., & Brown, R. E. (2017). Intrinsic membrane properties and cholinergic modulation of mouse basal forebrain glutamatergic neurons in vitro. *Neuroscience*, *352*, 249–261. https://doi.org/10.1016/j.neuroscience.2017.04.002

Yang, C., McKenna, J. T., Zant, J. C., Winston, S., Basheer, R., & Brown, R. E. (2014). Cholinergic neurons excite cortically projecting basal forebrain GABAergic neurons. *Journal of Neuroscience*, *34*(8), 2832–2844. https://doi.org/10.1523/JNEUROSCI.3235-13.2014

Yang, C., Thankachan, S., McCarley, R. W., & Brown, R. E. (2017). The menagerie of the basal forebrain: how many (neural) species are there, what do they look like, how do they behave and who talks to whom? *Current Opinion in Neurobiology*, *44*, 159–166. https://doi.org/10.1016/j.conb.2017.05.004

Zaborszky, L., Unal, C. T., & Golowasch, J. P. (2012). Adult mouse basal forebrain harbors two distinct cholinergic populations defined by their electrophysiology. *Frontiers in Behavioral Neuroscience*, *6*(MAY), 1–14. https://doi.org/10.3389/fnbeh.2012.00021

Zaborszky, L., van den Pol, A. N., & Gyengesi, E. (2012). The Basal Forebrain Cholinergic Projection System in Mice. In *The Mouse Nervous System*. https://doi.org/10.1016/B978-0-12-369497-3.10028-7

Zant, J. C., Kim, T., Prokai, L., Szarka, S., McNally, J., McKenna, J. T., Shukla, C., Yang, C., Kalinchuk, A. v., McCarley, R. W., Brown, R. E., & Basheer, R. (2016). Cholinergic neurons in the basal forebrain promote wakefulness by actions on neighboring non-cholinergic neurons: An opto-dialysis study. *Journal of Neuroscience*, *36*(6), 2057–2067. https://doi.org/10.1523/JNEUROSCI.3318-15.2016

Zeldenrust, F., Wadman, W. J., & Englitz, B. (2018). Neural coding with bursts—Current state and future perspectives. *Frontiers in Computational Neuroscience*, *12*(July), 1–14. https://doi.org/10.3389/fncom.2018.00048

Zhao, S., Ting, J. T., Atallah, H. E., Qiu, L., Tan, J., Gloss, B., Augustine, G. J., Deisseroth, K., Luo, M., Graybiel, A. M., & Feng, G. (2011). Cell type-specific channelrhodopsin-2 transgenic mice for optogenetic dissection of neural circuitry function. *Nature Methods*, *8*(9), 745–755. https://doi.org/10.1038/nmeth.1668

11. BIBLIOGRAPHY OF CANDIDATES PUBLICATIONS

11.1. List of publications related to this thesis

11.1.1. Articles

1. **Laszlovszky, T.**, Schlingloff, D., Hegedüs, P., Freund, T. F., Gulyás, A., Kepecs, A., & Hangya, B. (2020). Distinct synchronization, cortical coupling and behavioral function of two basal forebrain cholinergic neuron types. *Nature Neuroscience*, *23*(8), 992–1003. https://doi.org/10.1038/s41593-020-0648-0

2. Solari, N.†, Sviatkó, K. †, **Laszlovszky, T.** †, Hegedüs, P. †, & Hangya, B. (2018). Open source tools for temporally controlled rodent behavior suitable for electrophysiology and optogenetic manipulations. *Frontiers in Systems Neuroscience*, *12*(May), 1–14. https://doi.org/10.3389/fnsys.2018.00018

† Equal contribution

11.2. List of other publications

11.2.1. Articles

Domonkos, A., Nikitidou Ledri, L., **Laszlovszky, T**., Cserép, C., Borhegyi, Z., Papp, E., Nyiri, G., Freund, T. F., & Varga, V. (2016). Divergent *in vivo* activity of non-serotonergic and serotonergic VGluT3–neurones in the median raphe region. *Journal of Physiology*, *594*(13), 3775–3790. https://doi.org/10.1113/JP272036

12. ACKNOWLEDGEMENT

First of all, I would like to thank my supervisor, Balázs Hangya for the opportunity to work in his lab, all the energy and mentorship he provided during my graduate years. I am especially grateful for his guidance to learn programming, analytical skills, experimental techniques, critical thinking, and all the help he provided finalizing my doctoral studies. Furthermore, I would like to thank him that he provided the opportunity to participate in international conferences and neuroscience summer schools, meeting fascinating people, and broadening my horizons.

I would also like to thank all the present and past members of the Hangya lab (a.k.a. Planet36) for creating a stimulating work environment and helping me tackle all the theoretical and technical challenges during my PhD, and for all the fun that we had in the daily life of the lab. I thank Katalin Sviatkó, Nicola Solari, Diána Balázsfi, Sergio Martínez Bellver, Panna Hegedüs, Bálint Király, Márton Kajtor, Barnabás Kocsis for their support during my graduate years and all the ups and downs we went together. Finally, I would like to thank Katalin Lengyel for his excellent technical assistance throughout all the 12 years I spent in Koki.

I express special gratitude towards Viktor Varga for his invaluable help and support and the opportunity to work in his lab during my undergraduate years. Viktor always supervised my work with patience and both shaped and inspired my passion towards neuroscience. I would also like to thank Andor Domonkos, Márti Jelitai, Litsa Ledri for helping me obtaining theoretical and practical knowledge and showing me a level of excellence, which defined the standards I was aiming during my undergraduate years. I thank Tamás Freund for providing the possibility to work in his department and for organizing the Introduction to Neurobiology course during my bachelor studies which started my curiosity about neuroscience.

I cannot be grateful enough to my friends for being with me and supporting during the hard times as well.

Finally, I would like to thank the continuous support of my family, particularly my wife, Kata Melecsky; my parents, Csilla Siklódi and József Laszlovszky; my sisters, Ágnes and Andrea Laszlovszky, my grandmother, Gimama for the endless patience and support during my scientific career and my whole life enabling me to chase my dreams.